ACCURACY ENHANCEMENT FOR HIGH PRECISION GANTRY STAGE

TEO CHEK SING

NATIONAL UNIVERSITY OF SINGAPORE
2007

ACCURACY ENHANCEMENT FOR HIGH PRECISION GANTRY STAGE

TEO CHEK SING
(B.Eng., NATIONAL UNIVERSITY OF SINGAPORE)

A THESIS SUBMITTED
FOR THE DEGREE OF DOCTOR OF PHILOSOPHY
NUS GRADUATE SCHOOL FOR INTEGRATIVE SCIENCES AND ENGINEERING
NATIONAL UNIVERSITY OF SINGAPORE
2007

Acknowledgments

I would like to express my sincerest appreciation to all who had helped me during my study in the National University of Singapore (NUS). First of all, I would like to thank my Supervisors and Thesis Advisory Committee: Dr. Lim Ser Yong, Associate Professor Tan Kok Kiong and Assistant Professor Xiang Cheng for their helpful discussions, support and encouragement. I would also want to thank my Scholarship provider: the Agency for Science, Technology and Research (A*STAR), the staffs at the NUS Graduate School for integrative sciences and engineering (NGS), as well as the Singapore Institute of Manufacturing Technology (SIMTech) for the various supports and collaborations in the research works.

I would like to give my gratitude to all my friends in Mechatronics and Automation Lab. I would especially like to thank Dr. Huang Sunan, Dr. Tang Kok Zuea, Dr. Zhao Shao, Mr. Andi Sudjana Putra and Mr. Tan Chee Siong for their inspiring discussions and advice.

Finally, I would like to thank my family for their endless love and support. Specially, I would like to express my deepest gratitude to my wife Angela Chia li lin for her understanding and support.

Contents

Summary

Most industries are accelerating their moves toward higher accuracy and faster speed on the factory floor. This is certainly the case in the semiconductor industry. It needs systems that provide accurate and fast processing, control and inspection of wafer and die to make the next step in large-scale integration; with smaller feature size on larger wafer substrate. The same trend can be seen in other industries: aerospace, biomedical and storage media, where success rests on positioning with submicron tolerances. Manufacturers are always looking for systems that provide the highest and fastest performance in the smallest package and the lowest overall cost. The accuracy of a machine tool is the limiting factor in the accuracy of the finished parts. Errors in the machine tool motion produce a one-to-one error correspondence in the final workpiece. It is impossible to completely eliminate errors by design and/or manufacturing modifications. Hence, this study provides various methodologies for reducing and compensating for errors in real-time, thus improving the accuracy of workpieces.

Significant advances have been made in each control area, (pattern recognition, learning, adaptive control, robust control, knowledge-based systems) such that various opponents have advocated that the field of control engineering has realized its potential.

However, newer technologies and requirements challenge the control engineers to greater heights; precision engineering is precisely the challenge needed. The importance of ultra-precision motion systems, especially in the semiconductor industry, cannot be denied; component placement, lithography, and wafer inspection are just some of the related applications. Hence, the demand for faster output and better quality products lead to this author's research focus: Accuracy Enhancement for High Precision Gantry Stage. This report details the progress development the author has achieved within his candidature.

In this thesis, the platform of the study will be on long travel and ultra-precision motion system. Amongst the various configurations of such motion system, one of the most popular is the gantry stage; it consists of two motors, which are mounted on two parallel slides, moving another orthogonal member simultaneously in tandem. Using a particular class of direct drive linear motors: Permanent Magnet Linear Motors (PMLM), the gantry stage can be designed to provide high-speed and high-accuracy motion. Fitted with another orthogonal actuator as well as a vertical one, the system is capable of X, Y and Z motion. This configuration of gantry stage is also commonly referred as a H-type gantry stage, due to the 'H' shape that the three actuators (used for X-Y motion) formed. The application area is targeted at (but not restricted to) inspection system such as Micro X-ray 2-Dimensional/ Computed Tomography (CT) inspection. They are essential tools for internal defects detection in the semiconductor and electronics industries. Typical 2-Dimensional applications include the inspection of voids in Ball Grid Array (BGA), ball missing, ball misplacement or bridging, wire

bonding problem, wafer impurity, and other internal defects in advanced packaging. CT inspection is mainly used to inspect and localize an internal defect which cannot be properly determined with 2D inspection, or to provide 3D visualization and measurement of an internal structure or defect.

This thesis focuses on improving the accuracy achieved by motion system. These improvements are two fold: firstly, software-based corrective approaches are adopted to improve the accuracy of motion system, rather than to rely purely on the precise design and construction of the hardware; which is costly. Secondly, a model-based control strategy is proposed for the gantry stage to deal with nonlinear effects. Nonlinearities exist in any motion system; the demand for high accuracy motion increases the significant impact of these nonlinearities. Theoretical formulations are developed to analyze these issues, with extensive simulations and experimental results furnished to illustrate the effectiveness of the approaches.

List of Tables

List of Figures

List of Abbreviations

A/D	*Analog to Digital*
ASME	*American Society Mechanical Engineers*
BGA	*Ball Grid Array*
CIPM	*International Committee of Weights and Measures*
CMM	*Coordinate Measuring Machines*
CT	*Computed Tomography*
DAQ	*Data Acquisition*
DOF	*Degree Of Freedom*
DSP	*Digital Signal Processing*
et al.	*et alii*
etc.	*et cetera*
GUM	*Guide to the expression of Uncertainty in Measurement*
I/O	*Input/Output*
ILC	*Iterative Learning Control*
ISO	*International Organization for Standardization*
LUT	*Look Up Table*

PCB	*Printed Circuit Board*
PID	*Proportional Integral Derivative*
PMLM	*Permanent Magnet Linear Motor*
RBF	*Radial Basis Function*
SI Units	*International System of Units*
SIL	*Safety Integrity Level*
SVM	*Support Vector Machines*

Chapter 1

Introduction

Precision engineering is the multidisciplinary study and practice of design, metrology, and manufacturing at high precision. It draws on diverse historical roots dating from the invention of the seismoscope by Zhang Heng almost two thousand years ago and the development of the mechanical clock in Europe during the 13th century. Subsequently, these contributions cumulated towards the development of high-precision machine tools and instruments in the late 1800s and early 1900s with the ruling engines for the manufacture of scales, reticules and spectrographic diffraction gratings. Today, ultra-precision machine tools under computer control can position the tool relative to the workpiece with positioning accuracy that is much smaller than the diameter of a human's hair. These ultra-precision machine tools shall form the centerpiece for this thesis research development.

1.1 Current Trends and Challenges

Most industries are accelerating their moves toward higher accuracy and faster speed on the factory floor. This is certainly the case in the semiconductor industry. It needs

systems that provide accurate and fast processing, control and inspection of wafer and die to make the next step in large-scale integration; with smaller feature size on larger wafer substrate. The same trend can be seen in other industries: aerospace, biomedical and storage media, where success rests on positioning with submicron tolerances. Manufacturers are always looking for systems that provide the highest and fastest performance in the smallest package and the lowest overall cost. This section seeks to observe the trends for both stage manufacturers as well as emerging applications and subsequently, identified the challenges that these would posed for the next generations of control engineers.

Central to all the different industries/processes is a ultra-precision motion system that is capable of achieving the tight specifications in accuracy and speed. The development in control methodologies for such systems are matured. However, as our understanding continues to evolve in the design of precision machines, in order to develop machines with higher accuracies than their predecessors, new techniques are used and sometimes they bring along new issues for control engineers to resolve. Some of these new developing machines include:

- A decoupled air-bearing positioning stage developed in the Singapore Institute of Manufacturing Technology [1]:

  This system uses 3 linear motors to provide a planar motion (X, Y and θ_Z) of 300mm by 300mm and optical encoders, calibrated from a laser interferometer, for measurements. The positioning accuracy after compensation is 3micron with

repeatability of 1micron in a temperature-regulated environment. It is capable of acceleration up to 0.5g with a payload of 10kg.

- A Multi-Scale Alignment Positioning System stage currently being developed for the Center for Scalable and integrated Manufacturing [2]:

  This system uses 4 Lorentz motors to achieve 3 DOF (X, Y and θ_Z) with a working area of 10 mm by 10 mm. A laser interferometer is used for all measurements. It is developed to achieve critical dimensions of 5 nm and overlay of 10 nm in lithography applications with motion up to 0.5mm/s.

A noticeable trend in the above stages is the usage of linear actuators to provide 'Yaw' positioning at a higher resolution as compared to the standard rotary setup. However, this higher resolution brings about the issue of stricter requirement on the precise coordination between the linear actuators that provide both the linear as well as the angular motion. Even though the same actuation system is used for each actuators, we cannot simply assumed that their motion characteristic behaves identically at high precision.

Likewise, as new process methodologies are established, they bring along new challenges as well. A case in point comes from the emergence of flexible electronics, which bring about a new dimension for control, namely roll to roll manufacturing [3]. It is a process technique where the product sheet is continuously being processed, much like the newspaper printing process. Typical applications operate for substrate area of 300x300mm at resolution of 10micron in 30seconds, i.e. throughput of 120panels per

hour or equivalently, web speed of 0.6m/min. Unlike static pick-and-place operations, it can be seen that this next generation of technological methodology requires accurate continuous motion tracking to increase the process speed. For continuous motion at high precision, the dynamic effects of system cannot be ignored unlike static operations.

In addition to these outstanding issues, some of the essential characteristics of relevant applications are illustrated here. Although these would constraints the applicability of the proposed methodologies, it also simplifies the issues at hand so that the focus is clearer. The typical characteristics are:

- Wafer positioning and hence typically 2-D (X, Y and θ_z),
- Workspace corresponds to wafer size in the range of 100 to 450mm; however, sometimes localized process (such as step and repeat sequences) reduced the operational workspace to below 100mm,
- Accuracy of 1micron over 100mm (10ppm),
- Trajectory profile could be point to point, repetitive, or continuous profile tracking, and
- Motion with speed of 0.1m/s to 1m/s, and acceleration of $10m/s^2$ to $100m/s^2$ (1g to 10g).

1.2 Objective and Background

The main objective of this research work is to enhance the accuracy of machine tool. As encapsulated by the title of this thesis, Accuracy Enhancement for High Precision Gantry Stage, there are three parts to the discussion:

- 'Accuracy' must be clearly defined to facilitate the proper target setting.
- 'Enhancement Scope' is established to determine the area of implementing control methodology.
- 'High Precision Gantry Stage' is represented by the test platform used for verification of the proposed methodology

1.2.1 Accuracy

The accuracy performance of any machine tools is defined by how closely the measurement agrees to the international standard of length. It refers to the difference between the results of a measurement and the true value of the measurand, where international standards represent the "truth". Figure 1.1 aptly illustrate the term as well as differentiate it from two commonly mistaken concept: repeatability and resolution.

From the concept of traceability chain [4], the "truth" measurand is determined via justification in stating a measurement system as superior compared to another measurement system. For the purpose of this research, a Heidenhain two-coordinates encoder is chosen to be the reference "truth".

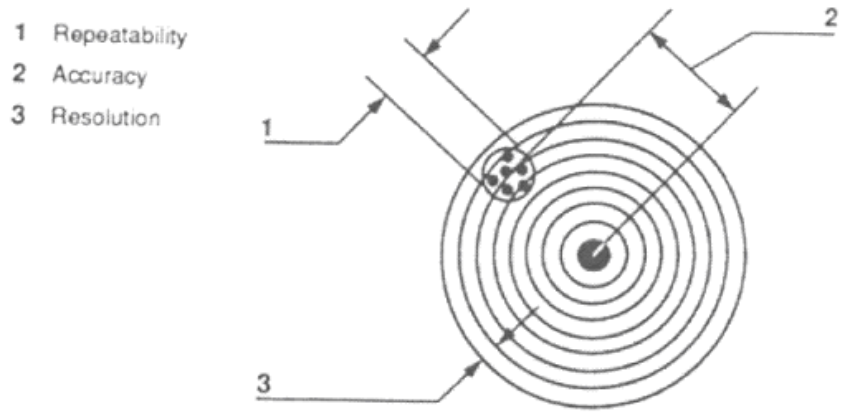

Figure 1.1: Accuracy vs Repeatability and Resolution, Source: [5]

The justification can be explained as follows: The accuracy of the motion achieved by the machine is mainly limited by the characteristics of the encoder used. These include 1) the accuracy of the graduation, 2) the interpolation error during signal processing in the incorporated or external interpolation and digitizing electronics, 3) the error from the scanning unit guideway along the scale, and 4) mechanical deficiency during setup which results in orthogonal error and Abbe error. Comparing the in-house encoder with the Heidenhain encoder, the advantages arise from the fact that the Heidenhain encoder has a higher accuracy grade, and a smaller grating pitch (which resulted in smaller interpolation error, hence a better representation of the actual position). Furthermore, with the scanning head mounted at the tool tip, the resulting Abbe error is minimized. Also, by having a two-axis scale housing, mounting guideway error and the effect of orthogonal error are also reduced significantly.

1.2.2 Enhancement Scope

From the above mentioned trends, we can establish a proper context for our research work. The two outstanding issues are the rising importance of dynamic effects and the emerging popularity of the H-type gantry stage.

Hence these two issues must be addressed within the research to enhance accuracy. Generally speaking, accuracy enhancement may be achieved based on two aspects, i) Improving Machine Accuracy via Compensation Schemes and ii) Improving Accuracy Performance via Advance Control Scheme. Simply put, the first scheme seeks to improve the accuracy grade of a machine tool by ensuring that the readout from the machine is accurate; The second scheme seeks to improve the tracking performance of a machine tool, hence achieving tighter tracking accuracy to enable a better processed end product.

(i) Improving Machine Accuracy via Compensation Schemes

There are bound to be positioning errors in whichever precision motion system used. Mechanically, careful design and precise construction of the motion system will reduce the positioning errors, but every subsequent micrometer/nanometer of error reduction results in exponential cost. Hence, there should be a balance between performance and cost of such motion system. Either should not be pursued at the total expense of the other. An important criterion for determining the trade-off between performance and cost depends upon the application. Thus, rather than relying purely on the precise mechanical design and construction of the hardware (which is costly), it would be highly desirable to adopt a corrective approach to improve the performance of precision motion

system. Error modeling and compensation is one of the viable means to improve system performance at a much-reduced cost compared to pure mechanical construction at high precision.

(ii) Improving Accuracy Performance via Advance Control Scheme

Proportional-Integral-Derivative (PID) controllers are now widely used in various industrial applications. The strong affinity with industrial applications is due largely to their simplicity and the satisfactory level of control robustness which they offer. However, when it comes to high precision application domains, conventional PID controllers usually do not suffice since they cannot compensate for the nonlinear dynamics (such as friction) of the system, which are significant in these domains. Model-based control strategies to deal with these nonlinear effects are considered as these nonlinear effects may be modeled and hence appropriately controlled.

1.2.3 High Precision Gantry Stage

Although the author do not have the luxury of using the start-of-the-art precision stage as a test platform, reasonably well-performed platforms have been setup in the NUS mechatronics and automation lab including a high performance Anorad G5300M1 machine, Figure 1.2, as well as a self-built H-type gantry stage, Figure 1.3. The Anorad machine shall be used for implementation of compensation schemes while the H-type gantry stage is used to verify the performance of the advance control scheme.

The reason for having separate setup lies with the poor repeatability of the self-built

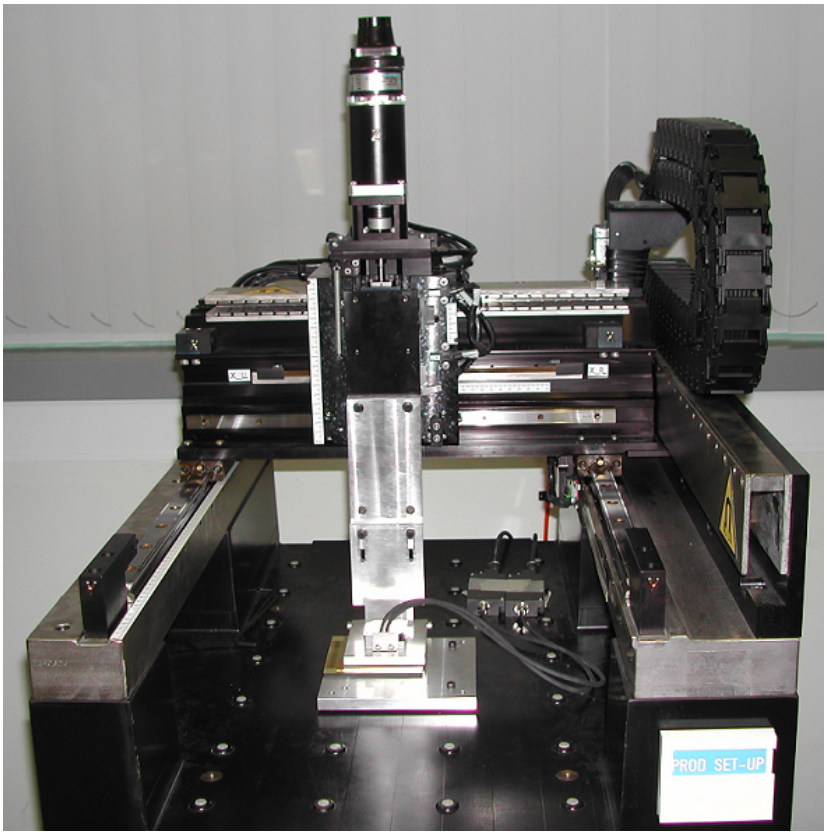

Figure 1.2: Anorad G5300M1 machine

H-type gantry stage. Due to its poor repeatability, the H-type gantry stage cannot be used to effectively demonstrate the feasibility of the compensation schemes. However, as the Anorad machine is not structured in the 'H' configuration, it cannot be used for the implementation of the advanced control scheme, which is modeled specifically for H-type stages.

The proposed methodologies are first simulated using MATLAB/SIMULINK, which offer a rich set of standard and modular design functions for both classical and modern control algorithms, to evaluate the feasibility of the proposed methodologies as well as the parameter performance characteristics. Once the simulations are acceptable, the

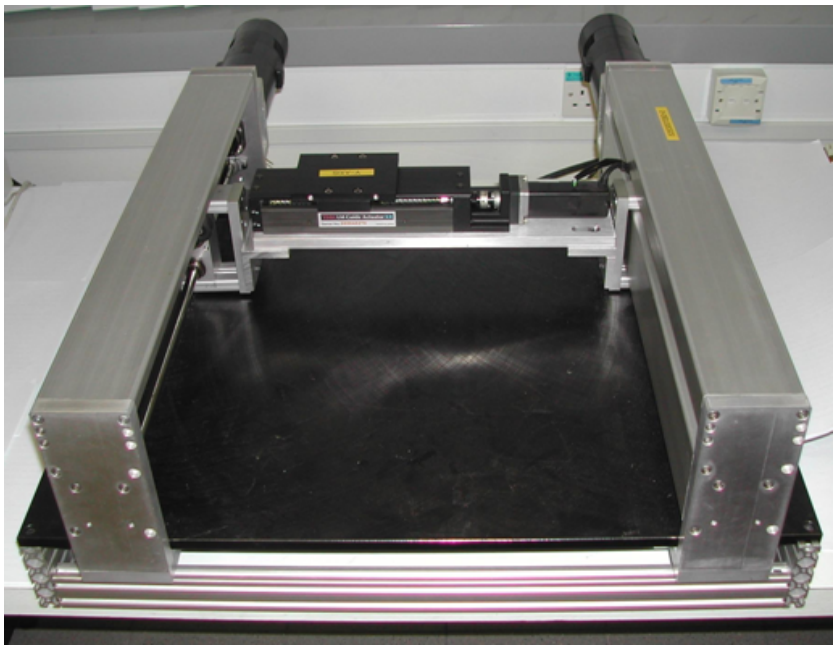

Figure 1.3: Self-built H-type Gantry Stage

program can then be implemented for real-time control of the setup.

The control card used for real-time control is the dSPACE DS1103 board. The DS1103 hardware consist of the following components:

- PowerPC 604e with 400 MHz
- 2 MBytes local SRAM
- 32 MBytes or 128 MBytes global DRAM
- 16 ADC channels, 16 bit
- ADC channels, 12 bit
- DAC channels, 14 bit
- 32 digital I/O channels, programmable in 8-bit groups

- Serial interfaces
- CAN interface

One of the benefit of using dSPACE is that it is well supported by popular software design and simulation tools, including MATLAB/SIMULINK. The Real-Time Interface (RTI) within the SIMULINK control block can be used to automatically generate the dSPACE compatible code to be run on the dSPACE hardware architecture. This reduces the implementation turn-time as the simulation programs can be directly used with some minor adjustment to the I/O setting, i.e. the simulated I/Os generated within SIMULINK are replaced with the actual system I/Os, which are represented in SIMULINK control block diagrams.

For real-time action on the control algorithm and supervision of important data on the PC screen, the ControlDesk software available with the DS1103 board shall be used. ControlDesk from dSPACE offers interactive control of SIMULINK and real-time applications up to the most complex automation tasks. It is seamlessly integrated within the dSPACE development platform. ControlDesk offers interactive control of MATLAB/SIMULINK and real-time applications, and provides a comprehensive design environment for designers to manage, instrument and automate their experiments. User interface is designed as avirtual instrument panel achieved simply via drag and drop operations from the Instrument Selector provided by ControlDesk. It enables the tuning of parameters and monitoring of signals online without regenerating the code. The control parameters can be changed on-line, while the motion along all axes can be

observed simultaneously on the display. Preselected variables of the controller algorithm are stored in memory and can be plotted off-line on the PC. They can also be imported into MATLAB for further analysis.

1.3 Contributions

Based on the identified issues and the test platform setup, three schemes were proposed to achieve the intended objective of enhancing the accuracy of high precision gantry stage. These contributions can be summarized as follows:

1.3.1 Static Geometric Compensation using Support Vector Machine Approach

Geometrical compensation is used to improve the accuracy of the precision motion system. Support Vector Machines (SVM) are used to model the geometrical errors, which are calibrated based on a dual-axis high-grade analog optical encoder. The model is subsequently included in the feedback control loop to compensate for the geometric errors in position readings. This proposed approach of modeling and compensation will reduce significantly the setup time required to model the error map as calibration of the precision motion system can be performed concurrently for both sets of axis. The proposed approach uses the support vector regression method as the basis for modeling the geometric errors; with motivation from the problems (such as computational requirements and optimization of neurons) associated with the look-up table and neural networks. Simulations and experimental results are provided to highlight the principles,

and the practical applicability of the proposed methodology. Finally, diagonal tests are performed to demonstrate that the proposed compensation approach is able to reduce the geometrical errors effectively.

1.3.2 Dynamic Compensation using Iterative Learning Control

Although static geometric compensation has its appeals, it is restricted to point-to-point positioning applications such as the component placement on a Printed Circuit Board (PCB) assembly line. For applications that require continuous trajectory tracking such as e-beam lithography, the static compensation model is inadequate as it fails to account for other factors such as effectors inertia, effectors directional velocities, computational delay, encoder feedback delay etc. Hence, utilizing the repetitive nature in a class of applications (such as 2-dimensional wafer inspection, where each subsequent wafer is inspected in the same repetitive sequence), the Iterative Learning Control (ILC) methodology can be used to provide dynamic geometric compensation.

1.3.3 Innovative Adaptive Control for Dynamic Model-based Gantry

Among the various configurations of ultra-precision motion system, one of the most popular is the H-type gantry stage. In this configuration, two motors are mounted on two parallel slides to move a stage simultaneously in tandem. The stage is modeled as a three-degree-of-freedom (3-DOF) system. Based on this structure, a mathematical model is built using the Lagrangian equation. With the model, an adaptive control method is formulated for improving the tracking error of the stage, with minimal a

priori information assumed of the model. The modeling of the gantry stage is detailed enough to address the main concerns and yet generic enough to cover various aspects of the gantry stage.

1.4 Organization of Thesis

This thesis is organized as follows: Chapter 2 provides a literature review of motion systems. It also provides an overview of the control algorithms that were used in such motion systems. The types of application that such systems may be applicable are also described. In Chapter 3, a geometric compensation scheme is developed and implemented to overcome the mechanical deficiency of motion system. Chapter 4 presents an innovative method to compensate for dynamic errors in applications where the processes are repetitive in nature. Next, in Chapter 5, a model-based adaptive controller is proposed to deal with the nonlinearities in gantry stage. Finally, conclusions and a few suggestions for future work are documented in Chapter 6.

Chapter 2

Review of Motion Systems: Mechanics, Control, and Applications

2.1 Introduction

A host of issues and considerations will considerably affect the accuracy of any motion system. Figure 2.1 appropriately summarizes these considerations from the initial process requirements to the final achieved objectives. The initial development consists of a specific process with a set of objectives. With these in mind, a designer will selects the appropriate equipments and determines the working environment. The environment and equipments used ultimately characterized the entire setup (or as a control engineer defines as the plants transfer function). Mechanical engineers used to achieve the objectives. However, as the requirements become more and more stringent, limitations in mechanical constructions together with the dominance and the increasing computation capability of computer point toward control methodology.

It is hoped that through this chapter, the reader can gain appreciative understanding of

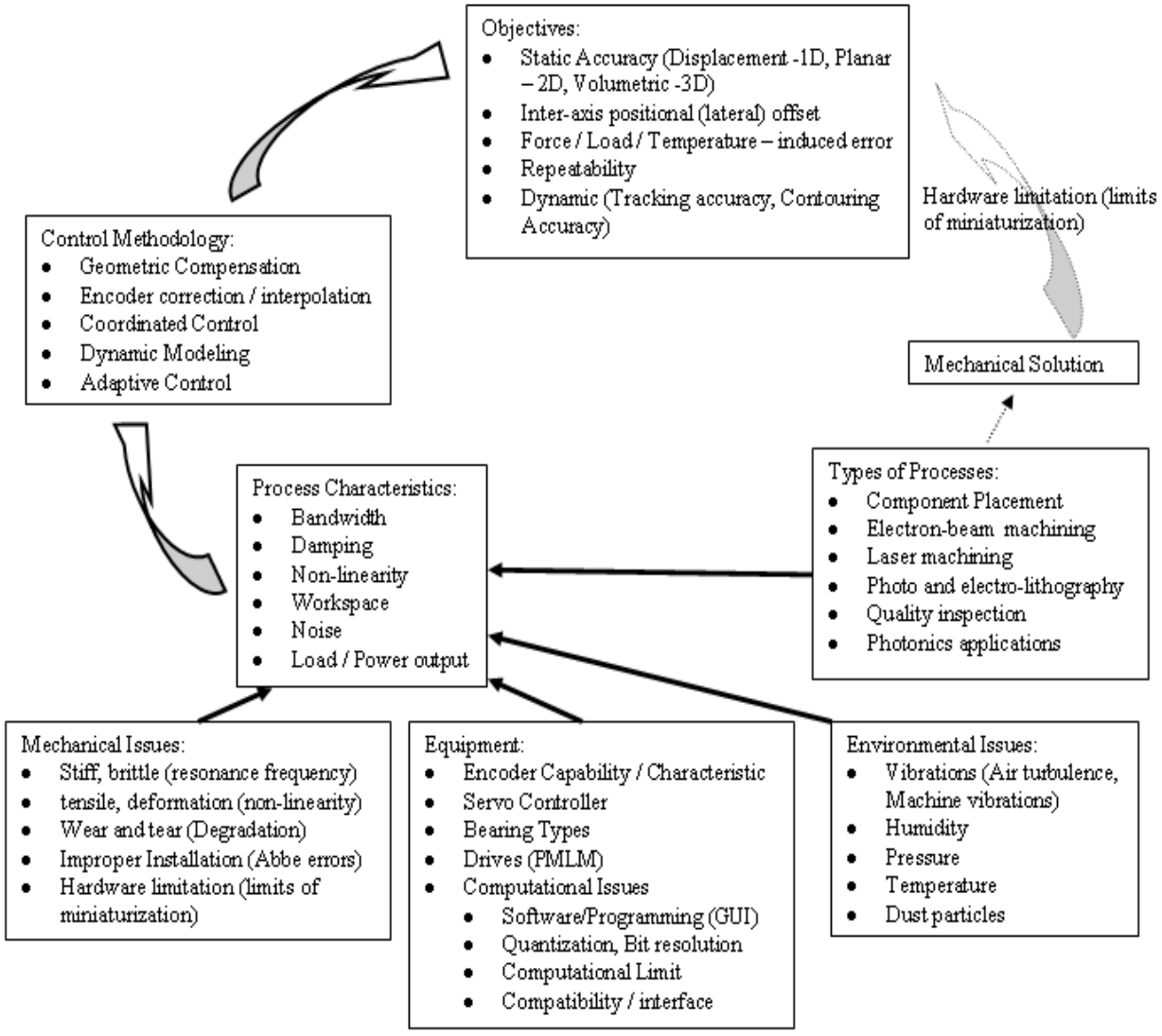

Figure 2.1: Development Workflow

the significance of various aspect of the motion system. This literature review is divided into three main focuses: the anatomy of the motion system, the control schemes, and the typical applications.

2.2 Anatomy of a Motion System

Although the focus of this research wishes to build on the non-mechanical aspect of accuracy enhancement, it is undeniable that mechanical factor forms a vital part in achieving the desired results. Several issues regarding the mechanical aspect need to be acknowledged or adhered. Slocum provides a comprehensive mechanical design perspective in [6]. There are six main considerations in the entire motion system, namely the basic configurations of a motion system, its structural material properties, the bearing systems, the drive systems, the displacement transducers (encoders) and the software and system integration.

2.2.1 Basic Configurations

As depicted in Figure 2.2, there are various configurations for motion system namely: Moving bridge, Fixed bridge, Cantilever, Horizontal arm, and Gantry.

The structural build of the motion system will significantly affect the performance under different applications. For example, when movement of a heavy load is required, the cantilever or horizontal arm configuration cannot be used with high performance as these configurations generally have lower resonance mode. This makes it difficult for the control designer to achieve stringent objectives with these designs.

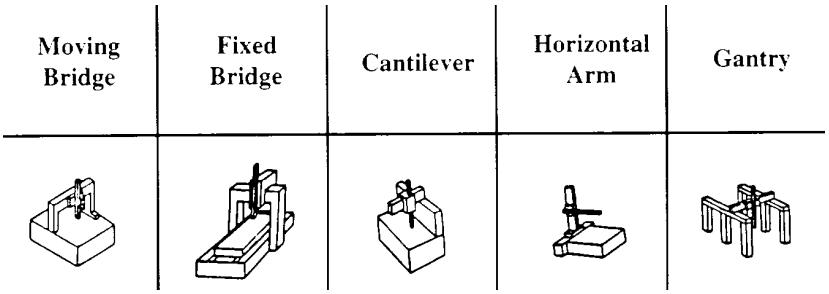

Figure 2.2: Motion System Configurations, Source: [4]

Amongst these configurations of motion systems, one of the most popular is the gantry; it consists of two motors which are mounted on two parallel slides moving another orthogonal member simultaneously in tandem. Fitted with another orthogonal actuator as well as a vertical one, the system is capable of X, Y and Z motion to facilitate automated processes in flat panel display, printed circuit board manufacturing, precision metrology, and circuit assembly where high part placement accuracy for overhead access is necessary. This configuration of gantry is also commonly referred as a H-type gantry, due to the 'H' shape that the three actuators (used for X-Y motion) formed. The gantry is equipped with a high force capability due to the dual drives, and it can yield high speed motion with no significant lateral offset when the two drives are appropriately coordinated and synchronized in motion. In certain applications such as in wafer steppers, the dual drives can also be used to produce a small "theta" rotary motion, without any additional rotary actuators. Park et al. gave a proper overview of such a structure and its dynamics in [7].

2.2.2 Structural Material Properties

With regards to the system build, though it is highly process-dependent, (for example, high speed demands high bandwidth while lithography requires dynamic tracking) the materials used for the plant may alter the plant characteristics. For example, the stiffness of the material used will affect the resonance mode while the usage of an air bearing stage reduces the damping factor. Some ideal properties of the structural material are:

- dimensional stability,
- infinite stiffness,
- weightlessness,
- high damping capacity,
- low coefficient of thermal expansion, and
- high thermal conductivity.

However, no material is capable of satisfying all the above listed properties. Knowing the desirable properties and their influence help in the selection of materials for the structural members. Depending of the structure requirements and applicability, different materials are chosen. For example, in a noise-free environment, high damping capacity reduces in priority whilst an effective temperature-controlled system places less stringent requirements on the thermal capability.

2.2.3 Bearing Systems

There are three categories of existing linear bearings: fluidstatic, sliding contact and rolling element bearings. Fluidstatic bearings, which include hydrostatic and aerostatic bearings, are the only types of bearings for machine tools that are truly frictionless and preloadable. The former use a cushion of high-pressure oil to float one structure above another while aerostatic air bearings utilize a thin film of air under pressure to provide the support of a load. Air bearings may be more durable in the long term because there are no wearing surfaces but precautions must be taken as air pressure variation can cause machine geometric errors to change. Furthermore, a sudden loss of air pressure will cause catastrophic failure and can damage the guide surfaces and bearings. Also, air bearings require filtration systems to prevent water and oil in the air lines from getting into the bearings. Also, the guideway surfaces, on which air bearings operate, need to be cleaned from time to time.

Sliding contact bearings for machine tools utilize a thin layer of low-friction material (such as light oil to grease to a solid lubricant such as graphite) bonded to the surface of the moving axis. They are high-stiffness medium friction bearings with excellent damping characteristics. The large surface contact areas that can be attained with this type of bearings allow machines to resist very high cutting and shock loads. However, their finite friction properties meant that power input to the high-speed axes would be more than double that required for a system with very low friction bearings such as the rolling element type. Also, finite friction sometimes leads to a condition known as

stick-slip, which can limit the accuracy and resolution of the system. Stick-slip is best characterized by trying to push a book to a desired position on a table. The initial force to get the book going impedes the accuracy to which it can be moved to a desired location.

Rolling element linear bearings are bearings which carry a load by placing round elements between the load and the main shaft. The relative motion of the pieces cause the round elements to "roll" with little sliding. There are many types of rolling element linear bearings such as ball, roller, needle, tapered roller, and thrust bearings. Generally they have very low friction characteristics, however, they cannot carry as much load (per area) and have poorer damping characteristics than sliding contact bearings. Furthermore, once worn out they cannot be refinished or adjusted with a gib. Thus they are used only on lower-powered (less than 7kW) machine to reduce the wear and tear. Their modularity, low cost, and low-friction properties are the main advantages. Both the rolling element linear bearings as well as the sliding contact bearings are contact hard bearings; i.e. the bearings are in direct contact with the motion system. Hard bearings can normally take higher loads, as compared with fluidstatic bearings. They have been primarily used for machines designed for rough factory environments such as grinding. For maintenance, the hard bearings need to be lubricated from time to time.

2.2.4 Drive Systems

To achieve precise positioning, direct drive linear motors are usually used. There are three motor options for direct drive linear motion: linear motors, voice-coil motors, and

piezoelectric motors. Which is the most practical depends almost completely on the amount of required motion range. If less than 40 microns of movement is required, piezoelectric motors are often the preferred choice. For distances up to 75mm, typically, voice coils are used. And for movements in the 75mm range or greater, linear motors are generally the way to go [6]. As this research focuses on long travel range, linear motors will be elaborated upon.

Linear motors are very popular for applications requiring linear motion at high speed and accuracy due to their mechanical simplicity. The increasingly widespread industrial applications of PMLMs in miniature system assembly and various key stages of semiconductor fabrication and inspection processes are self-evident testimonies of the effectiveness of PMLMs in addressing the high requirements associated with these application areas.

The most attractive features of linear motors for precision control include low thermal loss, simple mechanical structure, high achievable force density and high dynamic performance. Linear motors require no indirect coupling mechanisms such as gear boxes, chains and screws coupling. This greatly reduces the effects of external, contact-type nonlinearities such as backlash and frictional forces, especially when they are used with aerostatic or magnetic bearings. However, the advantages of using mechanical transmission, such as its inherent ability to reduce the effects of model uncertainties are consequently lost. This type of motor is also impractical for accurate motion control of high-speed, high-mass systems subjected to large cutting force.

Due to its working principle, the presence of uncertainties are prominent factors limiting the performance of a linear motor. These may arise due to external factors such as load changes or internal factors such as system parameters perturbation owing to prolonged use, and the various friction components and force ripples arising from imperfections in the underlying components. A reduction of these effects, either through proper physical design or via the control system, is of paramount importance if high-speed and high-accuracy motion control is to be achieved. Compensation via proper physical design usually introduces mechanical complexity and extra manufacturing costs. On the other hand, control algorithms have the advantage of preserving the maximum force achievable even in high-speed and high-accuracy motion. Thus control algorithm is preferred to compensate for these nonlinearities.

To complete the picture, the rest of the possible direct drive linear systems are briefly touched upon.

Voice-coil actuators are limited-motion devices that use a permanent-magnetic field and coil to produce a force proportional to the current applied to the coil. In its simplest form, a linear voice coil consists of a tubular coil of wire within a radially oriented magnetic field. Permanent magnets lining the inside diameter of a ferromagnetic cylinder produce the field. The magnets are arranged so the sides "facing" the coil are the same polarity. The core of ferromagnetic material completes the magnetic circuit. It sits on the coil's axial centerline and is connected on one end to the permanent magnet. When current flows through the coil, it generates an axial force on the coil and produces relative

motion between the field assembly and coil, providing the force is enough to overcome friction, inertia, and other forces from loads attached to the coil.

Piezo-electric materials change shapes when a voltage is applied, this unique property is used to control and drive the motion of piezo actuators. A case in point is the patented Nanomotion drive (http://www.nanomotion.com/). Under special electrical excitation drive and ceramic geometry of Nanomotion motors, longitudinal extension and transverse bending oscillation modes are excited at close frequency proximity. The simultaneous excitation of the longitudinal extension mode and the transverse bending mode creates a small elliptical trajectory of the ceramic edge, thus achieving the dual mode standing wave motor patented by Nanomotion. By coupling the ceramic edge to a precision stage, a resultant driving force is exerted on the stage, causing stage movement. The periodic nature of the driving force at frequencies much higher than the mechanical resonance of the stage allows continuous smooth motion for unlimited travel.

2.2.5 Displacement Transducers (Encoders)

An encoder is a device (transducer) that is used to convert rotary or linear motion into useful information. The primary parameters determined are speed, rate, velocity, distance, position, or direction. A typical application will use one or more of these parameters as feedback to the controller in a motion control system. Although there are various configurations of transducer, [9]-[11], the most popular choice is the incremental linear encoder as shown in Figure 2.3.

The incremental encoder is sometimes called a relative encoder, as nature of the phase-

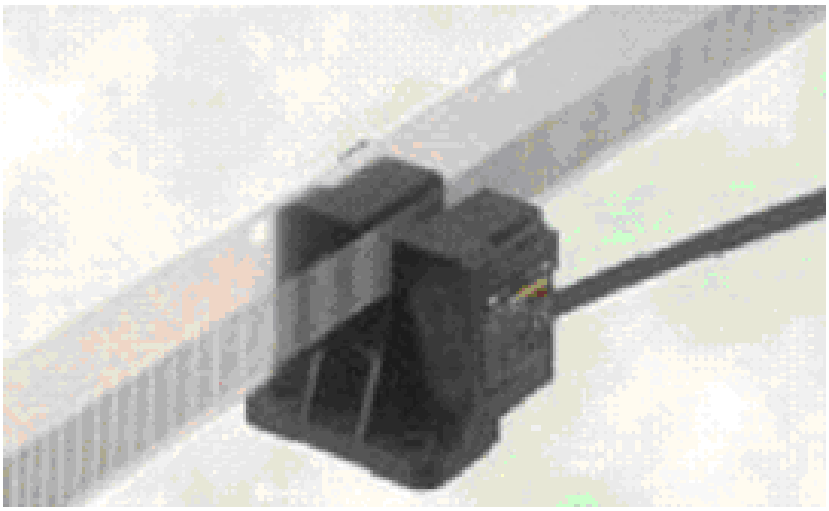

Figure 2.3: Incremental Linear Encoder, Source: [8]

quadrature output signals dictates that any resolution of angular position can only be relative to some specific reference. It consists of two tracks and two sensors whose outputs are called channels A and B. As the motor moves, pulse trains occur on these channels at a frequency proportional to the speed, and the phase relationship between the signals yields the direction of motion, the pulse trains are 90 degrees out of phase. This technique allows the decoding electronics to determine which channel is leading the other and hence ascertain the direction of rotation. The code disk pattern and output signals A and B are illustrated in Figure 2.4. By counting the number of pulses and knowing the resolution of the disk, the motion can be measured. Often a third output channel, called INDEX, yields one pulse per revolution, which is useful in counting full revolutions. It is also useful as a reference to define a home base or zero position.

As the signals from the two channels are a 1/4 cycle out of phase with each other, they are known as quadrature signals. This also has the added benefit of increased resolution;

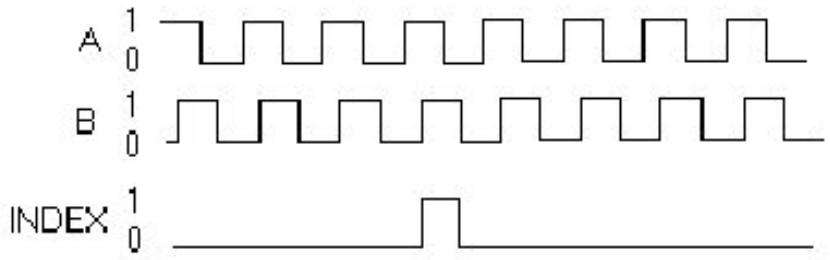

Figure 2.4: Incremental Encoder Signal Patterns

where unique output states allow for up to a four-fold increase in resolution. In addition to this, it is possible to provide further interpolation to obtain higher resolutions (limited by the wordlength of the servo system A/D converter and the bandwidth of the encoder) as described in [12].

2.2.6 Software and System Integration

One of the main reason precision has reach the level achieved now, begins with the advent of computers. However, it also brings along other issues such as quantization error, processing limit, open-architecture programming capability, software programming, and hardware interfacing compatibility. Faster DSP (Digital Signal Processing) processor and industry standards resolved most of these issues.

Over the course of the research, different types of software are used. They include Delta Tau's PMAC (Programmable Multi Axis Controller), Precision MicroDynamics's Motiontools, National Instruments's LabVIEW and dSPACE. Generally speaking, the faster (more bandwidth) the control card, the less versatile it's software is capable of controller manipulation. This is expected as any DSP processor requires a trade-off between the complexity of its software capability and its processing speed; with complexity,

redundant circuitry within the processor is required to deal with myriad potential configurations.

All the software comes with its own set of motion control, data acquisition (DAQ) libraries, and signal analysis tools. It will have some DAQ card for communication with the actuators and transducers. The actuators are normally integrated with the DAQ via servo amplifier systems while the transducers can be directly connected to any DAQ with an encoder card.

2.3 Control Schemes

Great advances have been made in each control area, for example, in pattern recognition, learning, adaptive control, robust control, knowledge-based systems, such that various opponents have advocated that the field of control engineering have realized its potential. However, newer technology and requirements challenge the control engineer to greater heights; precision motion control is one such challenge. The controller must plan and execute tasks for various system processes which may possess system characteristics such as those listed in Table 2.1. The control engineer needs to design a suitable controller which will effectively achieves the system characteristics that are desired. For example, in high speed applications, large bandwidth is required which brings along high frequency noise issues. In another case, limited DSP processing capability may require simpler control algorithm to reduce processing time in lieu of higher sampling time.

Figure 2.5 gives a broad overview of the locations where control schemes may be imple-

Table 2.1: List of System Characteristics

Multivariable	High impact	Time-varying
High speed	High bandwidth	Maintenance
Vibration	Nonminimum phase	Nonlinear
Repetitive	Noise	High acceleration
Range of motion	Applied loads	Preload
Size and configuration	Damping	Friction
Environmental sensitivity	Delay	Weight
Stiffness	Setpoint Trajectories	Cost
Uncertainties	Multi- I/Os	Discretized

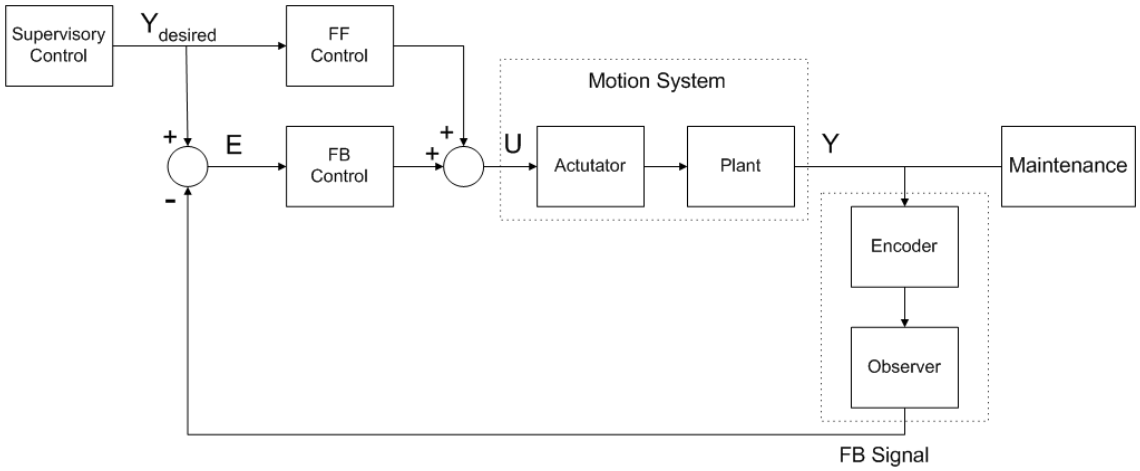

Figure 2.5: Control Structure

mented in one way or another to improve the system characteristics and performances. The locations are categorized under: Supervisory Control, Feed-Forward (FF) Control, Feed-Back (FB) Control, FB Signal, and Maintenance ("Motion System" has been discussed earlier on in this chapter). Each category is discussed and the latest development made by various researchers in each area expounded. A comprehensive list of the researches that are directly applicable for motion systems, in particular gantry stages, are examined.

2.3.1 Supervisory Control

Supervisory control develops an overview control outlook of the entire system such as the development of a multi-functional tele-operative system in [13] for automating bio-production processes; or operational decisions such as component allocation and process arrangement etc. [14].

Supervisory control seeks to optimize automated process by having an overview picture and providing the necessary support and control such as a "knowledge assistant" to guide the robot operator during the planning, execution, and post analysis stages of the characterization process [15]. Or it could simply be a scheduling problem issue such as a tightly coupled automated serial production line with deterministic processing time [16].

Above are four examples of research applications where supervisory control are employed. Although the tasks in each example are different, they have the same fundamental objective, i.e. to generate a desired trajectory. This objective is the primary function of any supervisory control scheme.

2.3.2 Feedforward Control

Feedforward controller attempts to correct errors in motion systems without any updated information on the status of the motion system, i.e. without feedback inputs. It is a term describing a kind of system which reacts to changes in its environment; a system which responds to a measured disturbance in a pre-defined way. Feed-forward control can

respond more quickly to known and measurable kinds of disturbances such as in [17], but cannot do much with indeterministic disturbances such as environmental noises, and unmodeled or unidentified system parameters (e.g.narrow-band disturbances with unknown frequencies as described in [18]).

The technique of using feedforward control always involve finding an appropriate model of the system and enhancing system performance by reacting to the predicted model error ([19], [20]). Variants of the feedforward control methodology include:

- Command Shaping - Altering the command input signal characteristics to optimize process speed and efficiency [21], [22].
- Control signal cleaning - Based on modeling properties of the system, the controller's signal is modified/filtered to provide a smoother control signal into the system [23], reducing effects such as chattering.

2.3.3 Feedback Control

Feedback control deals with any deviation from desired system behavior by measuring the system's variable (output) and react accordingly. There are simply too many control schemes which have been proposed by researchers; the following, however, are methods that had been applied to motion systems:

- PID - a linear model is developed/identified and traditional quantitative analyses are used to tune the PID parameters [24].
- Various model-based schemes:

  - Lagrange-based is the most common as describe in [25], [26].
  - Euler-Bernoulli beam method [27].
  - Mechanical spring-mass system [28].
  - Rigid bodies with joints constraints parameterized by manifold [29].

- H_∞ - It seeks to minimize certain weighting function (based on infinite norm) to optimize system performance [30]. Variants of the H_∞ include gain scheduling [31] and Fuzzy mixed H_2/H_∞ [32].

- Adaptive - Varying parameterized controller that is self-tuned according to certain Lyapunov function [33].

- Backstepping - It is based on identified models and mathematically working backwards (backstepping) to obtain a desired controller [34]. Variants include: Adaptive backstepping [35], and Discretized backstepping [36].

- Micro-synthesis - It manipulates the complementary sensitivity function for performance [37].

- Gain scheduling - Scheduling is incorporated by a user-defined continuous function, which alters the feedback error to the controller by scaling the input error accordingly [38], [39].

- Sliding mode control - Choosing a desired function response and forcing the system motion to "slide" in its vicinity [40].

- Neural network - A form of learning control; where the controller "learns" from previous outcome to improve subsequent control [41].

- Iterative Learning Control - Another form of learning control, specifically for periodic applications [42]-[44].

- Fuzzy logic - Ramy and Saman implemented a form of fuzzy-based control for a modeled XY-table in [28]. Fuzzy logic is a concept originally proposed by Lotfi Zadeh, [45] in 1965.

- Parametric-Tuning - Identify parameterized controller and tuned its parameter accordingly such as using genetic algorithm to tune a fuzzy sliding-mode controller [46], or using adaptive neuro-fuzzy inference system to tune a PID controller [47].

In addition to the above stated control schemes, novel control techniques have been developed for unique circumstances such as:

- Coordinated control - Single axis, dual drive system requires synchronization of both drives to prevent an inter-axis yaw error [48], [49].

- Oscillatory input - Faster production requires faster speed which results in oscillatory input with large amplitude. Averaging analysis is used in [50] to resolve this issue.

- Low damping - Contactless bearing system (magnetic and air-bearing) tends to have better performance as they have less friction, backlash, and hysteresis issues.

However, such low damped systems tend to be oscillatory. Resonant modes suppression is used in [51] to reduce the effects in magnetic bearing system. Space control is an example of low damped control and H_∞ control was used in [52] for space control.

Each control scheme has a main focus or issue to deal with, but in practical applications, various problems must be simultaneously dealt with. Sometimes, simply combining various control schemes for their individual benefits such as in [53]-[56] would work. However, priorities for different control schemes may clash with one another. Various techniques have been developed to deal with different integration issues:

- Different control schemes may be required for different stage of operation. In general, a smooth transition from one to the other control scheme is required to prevent discontinuity. Yokote et al. utilized the benefit of digital control for initial fast positioning and transiting to analog control for the final precise positioning in [57].

- Combining two different control scheme using mathematical analysis such as [58] which uses zero phase error tracking controllers and cross-coupled controllers to reduce tracking and contouring accuracy respectively.

- Integrating different control law scheme using nonlinear terminal laws to provide an interpolation between each control laws, each with its own precomputed terminal set [59].

- Using a supervisor to determine the switching instants among the elements of a family of compensator based on offline system evaluation [60].

2.3.4 Feedback Signal

The feedback signal may be used to refine certain system characteristics to improve system performance, the schemes developed before include: (the terms are straightforward and need no further elaboration)

- disturbance rejection [61]-[63],
- encoder interpolation [12], [64]-[66],
- friction compensation [67]-[71],
- geometric compensation [72]-[75],
- dynamic error compensation [76],
- force compensation [77],
- thermal compensation [78], and
- measurement noise compensation [79], [80].

2.3.5 Maintenance

As described earlier, traceability requires a laser interferometer to calibrate the motion system in general [81]-[83]. Such calibration should be conducted at least once per year

to ensure that the system is accurate. For system with higher wear and tear (such as grinding, diamond turning), more frequent calibration is required.

System diagnostics seek to maintain the integrity of the system performance by analyzing the output response characteristics. Examples include:

- assessing the durability of the software error compensation [84],
- detecting and isolating sensor faults [85], and
- determining the reliability of motion system in harsh environment [86].

Reliability of motion system meant that downtime must be minimize; the concept of Safety Integrity Level (SIL) [87] as described in ANSI/ISA 84.00.01-2004 (IEC 61511-1), is a measure of system integrity; the higher the SIL number, the better the safety integrity performance. The level of redundancy in both software and hardware determines the SIL number.

2.4 Typical Applications

Each control scheme conceptualized and developed should have an accompanying application. The main user of precision positioning systems can be classified under three categories, namely: product shaping, metrology and placement. Under product shaping, there are two further sub-categories: energy beam processes and molding processes.

Energy beam processes which deal with removal, accretion and surface shaping of product and include:

- Scanning tunneling microscope molecular manipulation,
- Ion beam figuring and reactive atomic plasma technology,
- Photon beam cutting, drilling, transformation, hardening and coating,
- Inert ion beam machining,
- Reactive ion beam etching, and
- Electron beam lithography.

Molding processes deals with the hard grinding / molding of product into shape such as:

- high pressure grinding (optical lens grinding),
- diamond turning, and
- lapping, polishing and elastic emission machining.

Product metrology deal with dimension measurement of the product. Some termed it: reverse engineering, which is the development of technical data for an existing part for which no technical data is available [88]. Metrology processes include:

- Coordinate measuring machine (CMM),
- Scanning probe CMM,
- Microtome,

- Digital volumetric imaging,
- Atomic force microscope,
- Scanning white light interferometry,
- Micro x-ray 2D inspection, and
- CT inspection.

Lastly, product placement, as the name suggest, deals with positioning of objects at specific location (pick and place system), includes:

- electronics components manufacturing and assembly,
- photonics / fibre optic alignment, and
- wafer mask alignment.

The various applications can be categorize by the following characteristics, which greatly assist the control designer in determining the control schemes to use:

- Trajectory type: wafer alignment (step motion) vs scanning probe CMM (continuous motion)
- Accuracy required: ion beam machining (0.1-0.3nm) vs turning and milling machines (0.1mm)
- Range of motion: atomic force microscope (100nm) vs flat panel display inspection (2m)

- Contact with component: CMM (contact) vs scanning white light interferometry (non-contact)
- Destruction of component: x-ray CT (non-destructive) vs slicing-scanning process (destructive)
- Force impact: CMM (minimal force) vs grinding (large force)

2.5 Conclusions

Although industrial standardization leads to most companies providing similar products, there are certain intrinsic values that a few products may have over their competitors. To achieve equivalent performance, careful consideration of the hardware details reduces the requirements on the control.

Different control schemes have been proposed to resolve specific issues. The control scheme that is chosen / designed depends on the characteristics of the motion system used, the objectives targeted and the application features.

Chapter 3

Static Geometric Compensation using Support Vector Machine Approach

3.1 Error sources

There are bound to be positioning errors in whichever precision motion system used. The major sources of errors are well documented in [89], and [90]; these include geometric, kinematics, thermal, and force-induced errors.

Geometric errors are concerned with the point to point accuracy within the motion system. Even with feedback from the encoder, the motion system may not position accurately due to the following: errors that arise in a machine on account of its poor basic design (such as Abbe error [6]), the poor workmanship during assembly resulting in errors such as straightness error, and also as a result of the components used on the machine (such as using a lower accuracy-grade encoder).

Kinematics errors arise due to factors such as effectors inertia, effectors directional velocities, directional stiffness, computational delay, and encoder feedback delay. In

effect, any errors arising from the motion of moving machine components are categorized as kinematics errors. Kinematics errors results in both poor tracking error and poor tracking accuracy. (N.B. tracking error depends on the trajectory and encoder reading while tracking accuracy reflects on the 'true' motion achieved by the end effector.) The tracking errors are particularly significant during the combined motion of different axes which result in contouring errors [53].

Continuous usage of a machine tool causes heat generation at the moving elements and this heat causes expansion of the various structural elements of the machine tool. It is this expansion of the structural linkages of the machine that leads to inaccuracy in the positioning of the tool. Such errors are called thermal errors.

The dynamic stiffness of all the components of the machine tool that are within the force-flux flow of the machine are responsible for errors caused as a result of the cutting action. As a result of the forces, the position of the tool tip with respect to the workpiece varies on account of the distortion of the various elements of the machine. Depending on the stiffness of the structure under the particular cutting conditions, the accuracy of the machine tool will vary.

3.1.1 Choice of Error Source for Compensation

There are various categories of error sources as mentioned earlier. It is noted in [89] that geometric errors formed one of the biggest sources of inaccuracy and hence they require priority for compensation first. To ensure the decoupling of geometric errors from the other error sources, a few considerations are required. Firstly, the focus should

be on positioning accuracy (setpoint tracking) so that kinematics errors are not in effect. Secondly, thermal effects can be minimized by having non productive warm up cycle, and operating in a temperature controlled environment. Lastly, the end effector is not forcibly restricted in its motion in order to eliminate force effects. These considerations would result in errors collation that mainly arise from geometric error sources.

3.2 Geometric Compensation for Geometric Errors

3.2.1 Reasons for Software Compensation

There are bound to be geometric error sources in any motion system. Mechanically, careful design and precise construction can reduce the error but every subsequent micrometer/nanometer of error reduction results in exponentially increasing cost. Hence, there should be a balance between manufacturing machine performance and cost. Either should not be pursued at the total expense of the other. An important criterion for determining the trade-off between performance and cost lies in the area of application. Thus, rather than relying purely on the precise design and construction of the hardware which is costly, it would be highly desirable to adopt a corrective approach to improve the performance of precision motion system. Error modeling and compensation is a viable candidate to improve system performance at a much-reduced cost as compared to purely constructing the machine at high precision.

3.2.2 Traditional Compensation Schemes

The early developments in error compensation are well documented in Evans [91]. Different methods were reported in the literature to model and compensate the errors. These methods include neural-based approaches ([92]-[95]), use of genetic algorithms [96], finite element analysis [97] and other analytical tools ([98]-[100]). In the industry, many of the manufacturers (e.g. Mitutoyo, Japan) have incorporated geometrical compensation within their systems [101]. Common to all these works and more is a model of the machine errors, which is either implicitly or explicitly used in the compensator. The error model is normally used off-line to analyze and correct the measurement data in the final displayed Look Up Table (LUT) form. The LUT is built based on points collected and calibrated in the operational working space of the machine to improve its precision and accuracy. It has several associated disadvantages; such as computational requirements and memory storage, which become clearly significant with increasingly stringent requirements.

3.2.3 Propose Methodology

Here, geometrical compensation using SVM is proposed to improve the accuracy of the precision motion system. A dual-axis high-grade analog optical encoder and SVM are used to calibrate and model the geometrical errors respectively. This proposed approach will reduce significantly the setup time required to model the error map as calibration of the precision motion system can be performed concurrently for both set of

axis. The proposed approach uses the support vector regression method as the basis for modeling. Simulations and experimental results are provided to highlight the principles and practical applicability of the proposed method resulting from such an approach. Finally, diagonal tests are performed to demonstrate that the proposed compensation approach is able to reduce the geometrical errors effectively.

Neural networks, being universal approximators, are good candidates for geometric compensation purposes [102]. But neural networks posed some shortcomings that can be effectively overcome using SVM. These shortcomings include the constraints associated with dimensionality and difficulty in determining the optimum number of neurons. Given the natural sparseness property of SVM, the decision boundary can be expressed in terms of a limited number of support vectors. Furthermore, the optimum number of support vectors automatically follows a convex solution. SVM are thus strong candidates for learning and generalization in huge dimensional input spaces, avoiding the dimensionality and optimization constraints.

The SVM, originated from the statistic learning theory [103], [104], is mostly used in regression and classification applications. SVM can be said to be closely related to:

- learning in reproducing kernel hilbert spaces,
- nonlinear classification, and
- regression by convex optimization with a unique solution and primal-dual interpretations.

The SVM is able to select the number of the basis functions systematically without the dimensionality constraint and the number of data points available. The common optimization problem of being trapped in local minima is also avoided in SVM applications due to its fundamental structural risk minimization principle [104]. SVM are believed to be able to generalize well on unseen data and overcome the problem of over-fitting, considering the many outstanding results reported in the literature [105]-[107]. All these attractive features suggest that SVM are strong candidates for regression purposes.

The SVM is derived from the statistical learning theory to approximate the non-linear function $f(.)$ for a given precision [104]. The current output y_k may be approximated by

$$y_k = w\varphi(x_k) + b, \tag{3.1}$$

where x_k represents the current input, $\varphi(x)$ is a nonlinear basis function, b is the bias, and w is the weighting. Posing as a constrained optimization problem, the formulation in primal space is

$$min\ P(w, \xi_i, b) = \frac{1}{2}w^T w + C\sum_{i=1}^{N}\xi_i, \tag{3.2}$$

where ξ_i, equated to $y_i - (w\varphi(x_i) + b)$, are the slack variables, and C is the regularization parameter. Subjecting it to the constraint $0 \leq \alpha_i \leq C$, for $i = 1, ..., N$, where α_i are the Langrangian multipliers, the problem can be expressed (in the dual space) using the Langrangian function

$$J(w, \alpha_i, b) = \frac{1}{2}w^T w + \sum_{i=1}^{N}\alpha_i(y_i - (w\varphi(x_i) + b)), \tag{3.3}$$

with a set of N training data pairs $\{x_i, y_i\}$, for $i = 1, ..., N$. By performing the optimization and satisfying the Karush-Kuhn-Tucker conditions [108],

$$\frac{\partial J}{\partial w} = 0 \Rightarrow w = \sum_{i=1}^{N} \alpha_i \varphi(x_i), \tag{3.4}$$

$$\frac{\partial J}{\partial b} = 0 \Rightarrow \sum_{i=1}^{N} \alpha_i = 0, \tag{3.5}$$

the parameters α_i and b are obtained. For this optimization process, the function call 'trainlssvm.m', which is part of a MATLAB toolbox developed by Suykens et al.[109] is used. The following transformation pair is specified:

$$K(x_k, x_i) = \varphi(x_k).\varphi(x_i), \tag{3.6}$$

where $K(x_k, x_i)$ is a symmetrical kernel satisfying Mercers condition [104], [110]. The Radial Basis Function (RBF) is selected for the kernel, i.e.,

$$K(x_k, x_i) = exp(-(x_k - x_i).(x_k - x_i)^T/\sigma), \tag{3.7}$$

where σ is a user-specified constant. Thus, noting (3.4) and (3.6), the output may finally be expressed as

$$y_k = f(x_k) = \sum_{i=1}^{N} \alpha_i K(x_k, x_i) + b. \tag{3.8}$$

3.3 Calibration of the Testbed - Two-axial Precision Motion System

In certain cases, for specific precision-dependent operations, the inherent accuracy of a commercial machine may be insufficient. This has resulted in the usage of a higher

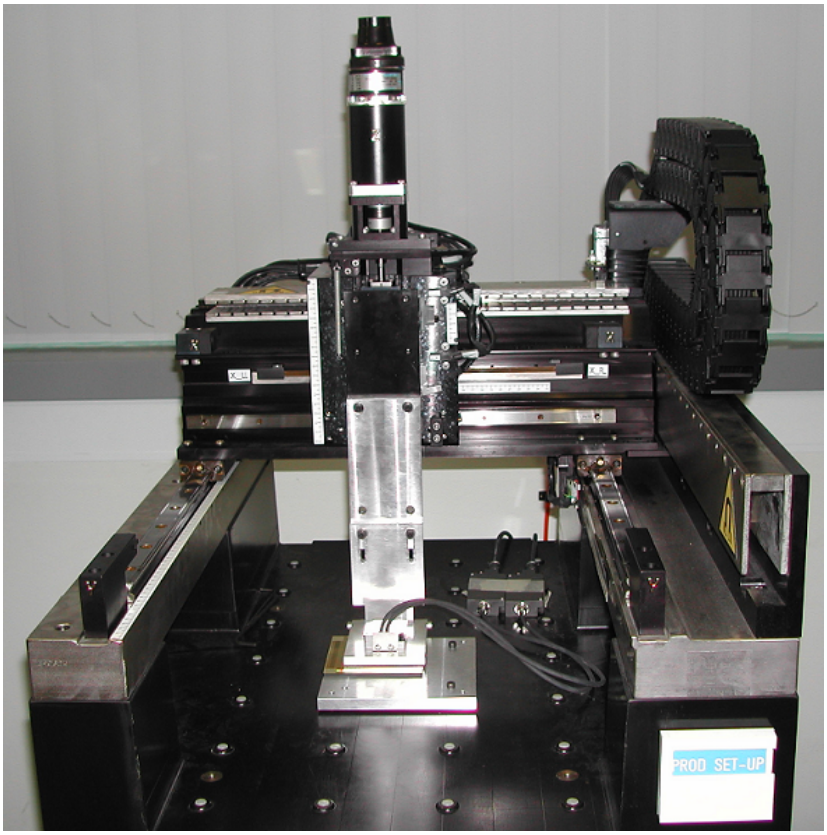

Figure 3.1: Two-axial Precision Motion Testbed

precision measurement system to assess the deviation of the tool-tip position from its true value and provide the necessary compensation. For an efficient and cost-effective solution, a Heidenhain two-coordinates encoder is used as the reference to calibrate a two-axial precision motion stage. The, linear motor driven, G5300M1 Anorad stage is manufactured by Anorad Corporation. Figure 3.1 shows a picture of the precision motion system used, while Table 3.1 details its specifications.

3.3.1 Reference Encoder

Normally, a laser interferometer is used to calibrate the machine. Today, laser interferometers can readily yield a measurement resolution of sub-nanometer. Although highly

Table 3.1: Specifications of G5300M1 Anorad Platform

Axis	X	Y
Travel	250mm	400mm
Drive Interface	LEA-S-2-S-NC	LEB-S-4-S-NC
Velocity	1.0m/s	
Acceleration	>1.0g's	>0.7g's
Resolution	$1\mu m$	
Straightness of Travel	$\pm 5\mu m$	
Flatness of Travel	$\pm 5\mu m$	
Repeatability (bi-directional)	$\pm 2.5\mu m$	
Repeatability (X to Y)	$\pm$ 10 arc seconds	

accurate, the laser interferometer requires stringent conditions to operate under; it is highly susceptible to pressure, temperature and humidity. Furthermore the calibration process is rather tedious and a high level of expertise is required to operate the laser interferometer. In addition, the high cost of a laser interferometer implies that probably only large companies can afford one. Hence, the usage of a 'low-cost' dual-axis encoder is proposed to simultaneously calibrate both axes.

A picture of the encoder used is shown in Figure 3.2. Its specifications are given in Table 3.2. As measuring standard, the encoder featured a planar phase-grating structure on a glass substrate. This makes it possible to ensure positions in a plane. The precision graduations are manufactured in a process (DIADUR) invented by Heidenhain, which involved graduations that are composed of an extremely thin layer of chromium on a substrate of glass. This allows the accuracy of the graduation structure to lie within the

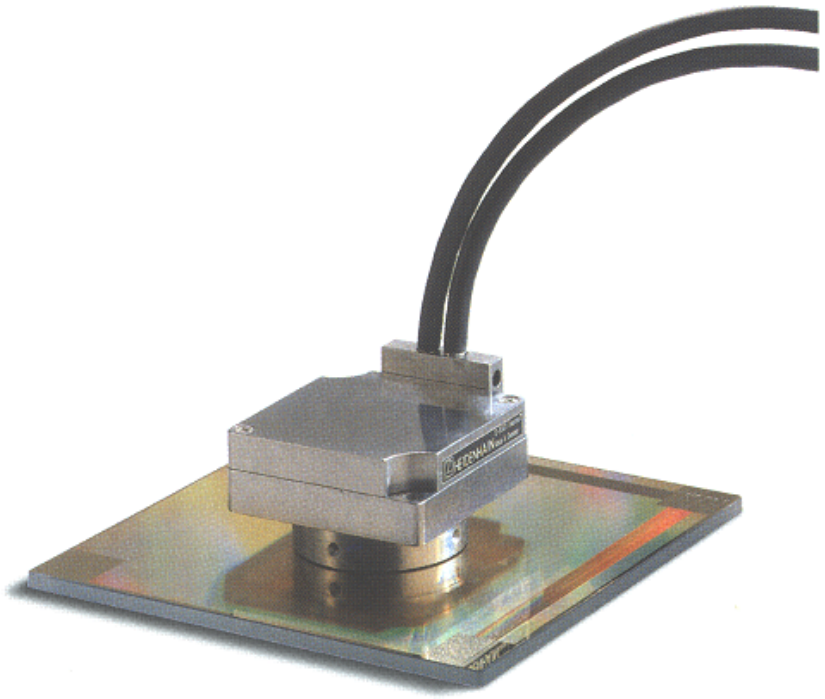

Figure 3.2: Heidenhain Dual-axial Encoder

micron and submicron range.

The accuracy of the motion achieved by the machine is mainly limited by the characteristics of the encoder used. These include 1) the accuracy of the graduation, 2) the interpolation error during signal processing in the incorporated or external interpolation and digitizing electronics, 3) the error from the scanning unit guideway along the scale, and 4) mechanical deficiency during setup which results in orthogonal error and Abbe error.

Hence, the usage of the Heidenhain encoder as a superior measurement system is justified by comparison of the encoder specifications on the Anorad with the Heidenhain encoder. The advantages arise from the fact that the Heidenhain encoder has a higher accuracy grade, and a smaller grating pitch (which resulted in smaller interpolation error,

Table 3.2: Heidenhain Dual-axial Encoder Specifications

Specifications	
Measuring standard	Two-coordinate DIADUR phase grating on glass
Grating period	$8\mu m$
Signal period	$4\mu m$
Thermal expansion Coefficient	$\alpha_{therm} \approx 8ppm/k$
Accuracy grade	$\pm 2\mu m$
Recommended measuring step	$1\mu m; 0.5\mu m; 0.1\mu m; 0.05\mu m; 0.011\mu m$
Measuring range	$68mm \times 68mm$ ($3.85in. \times 3.85in.$)
Reference mark	3mm after beginning of measuring range
Max. traversing speed	30m/min (depend on subsequent electronics)
Vibration (50 to 2000Hz)	$\leq 80m/s^2$
Shock (11ms)	$\leq 100m/s^2$

hence a better representation of the actual position). Furthermore, with the scanning head mounted at the tool tip, the resulting Abbe error is minimized. Also, by having a two-axis scale housing, mounting guideway error and the effect of orthogonal error are also reduced significantly.

3.3.2 Calibration Methodology

Error modeling typically begins with a calibration of the errors at selected points within the operational space of the machine. These errors are subsequently cumulated using the overall error model to yield the overall positional error and create the error map.

For the Anorad Machine, the tool attached to the table may move in either X or Y direction. The X and Y travel is capable of spanning a $250mm$ x $400mm$ 2D space. The present set of Heidenhain measuring range is $68mm$ x $68mm$. Accordingly, the calibration area is set to a $50mm$ x $50mm$ 2D space. Calibration is done at $1mm$ intervals

along the $50mm$ travel for the Y-axis and $10mm$ intervals along the $50mm$ travel for the X-axis. The start position for X-axis and Y-axis is defined as the origin (0,0) while the end position was (0,50), (10,50), (20,50), (30,50), (40,50) and (50,50) respectively for each of the six calibration line. A schematic diagram showing the calibration profiles of the table is shown in Figure 3.3.

A clear representation of the data collation control is illustrated by the schematic shown in Figure 3.4. The experimental sequences to obtain the error map are as follows:

1. Manually tune the PID controller to obtain stable output (N.B.: As performance specification is not crucial, tuning of the PID is not important.)

2. Home and zero the Anorad Machine at the origin (0, 0)

3. Perform stepped motion along the various calibration line, allowing sufficient settling time at each point.

4. Record the uncompensated error at each point and perform the next stepped motion along the calibration path.

5. Repeat the calibration steps (2, 3 and 4) at least thrice to obtain an average uncompensated error for each point.

6. With the uncompensated errors, perform the optimization process with the function call 'trainlssvm.m' in MATLAB to obtain the parameters α_i and b.

7. Generate the error map with Equation (3.1).

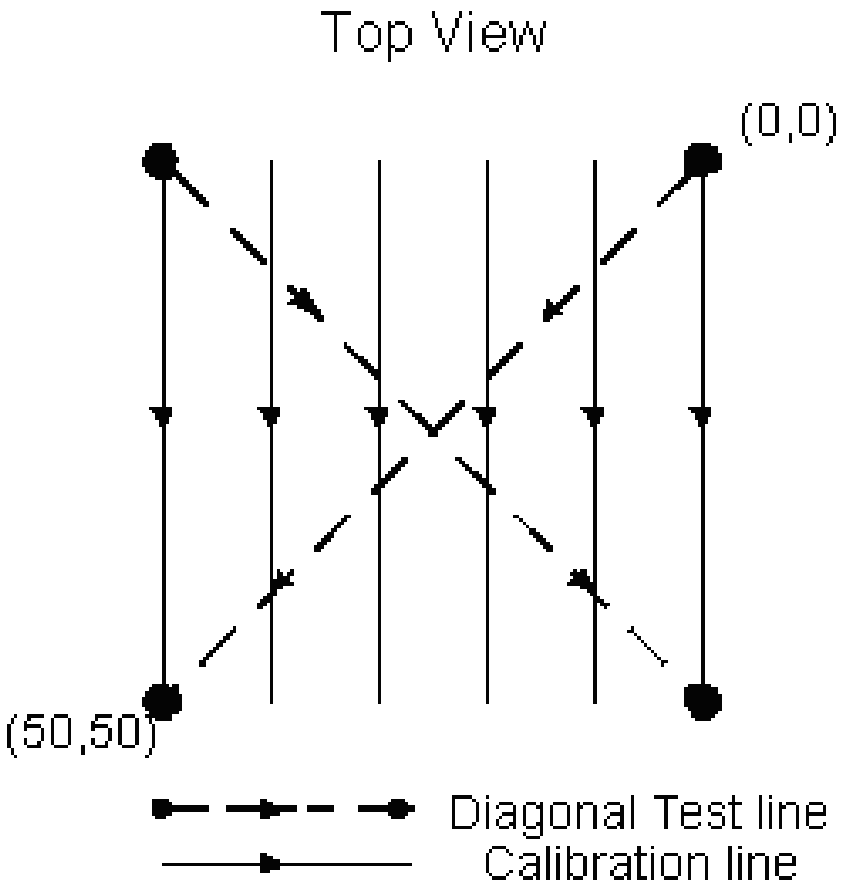

Figure 3.3: Calibration Path

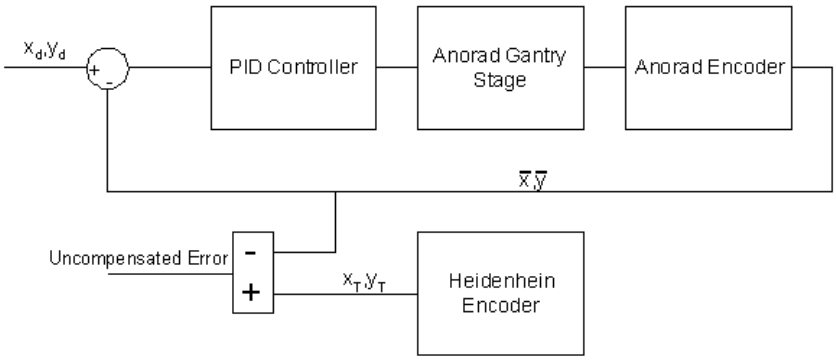

Figure 3.4: Schematic Diagram of Calibration Control

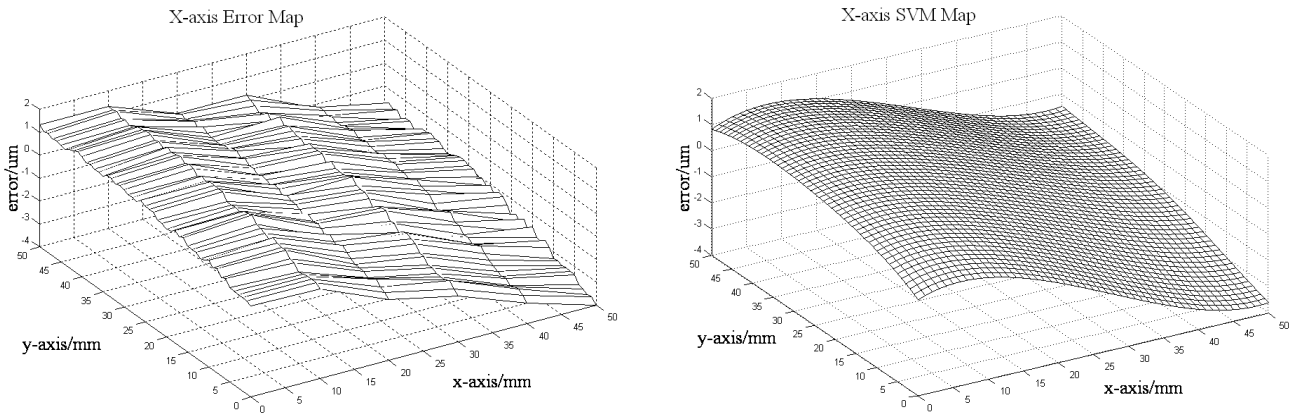

Figure 3.5: Error Map (left) and SVM Map (right) of the X-axis over the Entire Workspace

The final error map of both the X-axis and Y-axis is plotted on the left half of Figure 3.5 and Figure 3.6 respectively. The SVM map of the X-axis and Y-axis thus obtained is shown on the right half of Figure 3.5 and Figure 3.6 respectively. The adequacy of the resultant models is verified by the close fit of the model to the calibration lines. (N.B. It should be noted that comparison between the calibration lines of the error map and the same lines on the SVM map showed differences of less than 0.8micron. Refer to Appendix A for an explanation of this value.)

3.4 Real-time Error Compensation

The error compensation is implemented with the SVM as a S-function block in MATLAB/SIMULINK. Error compensation was then executed with servo control. A clear representation of the process is illustrated with the schematic diagram in Figure 3.7.

To assess the performance of the proposed method, the two actuators were made to move through the body diagonals of the working volume as shown in Figure 3.3. This

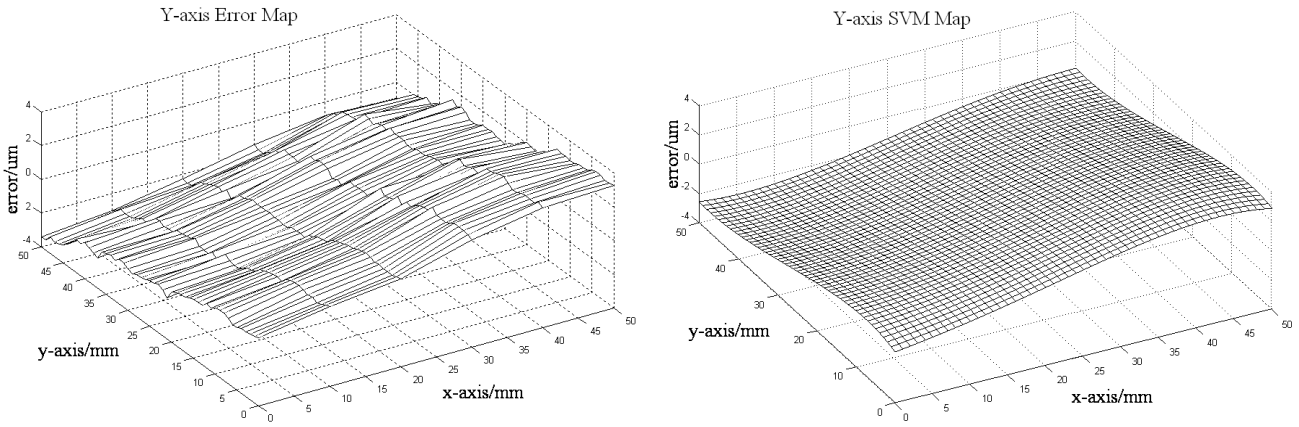

Figure 3.6: Error Map (left) and SVM Map (right) of the Y-axis over the Entire Workspace

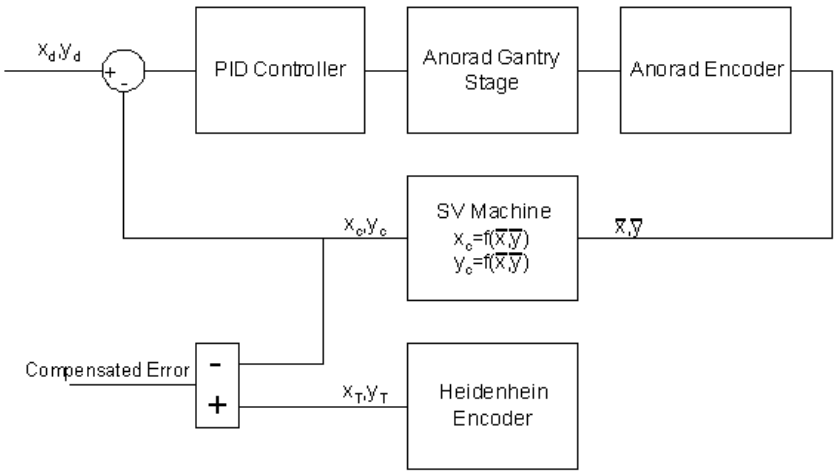

Figure 3.7: Schematic Diagram for Compensation

diagonal test is commonly used as noted in [111] even though it has its limitations [112]. 50 tested positioning points ($1mm$ apart) along each diagonal were collected and the resultant positional errors, before and after geometrical compensation, are shown in Figure 3.8 and 3.9. The results showed that the diagonal errors have been reduced from a maximum of $4\mu m$ to less than $1.8\mu m$.

It should be noted that there are two main factors which determines the compensation results, 1) the repeatability of the machine and 2) the accuracy of the error map. From experimental runs, the repeatability of the Anorad machine is less than $1\mu m$, while the SVM error mapping obtained (comparing the two diagrams in Figure 3.5 and Figure 3.6) showed that the compensation deviate from the measured position by approximately $\pm 0.8\mu m$ (maximum). Lastly, it is noted that the SVM map obtained in Figure 3.5 and Figure 3.6 are also influenced by the repeatability of the Anorad machine. Hence, the overall compensation will lie between a $\pm 2.8\mu m$ (1+0.8+1) error region as the worst case scenario. This also implies that for an initially uncompensated positional error which is small, it is possible for the compensated error to increase, but constrained within the $\pm 2.8\mu m$ error region.

3.5 Conclusions

A new method for geometrical error compensation of precision motion systems using support vector machines is proposed here. Although geometric compensation is not new, the traditional methods such as the look-up table are found wanting as higher

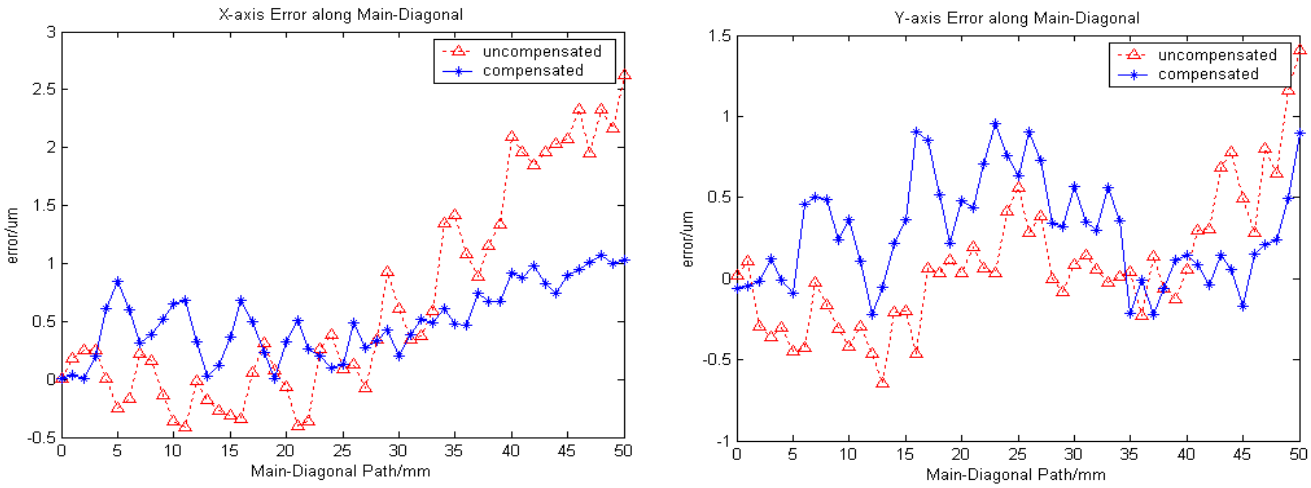

Figure 3.8: Comparison of Main-Diagonal Error for X-axis (left) and Y-axis (right)

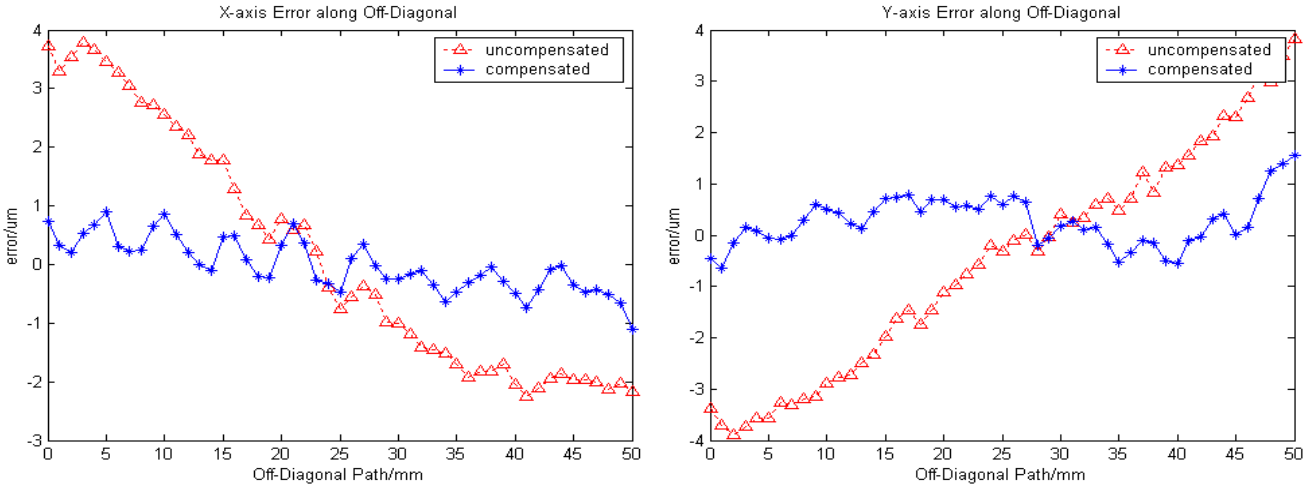

Figure 3.9: Comparison of Off-Diagonal Error for X-axis (left) and Y-axis (right)

accuracy compensation places increasing demand on computational requirements and memory storage. Neural networks are good candidates for geometric compensation, but they pose some shortcomings such as dimensionality and the number of optimum neurons. These issues are effectively overcome using SVM.

Furthermore, for an efficient and cost-effective solution, a Heidenhain two-coordinates encoder is used as the reference to calibrate the motion system instead of the usual laser

interferometer.

The compensation scheme is carried out with respect to an overall geometrical error model which is constructed from the individual error components associated with each axis of the machine. These error components are modeled using support vector regression method. The adequacy and clear benefits of the proposed approach are illustrated from an application to the dual-axial Anorad stage.

The following are findings which are significant for any user of such compensation scheme:

- The maximum achievable accuracy is at least twice the repeatability of the machine.

- The ability of any compensator to effectively map and interpolate the error map is another factor in achievable accuracy

- By increasing the resolution of the weight vector w, higher accuracy mapping is obtained. However, the SVM tends to "over-compensate" (resulting in an unnatural mapping) for large errors with fine resolution of compensation.

- Due to the previous point, the compensation capability of the compensator is limited. Based on simulation results, it is found that such compensation can, at most, reduce errors by a factor of 10; i.e., if the initial errors are very large (said 1mm), the compensation can only reduce errors to 100μm; no less.

- Lastly, it should be noted that, in terms of computational time and resources, the

main difference between SVM and LUT lies with SVM ability to identify support vectors in the arrays of calibration points; thus reducing substantially the amount of calibration data required to build the error map.

Chapter 4

Dynamic Compensation using Iterative Learning Control

4.1 Needs for Dynamic Compensation

Common to all the works on geometric compensation is a static geometric model of the machine errors, which is obtained (or derived) from measurements of the machine and reference encoders at various predetermined points over the workspace. This methodology is lacking in three aspects:

- The calibration process for geometric compensation requires the collection of many points. For a $1m^2$ workspace with $1mm$ of calibration resolution, 1 million data points are required. This is required for all static compensation schemes; whether Neural Network, SVM or LUT.

- The success of the compensation scheme is highly dependent on the interpolation characteristics between the calibration points by the software.

- Most significantly, dynamic errors cannot be included in the compensation schemes and hence these geometric compensation schemes are restricted to point-to-point

positioning applications such as the component placement on a PCB-assembly line. For applications that require continuous trajectory tracking such as e-beam lithography, the static compensation model is inadequate as it fails to account for other factors such as effectors inertia, effectors directional velocities, directional stiffness, computational delay, encoder feedback delay etc. In effect, any positioning error that arises from the movement of the motion system is classified as dynamic error.

To the best of the author's knowledge, there has been no reported paper on compensation schemes which may resolve the above issues.

4.2 Compensation Methodology

Since Arimoto et al. [113] proposed their iterative learning control (ILC) strategies; ILC has been gaining favor; and although ILC has traditionally been used for tracking control, there are instances where it has been used in different settings such as those reported in Norrlof [114] and Moore [115]. Likewise, ILC is used to provide dynamic geometric compensation. With its learning capability, it is suitable for tackling the problem where the compensation map is unknown or too complex to formulate; ILC provides a simple and elegant method of compensation under these circumstances.

4.2.1 Compensation Scheme and its Advantages

With the basic knowledge of ILC, a compensation scheme is developed as illustrated in Figure 4.1. Using a reference encoder, an ILC block is constructed to provide dynamic geometric compensation for error between the reference encoder and the plant encoder.

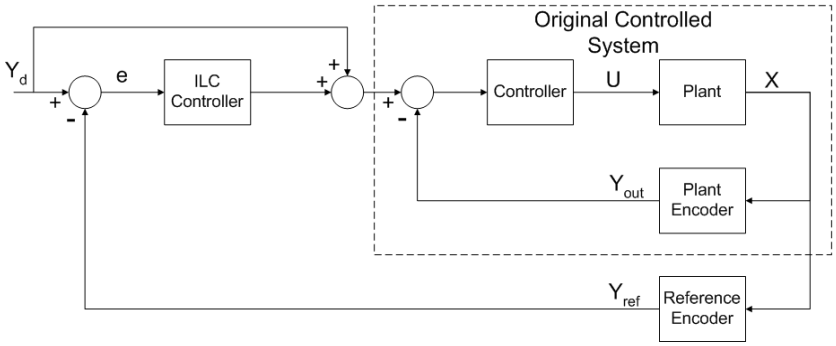

Figure 4.1: ILC Training Scheme

After the ILC controller has successfully recorded the necessary compensation trajectory, the reference encoder is removed and the original controlled system operates with improved performance with a "desired" trajectory setting.

An additional benefit from this methodology is that there is no need for modifications to the existing setup of the plant. This allows the system to retain the intrinsic properties provided by the existing controller.

It should be noted that using a simple LUT to replace the ILC controller is not feasible as the actual dynamic error compensation data is unavailable. It is only with each iterative step that the system moves closer and closer to the desired path and hence the achieved dynamic compensation. Upon compensation, the ILC controller stopped learning and behaves like a LUT. Also, the plant encoder cannot be directly replaced by the reference encoder for the compensation process as the control loop would be different using the plant encoder and the reference encoder.

4.2.2 Theoretical Analysis

First of all, the notations will be properly defined. Let the subscript i denote the iteration number of operation, k the sampling instance of a desired periodic trajectory with period T_D. Each sampling instance is T seconds long, and N samples are contained within each period, thus $T_D = NT$. Hence, $X_i(t_k)$, is the value of the system state (X) at the k^{th} instance of the i^{th} iteration. Furthermore, $\Delta X_i(t_k) = X_i(t_k) - X_{i-1}(t_k)$. Secondly, readers are encouraged to refer to Figure 4.2 for a better understanding of the use of the variables. The schematics are identical to Figure 4.1 except that the blocks are readjusted for ease of mathematical analysis. It should be highlighted that the output of the original controlled system (Y_{out}) has been split into three portions: firstly the linear state space model characterized by matrices A, B, and C, secondly, the internal nonlinearities and input noise ($D_{1,i}(t)$), and thirdly, the external noise and the dynamic error sources ($D_{1,i}(t)$). The dynamic error sources are determined based on the differences between the two encoders (Y_{out} and Y_{ref}), which are now merged together to form an unknown "error model".

Based on Figure 4.2, the original feedback plant may be described in state space form as follows:

$$\begin{aligned} \dot{x_i}(t) &= Ax_i(t) + Bu_i(t) + D_{1,i}(t), \\ y_i(t) &= Cx_i(t) + D_{2,i}(t), \end{aligned} \tag{4.1}$$

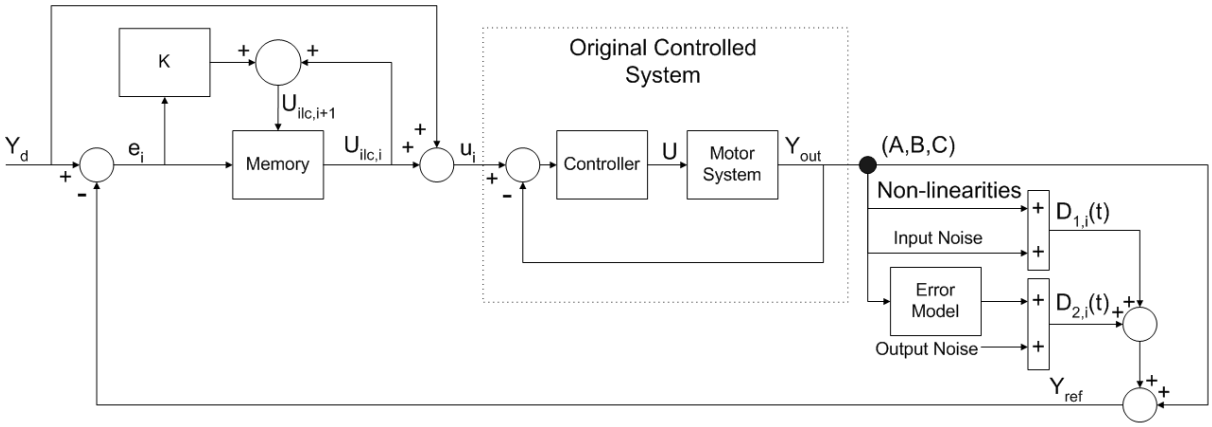

Figure 4.2: Schematics for Analysis

The system will be analyzed at each sampling instant via a discrete time approach. The solution of the state space (4.1) at the sampling instant t_k can be formulated as

$$x_i(t_{k+1}) = e^{A(t_{k+1}-t_0)}x_i(t_0) + \int_{t_0}^{t_{k+1}} e^{A(t_{k+1}-\tau)}Bu_i(\tau)d\tau + \int_{t_0}^{t_{k+1}} e^{A(t_{k+1}-\tau)}D_{1,i}(\tau)d\tau. \quad (4.2)$$

With the solution of Equation (4.2), the deviation in tracking accuracy at the i^{th} iteration of the t_{k+1} instant, $e_i(t_{k+1})$(between the desired trajectory and the reference encoder) may be formulated as follows:

$$
\begin{aligned}
e_i(t_{k+1}) &= y_d(t_{k+1}) - y_i(t_{k+1}) \\
&= y_d(t_{k+1}) - y_{i-1}(t_{k+1}) - (y_i(t_{k+1}) - y_{i-1}(t_{k+1})) \\
&= e_{i-1}(t_{k+1}) - C(x_i(t_{k+1}) - x_{i-1}(t_{k+1})) - \Delta D_{2,i}(t) \\
&= e_{i-1}(t_{k+1}) - C\int_{t_0}^{t_{k+1}} e^{A(t_{k+1}-\tau)} B\Delta u_i(\tau)d\tau - Ce^{A(t_{k+1}-t_0)}\Delta x_i(t_0) \\
&\quad -C\int_{t_0}^{t_{k+1}} e^{A(t_{k+1}-\tau)}\Delta D_{1,i}(\tau)d\tau - \Delta D_{2,i}(t) \\
&\equiv e_{i,1}(t_{k+1}) + e_{i,2}(t_{k+1}) + e_{i,3}(t_{k+1}), \qquad (4.3)
\end{aligned}
$$

where $\Delta x_i(t_0) = x_i(t_0) - x_{i-1}(t_0)$, $\Delta u_i(t_k) = u_i(t_k) - u_{i-1}(t_k)$, and $\Delta D_{\alpha,i}(t_k) = D_{\alpha,i}(t_k) - D_{\alpha,i-1}(t_k)$ (for $\alpha = 1, 2$), and the symbolic terms: $e_{i,1}(t_{k+1}), e_{i,2}(t_{k+1})$, and $e_{i,3}(t_{k+1})$ are expressed as:

$$
\begin{aligned}
e_{i,1}(t_{k+1}) &= e_{i-1}(t_{k+1}) - C\int_{t_0}^{t_{k+1}} e^{A(t_{k+1}-\tau)} B\Delta u_i(\tau)d\tau, \qquad (4.4) \\
e_{i,2}(t_{k+1}) &= -Ce^{A(t_{k+1}-t_0)}\Delta x_i(t_0), \qquad (4.5) \\
e_{i,3}(t_{k+1}) &= -C\int_{t_0}^{t_{k+1}} e^{A(t_{k+1}-\tau)}\Delta D_{1,i}(\tau)d\tau - \Delta D_{2,i}(t). \qquad (4.6)
\end{aligned}
$$

A standard P-type ILC update law is proposed as:

$$
u_i(t_k) = u_{i-1}(t_k) + Ke_{i-1}(t_{k+1}). \qquad (4.7)
$$

This control law updates the control signal '$u_i(t_k)$' by computing the $(k+1)^{th}$ instance of the previous $(i-1)^{th}$ cycle and used it as a feedforward compensation for the current

k^{th} instance of the current i^{th} cycle. The parameter 'K' in the control law determines the speed of learning. Higher 'K' results in larger adjustment of the control signal in each iteration.

Substituting Equation (4.7) into the first term of Equation (4.3), it may be expressed as:

$$\begin{aligned} e_{i,1}(t_{k+1}) &= e_{i-1}(t_{k+1}) - C\int_{t_0}^{t_{k+1}} e^{A(t_{k+1}-\tau)}B\Delta u_i(\tau)d\tau, \\ &= e_{i-1}(t_{k+1}) - C[\int_{t_0}^{t_1} e^{A(t_{k+1}-\tau)}d\tau B\Delta u_i(t_0) \\ &\quad + \int_{t_1}^{t_2} e^{A(t_{k+1}-\tau)}d\tau B\Delta u_i(t_1) + \cdots + \int_{t_k}^{t_{k+1}} e^{A(t_{k+1}-\tau)}d\tau B\Delta u_i(t_k)] \\ &= [I - C\int_{t_k}^{t_{k+1}} e^{A(t_{k+1}-\tau)}d\tau BK]e_{i-1}(t_{k+1}) - C\int_{t_{k-1}}^{t_k} e^{A(t_{k+1}-\tau)}d\tau BKe_{i-1}(t_k) \\ &\quad - \cdots - C\int_{t_0}^{t_1} e^{A(t_{k+1}-\tau)}d\tau BKe_{i-1}(t_1). \end{aligned} \tag{4.8}$$

Let

$$E(k) = I - C\int_{t_{k-1}}^{t_k} e^{A(t_k-\tau)}d\tau BK, \tag{4.9}$$

$$\bar{E}(k) = -C\int_{t_{k-1}}^{t_k} e^{A(t_{k-1}-\tau)}d\tau BK. \tag{4.10}$$

Thus, the deviation in tracking accuracy at each time instant is:

$$
\begin{aligned}
e_{i,1}(t_1) &= E(1)e_{i-1}(t_1), \\
e_{i,1}(t_2) &= E(2)e_{i-1}(t_2) + \bar{E}(1)e_{i-1}(t_1), \\
&\vdots \\
e_{i,1}(t_k) &= E(k)e_{i-1}(t_k) + \bar{E}(k-1)e_{i-1}(t_{k-1}) + \cdots + \bar{E}(1)e_{i-1}(t_1). \qquad (4.11)
\end{aligned}
$$

Finally, considering all N sampling instances, where $e_i = [e_i(t_1), e_i(t_2), \cdots, e_i(t_N)]^T$, and substituting Equation(4.11) into Equation(4.3):

$$
e_i = \mathbf{E}e_{i-1} - H_1\Delta x_i(0) - H_2, \qquad (4.12)
$$

where the parameters $\mathbf{E}$, H_1 and H_2 are as follows:

$$
\mathbf{E} = \begin{bmatrix}
E(1) & 0 & \cdots & 0 & 0 \\
\bar{E}(1) & E(2) & \cdots & 0 & 0 \\
\bar{E}(1) & \bar{E}(2) & \cdots & 0 & 0 \\
\vdots & \vdots & \ddots & \vdots & \vdots \\
\bar{E}(1) & \bar{E}(2) & \cdots & E(N-1) & 0 \\
\bar{E}(1) & \bar{E}(2) & \cdots & \bar{E}(N-1) & E(N)
\end{bmatrix}, \qquad (4.13)
$$

$$
H_1 = \begin{bmatrix}
Ce^{A(t_1-t_0)} \\
Ce^{A(t_2-t_0)} \\
\vdots \\
Ce^{A(t_N-t_0)}
\end{bmatrix}, \qquad (4.14)
$$

$$
H_2 = \begin{bmatrix}
C\int_{t_0}^{t_1} e^{A(t_1-\tau)}\Delta D_{1,i}(\tau)d\tau + \Delta D_{2,i}(t_1) \\
C\int_{t_0}^{t_2} e^{A(t_2-\tau)}\Delta D_{1,i}(\tau)d\tau + \Delta D_{2,i}(t_2) \\
\vdots \\
C\int_{t_0}^{t_N} e^{A(t_N-\tau)}\Delta D_{1,i}(\tau)d\tau + \Delta D_{2,i}(t_N)
\end{bmatrix}. \qquad (4.15)
$$

Noting that with a constant sampling time (i.e. $t_k - t_{k-1} = t_{k-1} - t_{k-2} = \cdots = t_2 - t_1 = T$):

$$I - C\int_{t_{k-1}}^{t_k} e^{A(t_k-\tau)}d\tau BK = I - C\int_0^T e^{A\tau}d\tau BK. \tag{4.16}$$

Since the matrix $\mathbf{E}$ in Equation (4.13) is in a lower block triangular form, e_i is convergent if $\|E(k)\| < 1$ for all $k = 1, 2, \cdots, N$. Thus:

$$\begin{aligned} \|E(k)\| < 1, \text{for all } k = 1, 2, \cdots, N \\ \|I - C\int_{t_{k-1}}^{t_k} e^{A(t_k-\tau)}d\tau BK\| < 1, \text{for all } k = 1, 2, \cdots, N \\ \|I - C\int_0^T e^{A\tau}d\tau BK\| < 1, \end{aligned} \tag{4.17}$$

which is guaranteed (in single input, single output cases) by manipulating K. Furthermore, for ILC, the system is exactly re-initialized at $X_i(0)$ for each cycle and hence $\Delta X_i(0) = 0$. Notice that

$$\begin{aligned} \|H_2\| &= \sqrt{\lambda_{max}({H_2}^T H_2)} \leq \sqrt{\|{H_2}^T H_2\|} \\ &\leq \|C_1\| e^{\|A\|NT} T\sqrt{N} d_{1,D} + d_{2,D}, \end{aligned} \tag{4.18}$$

where $\|D_{1,i}(t_k) - D_{1,i-1}(t_k)\|$ is assumed to be less than $d_{1,D}$ and $\|D_{2,i}(t_k) - D_{2,i-1}(t_k)\| \leq d_{2,D}$ for all t_k and i. Also, Equation (4.12) may be formulated as

$$e_i = e_0 + (I + \mathbf{E} + \mathbf{E}.\mathbf{E} + \mathbf{E}.\mathbf{E}.\mathbf{E} + ...\mathbf{E}^{i-1})H_2, \tag{4.19}$$

where $\mathbf{E}^i$ is the matrix multiplication of the matrix $\mathbf{E}$ with itself by i number of times. Utilizing the condition in Equation (4.17), $\mathbf{E}$ is a lower triangle matrix with a maximum eigenvalue less than 1. Thus, the matrix power series: $(I + \mathbf{E} + \mathbf{E}.\mathbf{E} + \mathbf{E}.\mathbf{E}.\mathbf{E} + ...)$, with infinite terms, converges. Assume that this power series is bounded by α. Finally, it may be concluded that

$$\lim_{i \to \infty} \|e_i\| \leq e_0 + \alpha(\|C_1\| e^{\|A\| NT} T\sqrt{N} d_{1,D} + d_{2,D}). \tag{4.20}$$

This equation showed that the error is bounded and this value is determined by the first cycle of deviation in tracking accuracy e_0, the sampling time T and the iterative changes in $d_{1,D}$ and $d_{2,D}$. It is highlighted here that the feedforward controller (with proportional unity gain) provides a simple yet appropriate feedforward control signal for the original closed-loop system to reduce e_0. Also, subsequently in this paper, it is shown that reducing $d_{1,D}$ and $d_{2,D}$ would improve the tracking performance. Since the period $TN = T_D$ is a fixed constant, the term $T\sqrt{N}$ showed that a smaller sampling time results in a smaller upper bound.

4.3 Software Simulation

The proposed control methodology is first tested using software simulation. The main considerations that were encountered are in the selection of a suitable model for the motion system as well as a model for replicating the dynamical error map.

For the first issue, as the motors for the motion system are based on Permanent Magnet

Linear Motors (PMLMs), its dynamics can be expressed as follows:

$$\ddot{x} = -\frac{K_e K_t + R_a}{R_a M}\dot{x} + \frac{K_t}{R_a M}u - \frac{1}{M}F_{load}, \tag{4.21}$$

where x is the position moved by the PMLM, u is the input actuation voltage to the PMLM and f_{load} refers to the force required to move the load. The physical parameters of the PMLM used in the simulations are listed in Table 4.1. Interested readers are referred to [116] for the full derivation of this equation.

Table 4.1: PMLM Parameters

Content	Units	LDL3810
Force Constant(K_t)	N/Amp	125
Resistance (R_a)	Ohms	16.4
Back EMF (K_e)	volt/m/sec	125
Slide Weight (M)	kg	5.9

As for the second issue, the exact dynamical geometric error cannot be determined; thus the author decided to use a static geometric error model (Figure 4.3) based on a previous static geometric error compensation paper conducted. Interested readers are referred to [117] for the detailed modeling concept. Although this geometric error model may not be a proper model ideally, it possesses intrinsically some geometric properties. Furthermore, this model has its own uncertain factors (computational lag, unknown velocities profile) which would test the ability of the ILC to dynamically compensate the error.

Theoretically, any waveform may be used as the desired trajectory. Varying frequencies of sinusoidal waveform were used to assess the applicability of the proposed methodology.

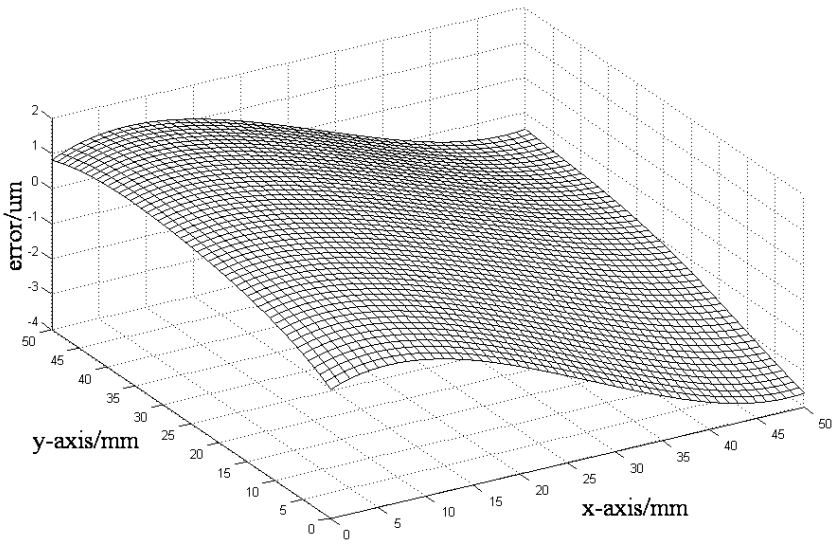

Figure 4.3: Assumed Geometric Error Model

However, for the presentation here and in the subsequent hardware implementation, the desired trajectory was chosen to be a fifth order polynomial as shown in the position profile of Figure 4.4. The rationale for such a trajectory lies in its practical implementation considerations such as zero initial position, velocity and acceleration, which are illustrated in their respective profile in the same figure. Interested readers should refer to the appendix where simulation results showed that the proposed methodology is able to compensate for all frequencies of sinusoidal waveform subjected to the limits of the sampling time (for proper compensation, the minimum samples in each iteration is approximately 50 samples).

The algorithms specified earlier and the simulation models are constructed and simulated using SIMULINK/MATLAB. The control performances will be assessed via the deviation in tracking accuracy of the system.

From Figure 4.5, it can be seen that the proposed methodology is indeed capable of

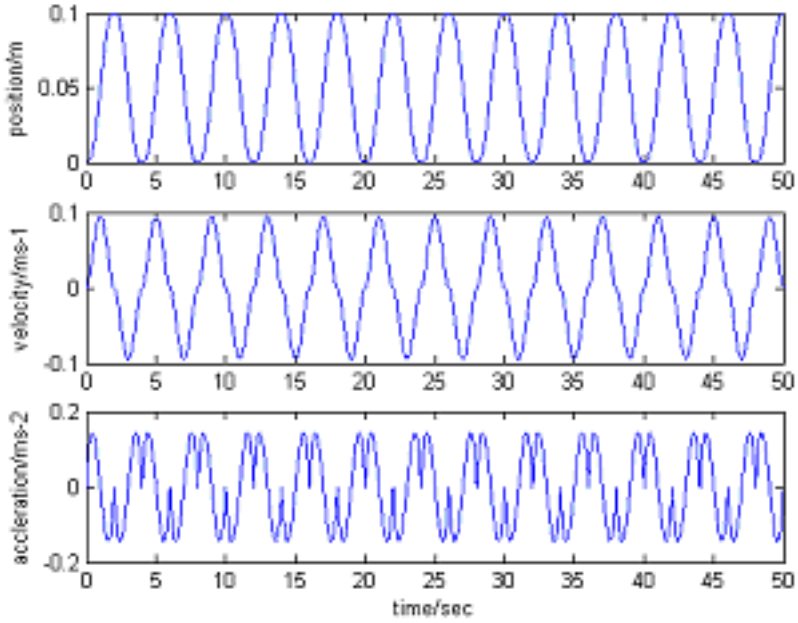

Figure 4.4: Desired Trajectory

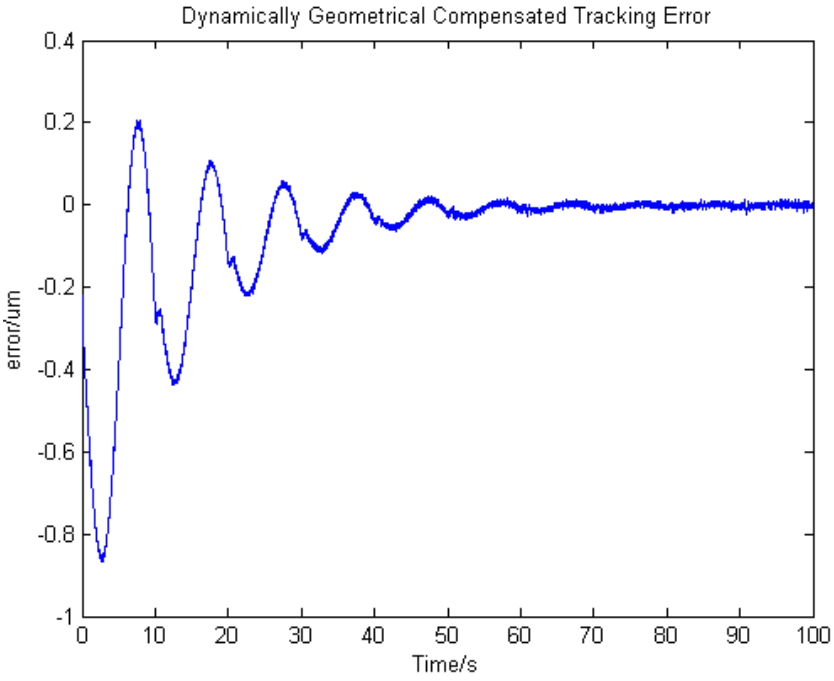

Figure 4.5: Deviation in Tracking Accuracy

reducing the deviation in tracking accuracy.

4.4 Hardware Implementation and Results

Similar to Chapter 3, the Anorad stage is the platform for testing the compensation scheme while the Heidenhain two-coordinates encoder is used as the reference for calibration.

Again, as in the simulated environment, the performance indicator is the deviation in tracking accuracy. Comparing Figure 4.6, (the deviation in tracking accuracy of the uncompensated system) with Figure 4.7, (the implemented methodology), it can be seen that the deviation in tracking accuracy drops from the initial maximum uncompensated error of $22\mu m$ to $16\mu m$ by the second iteration. However, as the ILC acts as an integrator, high frequency terms, such as measurement noise, will be summed up during the learning iterations. Thus, due to the noisy measurement, it is observed that the deviation in tracking accuracy actually increase in subsequent iterations in Figure 4.7. Again, interested readers are refered to the appendix, where the effects of sensor noise are simulated.

Generally, a low-pass filter may mitigate some of the effects. Thus, a simple output-averaging algorithm (which takes the average of the latest fifty output value as the actual present output value) is incorporated for the reference encoder. Comparing Figure 4.7 and 4.8, it can be seen that with the filter, the deviation in tracking accuracy is reduced significantly to a maximum of $9\mu m$ by the 4^{th} iteration. Of course, no filter is ideal

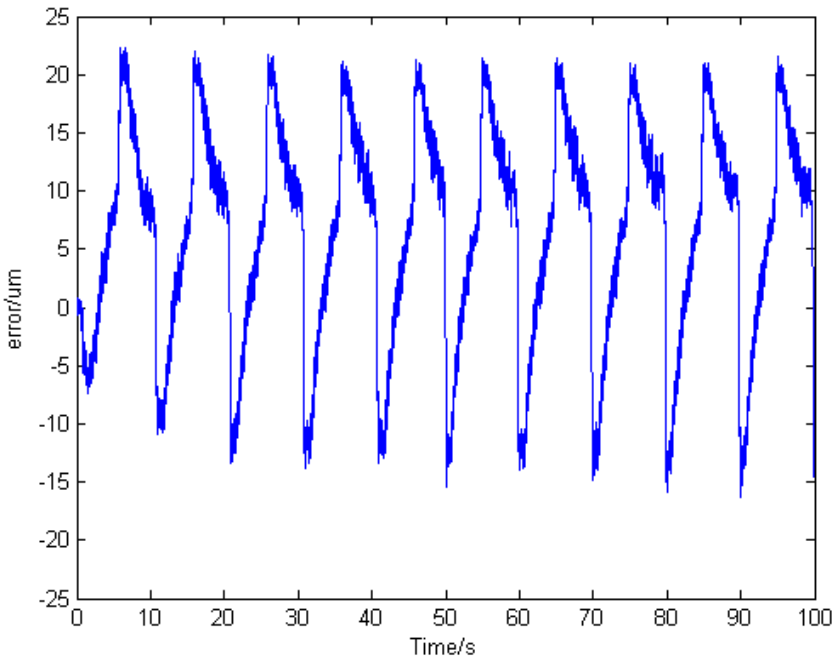

Figure 4.6: Uncompensated Deviation in Tracking Accuracy

except in its mathematical form and thus in practice, learning must cease once the performance specifications are satisfied to ensure long-term stability. In this case, as the 5^{th} subsequent iteration was not providing further improvements, learning is stopped and the ILC actually operates as a look-up table from the 6^{th} iterations without the reference encoder. These improvements are clearly summarized and displayed in Figure 4.9; however instead of simply observing the maximum error, the average absolute error over each iteration is computed in this figure. The average absolute error over each iteration is calculated by take the average of all the absolute value of the error in one iteration. i.e. $AAE_i = \frac{1}{N}\sum_{t=1}^{N} \|e_i(t)\|$, where AAE_i is the average absolute error in the i^{th} iteration, N is the number of samples in each iteration and $e_i(t)$ is the output error of the 't' instance in the i^{th} iteration.

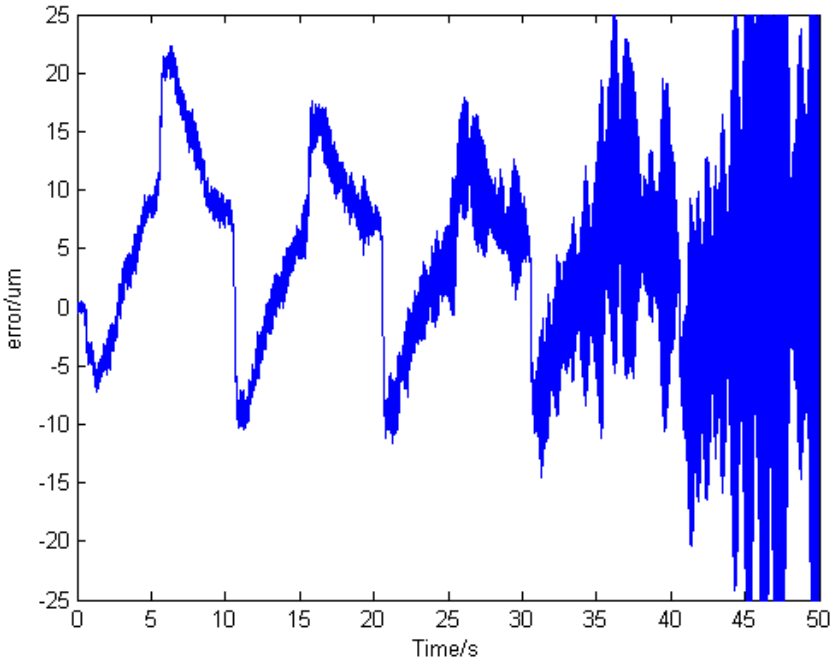

Figure 4.7: Deviation in Tracking Accuracy (w/o averaging filter)

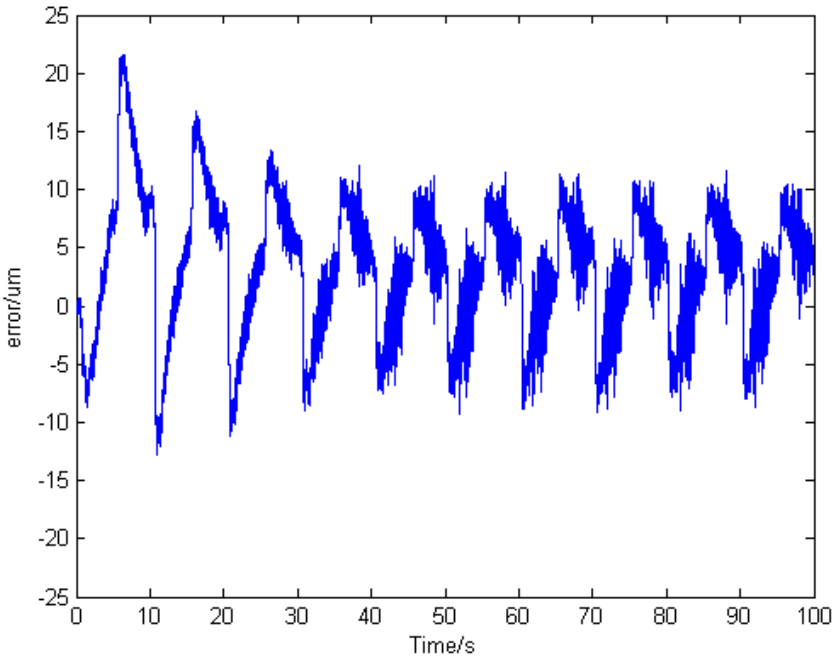

Figure 4.8: Deviation in Tracking Accuracy (with averaging filter)

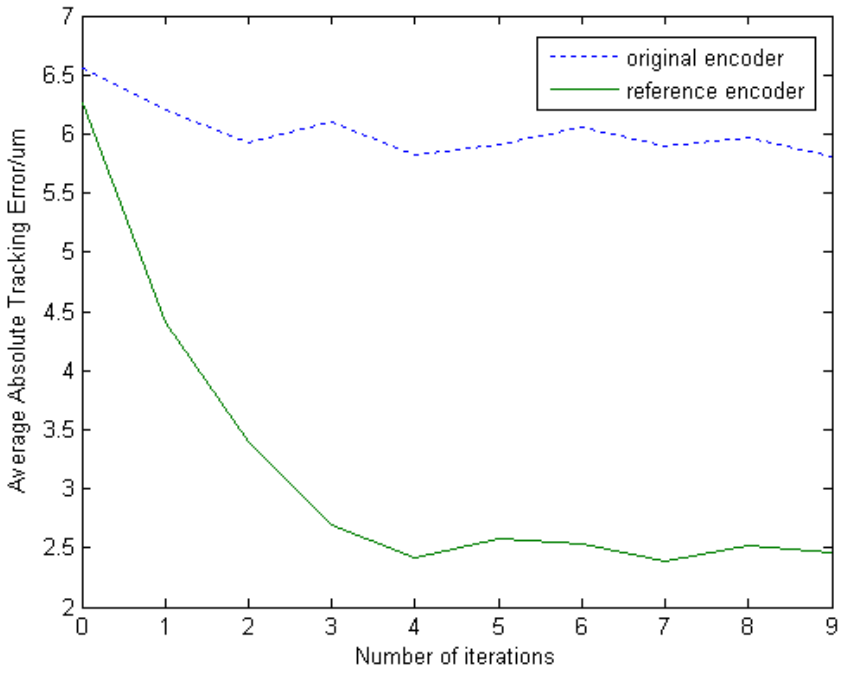

Figure 4.9: Average Deviation in Tracking Accuracy per Iteration

On a further note, the impact of the proposed methodology is compared using the reference encoder in one scenario whilst using the system's original encoder as input for the ILC controller in the other scenario. The improvement achieved using only the system's original encoder is depicted in Figure 4.10. As the maximum error in this case is $16\mu m$, it may be inferred that the ILC helps improve the tracking error of the original controller by $6\mu m$ $(22 - 16 = 6\mu m)$whilst dynamically compensating for $7\mu m$ of error $(16 - 9 = 7\mu m)$.

4.5 Conclusions

Here, a first attempt on dynamic geometric compensation is made using ILC, by utilizing the repetitive nature of the targeted applications. The algorithms are derived and they showed that the error is bounded. Based on the proposed methodology, simulation and

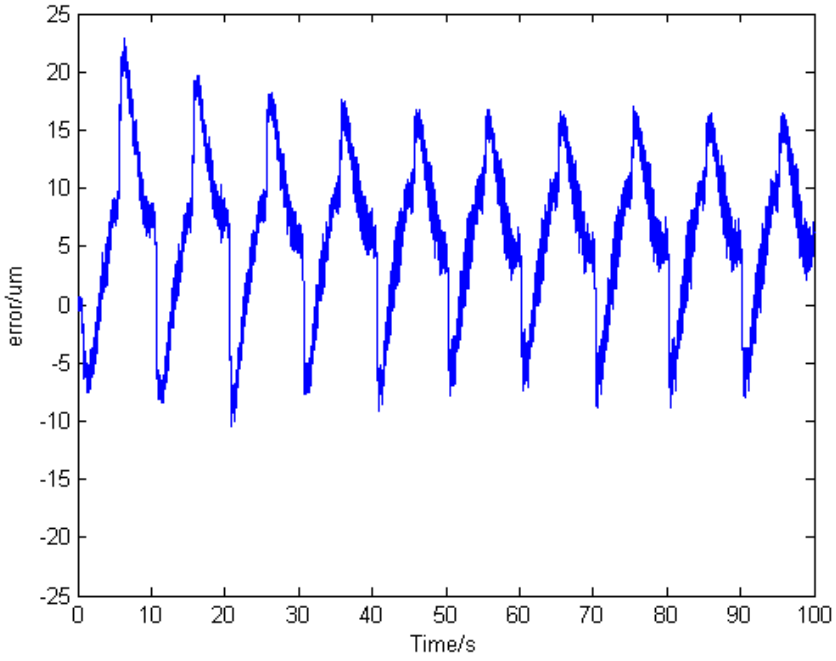

Figure 4.10: Tracking Error using System Original Encoder for ILC Control Input

hardware experiment were implemented. The results in both cases showed that the proposal is indeed feasible and applicable.

The following are findings which are significant for any user of such compensation scheme:

- The desired trajectory achievable is dependent on the sampling time of the system. Generally, a minimum of 50 samples per iteration is required. Hence the maximum frequency of the desired trajectory is constrained as follows: $F_{max} \leq \frac{1}{50T_{sample}}$, where F_{max} is the maximum frequency component of the desired trajectory and T_{sample} is the sampling time.

- A larger ILC gain 'K' results in faster learning but it is capped by the stability condition as stated in Equation 4.17. Furthermore, a well-tuned original controller

allows larger ILC gain to be used.

- Sensor noise will destabilize the ILC. Although filtering improves the performance, learning must terminate when performance objective are reached as subsequent learning will still destabilize the system. One possibility is the application of reset control with the ILC to remove the disadvantage of the integrative effect.

Chapter 5

Innovative Adaptive Control for Dynamic Model-based Gantry

As the demand for precision increases, the tuning of the controller should no longer be based on a static model of the plant. Dynamic modeling of the plant allows the controller to perform more effectively by considering the nonlinear dynamics of the plant. Of course, the time-varying plant will require a time-varying controller and hence the proposal of a model-based adaptive controller.

5.1 Significance of Control Methodology

Various research papers on independent axis control of motion systems have been published, including [118]-[121], but this is a first attempt on implementing a model-based adaptive control on a full-scale, actual H-type gantry stage. The use of Lagrangian equation to model motion systems is not uncommon, [122] and [123], but none have been developed for such a configuration of H-type gantry stage.

Based on the Lagrangian model, the adaptive controller of the control system is designed. Adaptive control schemes, such as those described by Slotine et al. in [124],

have long been in existence, but existing adaptive control cannot be used directly in this gantry stage to achieve high dynamic accuracy. Although the various adaptive control schemes may be applied; due to its special structure, which has two parallel channels with a cross bar, the existing adaptive control needs to be modified to accommodate for this arrangement. Otherwise, uncoordinated movement of the parallel channels may damage the system.

The modeling of the gantry stage is based on Lagrangian equation; the model is detailed enough to address the main concerns and yet generic enough to cover various aspects of the H-type gantry stage. Furthermore, minimal *a priori* information, namely the length and width of the stage, regarding the stage need to be measured. To the best of the author's knowledge, this is the first time an adaptive control scheme has been applied to such a configuration of gantry stage.

5.2 Dynamic Modeling of the Gantry Stage

Prior to the modeling of the gantry stage, a brief description of the typical gantry setup will provide a good basis for the subsequent discussion.

5.2.1 Brief Description of a Typical Gantry Stage

An example of a precision gantry stage is shown in Figure 5.1. This gantry system [1] consists of four sub-assemblies, viz., the X and Y-axis sub-assemblies, the planar platform, and two orthogonal guide bars.

Another setup of H-type gantry stage is shown in Figure 5.2. It consists of two X-axis

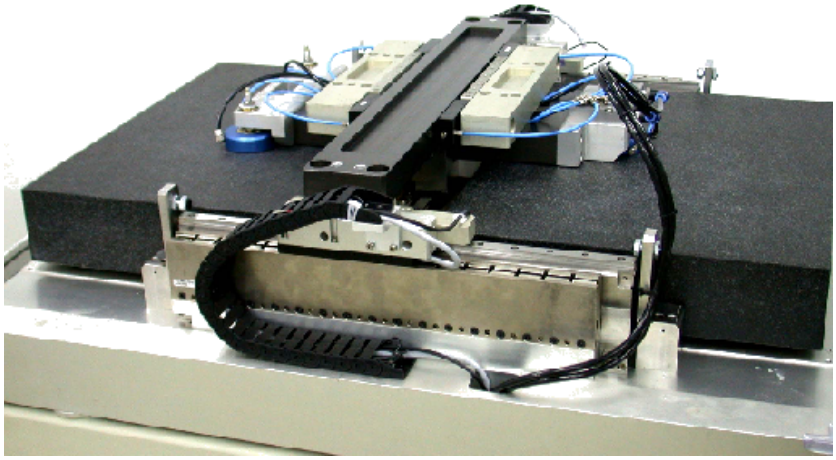

Figure 5.1: Example of a Precision Gantry Stage

servomotors: SEM's MT22G2-10 and a Y-axis servomotor: Yaskawa's SGML-01AF12. Further specifications regarding this stage will be provided in subsequent section accordingly, as this setup is the test bed for real-time experimentation.

Both of the above gantry stages may be considered as a 3-DOF servomechanism, which can be adequately described by the schematics in Figure 5.3. Two servomotors carry a gantry on which a slider holding the load (e.g., the tool) is mounted. One motor yields a linear displacement x_1 (measured from origin O), while the other yields a linear displacement x_2. Ideally $x_1 = x_2$, but they may differ owing to different dynamics exhibited by each of the motor, and also the dynamic loading present due to the translation of the slider along the gantry. The central point C of the gantry is thus constrained to move along the dashed line with two degrees of freedom. The displacement of this central point C from the origin O is denoted by x. The gantry may also rotate about an axis perpendicular to the plane of Figure 5.3 due to deviation between x_1 and x_2, and this rotational angle is denoted by θ. The slider motion relative to the gantry is represented

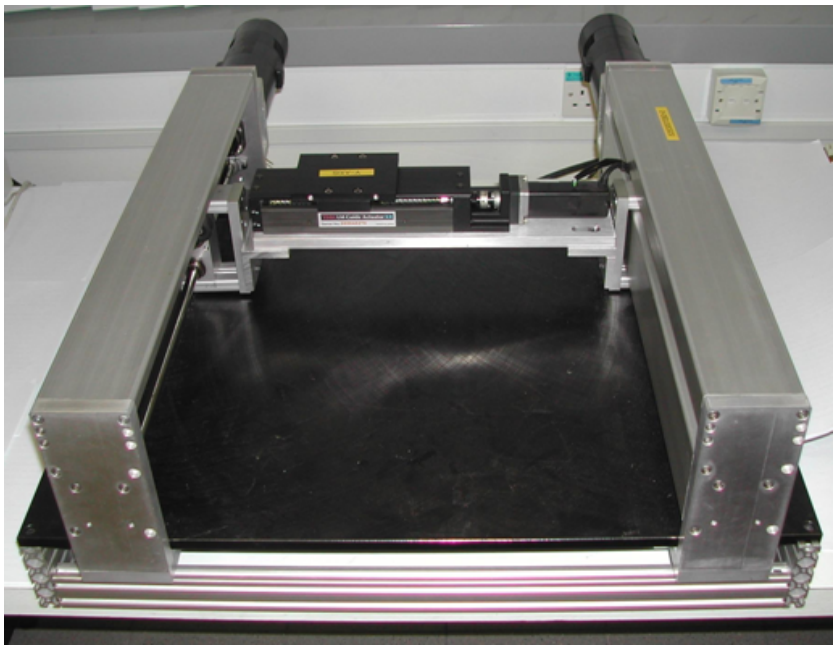

Figure 5.2: Another Structurally Similar Gantry Stage

by y. It is also assumed that the gantry is symmetric and the distance from C to the slider mass center S is denoted by $d = w + v$.

With the formulation of the system under study, it is imminent to proceed with the dynamic modeling of the gantry stage.

5.2.2 Lagrangian-based Modeling

Let m_1, m_2 denote the mass of the gantry and slider respectively, l denotes the length of the gantry, I_1, I_2 denote the moment of inertia of the gantry and slider respectively, (assume that $I_1 = m_1(l/2)^2, I_2 = m_2(\frac{l}{2} + y)^2$) and $X = [x\ \theta\ y]^T$ where $x = x_1 + \frac{x_2 - x_1}{2}$. (refer to Figure 5.3)

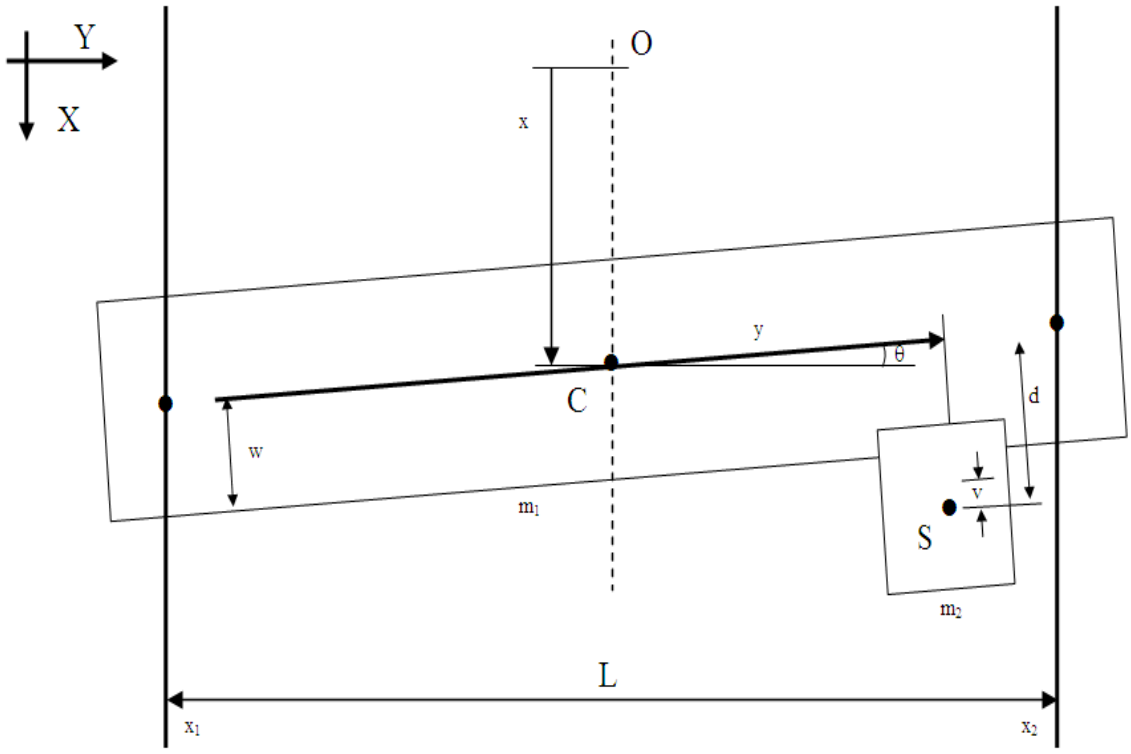

Figure 5.3: Three DOF Structure

The positions of m_i, $i = 1, 2$ are given by

$$x_{m1} = x, \tag{5.1}$$

$$y_{m1} = 0, \tag{5.2}$$

$$x_{m2} = x + dcos\theta - ysin\theta, \tag{5.3}$$

$$y_{m2} = ycos\theta + dsin\theta, \tag{5.4}$$

which lead to the corresponding velocities as

$$v_{m1} = \begin{bmatrix} \dot{x} \\ 0 \end{bmatrix}, \tag{5.5}$$

$$v_{m2} = \begin{bmatrix} \dot{x} - d\dot{\theta}sin\theta - \dot{y}sin\theta - y\dot{\theta}cos\theta \\ \dot{y}cos\theta - y\dot{\theta}sin\theta + d\dot{\theta}cos\theta \end{bmatrix}. \tag{5.6}$$

Thus, the total kinetic energy may be computed as

$$\begin{aligned} K &= \frac{1}{2}m_1 v_{m1}^T v_{m1} + \frac{1}{2}m_2 v_{m2}^T v_{m2} + \frac{1}{2}(I_1 + I_2)\dot{\theta}^2 \\ &= \frac{1}{2}(m_1 + m_2)\dot{x}^2 + \frac{1}{2}(I_1 + I_2 + m_2 y^2 + m_2 d^2)\dot{\theta}^2 \\ &\quad + \frac{1}{2}m_2\dot{y}^2 - \dot{x}\dot{\theta}m_2[dsin\theta + ycos\theta] - \dot{x}\dot{y}m_2 sin\theta \\ &\quad + \dot{\theta}\dot{y}m_2 d, \end{aligned} \tag{5.7}$$

which can be further written as

$$K = \frac{1}{2}\dot{X}^T D\dot{X}, \tag{5.8}$$

where D is the inertia matrix given by:

$$D = \begin{bmatrix} m_1 + m_2 & -m_2 dsin\theta - m_2 ycos\theta & -m_2 sin\theta \\ -m_2 dsin\theta - m_2 ycos\theta & I_1 + I_2 + m_2 y^2 + m_2 d^2 & m_2 d \\ -m_2 sin\theta & m_2 d & m_2 \end{bmatrix}. \tag{5.9}$$

Next, the elements of the Coriolis and centrifugal matrix C are derived from:

$$C_{ij} = \sum_{k=1}^{3}(c_{ijk}\dot{q_k}), \tag{5.10}$$

where $\dot{q_1}$, $\dot{q_2}$ and $\dot{q_3}$ represents the derivative of x, θ and y respectively, and c_{ijk}, the Christoffel symbols, are computed as

$$c_{ijk} = \frac{1}{2}[\frac{\partial d_{ij}(q)}{\partial q_k} + \frac{\partial d_{ik}(q)}{\partial q_j} + \frac{\partial d_{jk}(q)}{\partial q_i}], \tag{5.11}$$

where d_{ij} represents the element in the i^{th} row and j^{th} column of the inertia matrix D.

Substituting the assumed inertia equation I_1 and I_2 into Equation (5.9) and computing Equation (5.11), matrix C is obtained as

$$C = m_2 \begin{bmatrix} 0 & y\dot{\theta}sin\theta - d\dot{\theta}cos\theta - \dot{y}cos\theta & -\dot{\theta}cos\theta \\ y\dot{\theta}sin\theta - d\dot{\theta}cos\theta - \dot{y}cos\theta & (ysin\theta - dcos\theta)\dot{x} - (\frac{l}{2} + 2y)\dot{y} & (\frac{l}{2} + 2y)\dot{\theta} - \dot{x}cos\theta \\ -\dot{\theta}cos\theta & (\frac{l}{2} + 2y)\dot{\theta} - \dot{x}cos\theta & 0 \end{bmatrix}. \tag{5.12}$$

Finally, the dynamic model is expressed as

$$D\ddot{X} + C\dot{X} + BF = BU, \tag{5.13}$$

where

$$B = \begin{bmatrix} 1 & 1 & 0 \\ lcos\theta & -lcos\theta & 0 \\ 0 & 0 & 1 \end{bmatrix}, \tag{5.14}$$

$$F = [F_{x1}, F_{x2}, F_y]^T, \tag{5.15}$$

$$U = [u_{x1}, u_{x2}, u_y]^T. \tag{5.16}$$

F_{x1}, F_{x2}, F_y are the frictional forces, and u_{x1}, u_{x2}, u_y are the generated mechanical forces along x_1, x_2 and y respectively. The frictional forces, F, are assumed to be adequately described by the Tustin model,

$$F_z = d_z\dot{z} + f_z sgn(\dot{z}), \tag{5.17}$$

for $z = x_1, x_2, y$. It is a simple and often adequate approach to regard friction force as a static nonlinear function of the velocity, where d_z is the viscous friction coefficient, and f_z covers the level of static friction, the level of Coulomb friction and the Stribeck effect. The Tustin model has proven to be useful and it has been validated adequately in many successful applications, including [67] and [125].

NB: For other unmodeled higher order terms, they can be regarded as a form of disturbances to the system. The feedback gain of the proposed adaptive controller may be increased so as to suppress the disturbance and enhance the robustness of the system. In this case, although asymptotic stability is not guaranteed, the tracking error will converge to a very small neighborhood of zero.

5.3 Proposed Control Methodology

For the actual real system, it is a challenging and difficult task to obtain the exact values of the parameters of the model m_1, m_2, d_i and f_i $(i = x_1, x_2, y)$ accurately. To this end, an adaptive controller will be designed based on the dynamic Lagrangian model described earlier, which does not require accurate estimates of the model parameters.

Define the filtered error $s = \Lambda e + \dot{e}$ where $e = X_d - X$, and X_d, representing the desired trajectories, is twice differentiable; Λ is a user-defined parameter. Thus, (5.13) can be expressed as

$$D\dot{s} = D(\Lambda\dot{e} + \ddot{X}_d) + C\dot{X} + BF - BU. \tag{5.18}$$

The parameters D, C, and F may be further expressed as follows:

$$D = m_1 D_0 + m_2 D_1, \tag{5.19}$$

$$C = m_2 C_0, \tag{5.20}$$

$$F = \sum_{i=1}^{3} (d_i F_{0i} + f_i F_{1i}), \tag{5.21}$$

where the various coefficients (D_0, D_1 etc) are expressed in Equation (5.22) through

Equation (5.30):

$$D_0 = \begin{bmatrix} 1 & 0 & 0 \\ 0 & (l/2)^2 & 0 \\ 0 & 0 & 0 \end{bmatrix}, \tag{5.22}$$

$$D_1 = \begin{bmatrix} 1 & -dsin\theta - ycos\theta & -sin\theta \\ -dsin\theta - ycos\theta & (\frac{l}{2}+y)^2 + y^2 + d^2 & d \\ -sin\theta & d & 1 \end{bmatrix}, \tag{5.23}$$

$$C_0 = \begin{bmatrix} 0 & y\dot{\theta}sin\theta - d\dot{\theta}cos\theta - \dot{y}cos\theta & -\dot{\theta}cos\theta \\ y\dot{\theta}sin\theta - d\dot{\theta}cos\theta - \dot{y}cos\theta & (ysin\theta - dcos\theta)\dot{x} - (\frac{l}{2}+2y)\dot{y} & (\frac{l}{2}+2y)\dot{\theta} - \dot{x}cos\theta \\ -\dot{\theta}cos\theta & (\frac{l}{2}+2y)\dot{\theta} - \dot{x}cos\theta & 0 \end{bmatrix}, \tag{5.24}$$

$$F_{01} = [\dot{x}_1, 0, 0]^T, \tag{5.25}$$

$$F_{02} = [0, \dot{x}_2, 0]^T, \tag{5.26}$$

$$F_{03} = [0, 0, \dot{y}]^T, \tag{5.27}$$

$$F_{11} = [sgn(\dot{x}_1), 0, 0]^T, \tag{5.28}$$

$$F_{12} = [0, sgn(\dot{x}_2), 0]^T, \tag{5.29}$$

$$F_{13} = [0, 0, sgn(\dot{y})]^T. \tag{5.30}$$

Let

$$V = \frac{1}{2}\dot{D} = m_2 V_0. \tag{5.31}$$

Thus, V_0 may be expressed as:

$$V_0 = \frac{1}{2}\begin{bmatrix} 0 & -d\dot{\theta}cos\theta - \dot{y}cos\theta + y\dot{\theta}sin\theta & -\dot{\theta}cos\theta \\ -d\dot{\theta}cos\theta - \dot{y}cos\theta + y\dot{\theta}sin\theta & 2(\frac{l}{2}+y)\dot{y} + 2y\dot{y} & 0 \\ -\dot{\theta}cos\theta & 0 & 0 \end{bmatrix}. \tag{5.32}$$

Now the filtered error Equation (5.18) can be re-written as

$$\begin{aligned} D\dot{s} &= -Vs + m_1 D_0(\Lambda\dot{e} + \ddot{X}_d) + m_2[V_0 s + D_1(\Lambda\dot{e} + \ddot{X}_d) + C_0\dot{X}] \\ &\quad + \sum_{i=1}^{3}(d_i BF_{0i} + f_i BF_{1i}) - BU. \end{aligned} \tag{5.33}$$

An adaptive controller is proposed as follows:

$$\begin{aligned} U &= B^{-1}Ks + \hat{m}_1 B^{-1} D_0(\Lambda\dot{e} + \ddot{X}_d) + \hat{m}_2 B^{-1}[V_0 s + D_1(\Lambda\dot{e} + \ddot{X}_d) + C_0\dot{X}] \\ &\quad + \sum_{i=1}^{3}(\hat{d}_i F_{0i} + \hat{f}_i F_{1i}), \end{aligned} \tag{5.34}$$

with the following adaptation rules:

$$\dot{\hat{m}}_1 = \gamma_1 s^T D_0(\Lambda\dot{e} + \ddot{X}_d), \tag{5.35}$$

$$\dot{\hat{m}}_2 = \gamma_2 s^T[V_0 s + D_1(\Lambda\dot{e} + \ddot{X}_d) + C_0\dot{X}], \tag{5.36}$$

$$\dot{\hat{d}}_i = \gamma_{3i} s^T B F_{0i}, \tag{5.37}$$

$$\dot{\hat{f}}_i = \gamma_{4i} s^T B F_{1i}, \tag{5.38}$$

where $K > 0$ is positive definite, and $\hat{m}_1, \hat{m}_2, \hat{d}_i, \hat{f}_i$ are estimates of m_1, m_2, d_i, f_i, respectively.

5.4 Stability Analysis

In this section, Lyapunov theorem is used to show that the proposed adaptive controller can guarantee the stability of the closed-loop system, and the filtered error s will approach zero as $t \to \infty$.

Define the Lyapunov function

$$v = s^T D s + \frac{1}{\gamma_1}\tilde{m}_1^2 + \frac{1}{\gamma_2}\tilde{m}_2^2 + \sum_{i=1}^{3}(\frac{1}{\gamma_{3i}}\tilde{d}_i^2 + \frac{1}{\gamma_{4i}}\tilde{f}_i^2), \tag{5.39}$$

where $\tilde{m}_1, \tilde{m}_2, \tilde{d}_i, \tilde{f}_i$ are the estimation error of m_1, m_2, d_i, f_i respectively. Differentiat-

ing v and substituting in Equation (5.33) and the control law: Equation (5.34)

$$\begin{aligned}\dot{v} &= -2s^T Ks + 2\tilde{m}_1 s^T D_0(\Lambda\dot{e} + \ddot{X}_d) + 2\tilde{m}_2 s^T[V_0 s + D_1(\Lambda\dot{e} + \ddot{X}_d) + C_0\dot{X}] \\ &\quad +2\sum_{i=1}^{3} s^T(\tilde{d}_i BF_{0i} + \tilde{f}_i BF_{1i}) - 2\frac{1}{\gamma_1}\tilde{m}_1\dot{\hat{m}}_1 - 2\frac{1}{\gamma_2}\tilde{m}_2\dot{\hat{m}}_2 \\ &\quad -2\sum_{i=1}^{3}(\frac{1}{\gamma_{3i}}\tilde{d}_i\dot{\hat{d}}_i + \frac{1}{\gamma_{4i}}\tilde{f}_i\dot{\hat{f}}_i). \end{aligned} \tag{5.40}$$

Incorporating the adaptive laws (5.35)-(5.38), $\dot{v}$ becomes

$$\dot{v} = -2s^T Ks. \tag{5.41}$$

This implies that $s, \hat{m}_1, \hat{m}_2, \hat{d}_i, \hat{f}_i$ are bounded. Based on the defined filtered error equation, since Λ is positive definite and s is bounded, it follows that e is bounded. This also implies that $\dot{e}$ is bounded, and in turn, that $X, \dot{X}$ are bounded. Furthermore, from (5.33), it can be concluded that $\dot{s}$ is bounded, and from (5.41) together with the definition of v jointly imply that

$$\lim_{t\to\infty}\int_0^t -2s^T(\tau)Ks(\tau)d\tau = \lim_{t\to\infty} v(t) - v(0). \tag{5.42}$$

Finally, applying Barbalat's lemma [126], $\lim_{t\to\infty} s(t) = 0$.

5.5 Simulation

To verify the effectiveness of the proposed approach, the results of using three decoupled PID controllers on each individual axis are compared with the developed adaptive controller applied to a software version of the dynamic gantry model. A MATLAB simulation is setup in each case. The gantry's parameters are selected as follows: masses

$m_1 = 1kg$ and $m_2 = 1kg$, length $l = 0.415m$, distance $d = 0.015m$ and the friction parameters are $d_1 = d_2 = d_3 = 1$, and $f_1 = f_2 = f_3 = 1$. The desired trajectories (position, velocity and acceleration) are as depicted in Figure 5.4. The trajectory would span a distance of 0.01m, periodically in 4s. The maximum velocity and acceleration attained are $0.094m/s$ and $0.145m/s^2$ respectively.

For the PID controllers, the following PID control law is used:

$$u = K_p e + K_i \int e + K_d \frac{\partial e}{\partial t}. \tag{5.43}$$

Using independent axis control, and assuming identical dynamics for each axis; in this simulation, all three PID controller are tuned as K_p=400, K_i=50 and K_d=30. The adaptive controller parameters are configured as: $\gamma_1 = 45000$, $\gamma_2 = 2800$, $\gamma_{31} = 4000$, $\gamma_{32} = 4000$, $\gamma_{33} = 28000$, $\gamma_{41} = \gamma_{42} = \gamma_{43} = 100$, K=diag(100 10 10), and Λ equates the identity matrix, i.e. Λ=diag(1 1 1).

The simulation results showing the error responses for individual axes are depicted in Figure 5.5, whilst the inter-axis offset error is shown in Figure 5.6. The control signals coming from the controller are recorded in Figure 5.7. The data collated from the PID-based simulations are represented in dotted lines whilst solid lines represent the adaptive-based simulations. The time histories of the estimated parameters m_1, m_2, d_1, d_2, d_3, f_1, f_2 and f_3 are shown in Figure 5.8.

For a short time duration from $t = 0$ to $t = 3$, the PID control outperforms the adaptive controller. This is expected as the learning parameters have been initialized to zero with no apriori knowledge assumed. Subsequently, after some parameter adaptation,

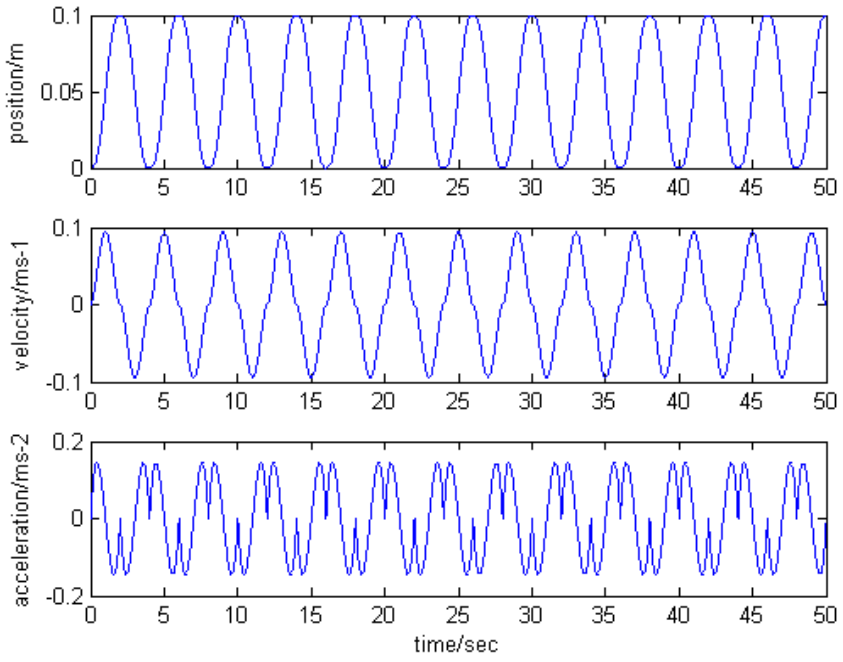

Figure 5.4: Desired Position, Velocity and Acceleration Trajectories for x_1, x_2 and y

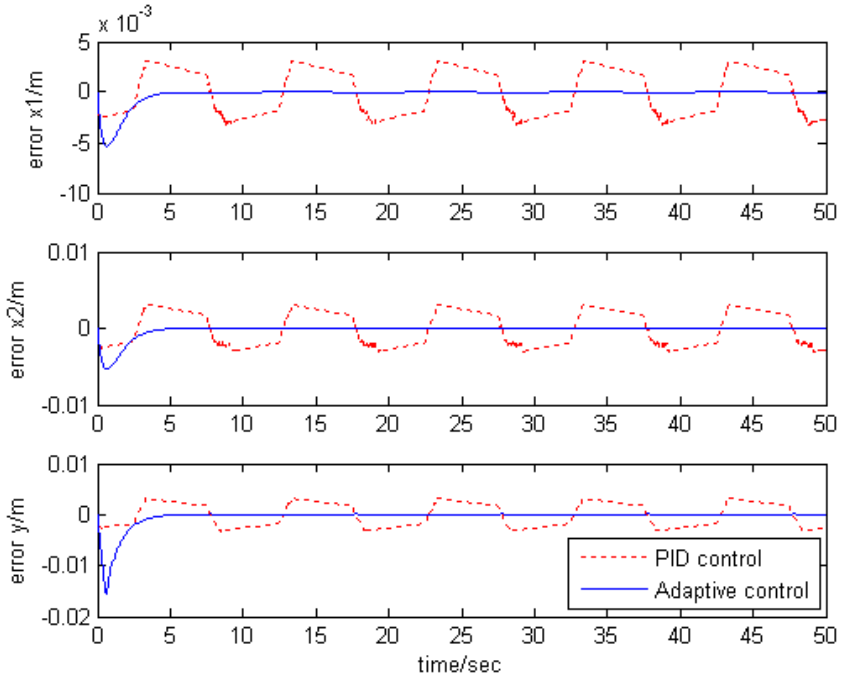

Figure 5.5: Simulated Tracking Error for x_1, x_2 and y

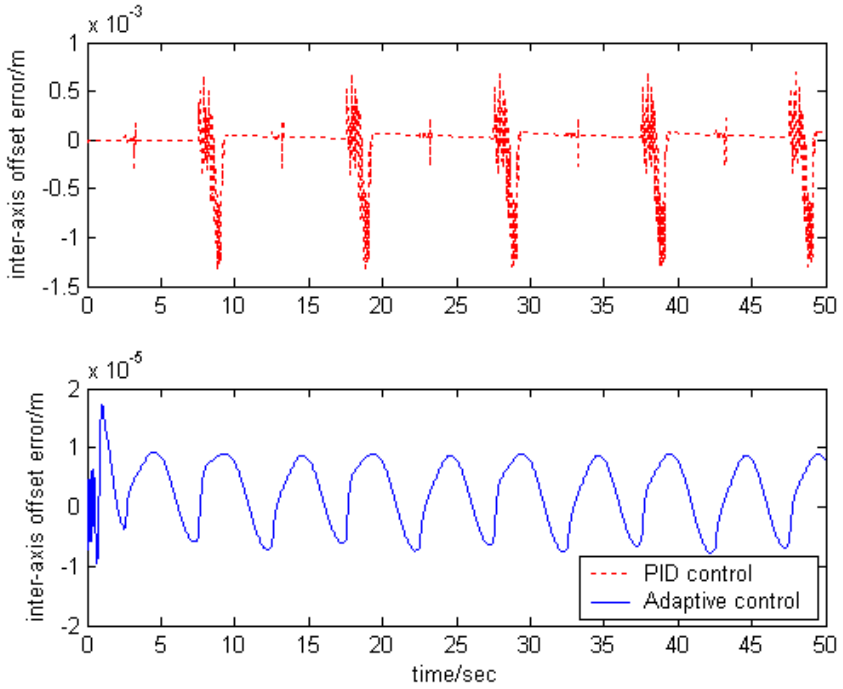

Figure 5.6: Simulated Inter-axis Offset Error Between x_1 and x_2 using (a) PID Control and (b) Adaptive Control

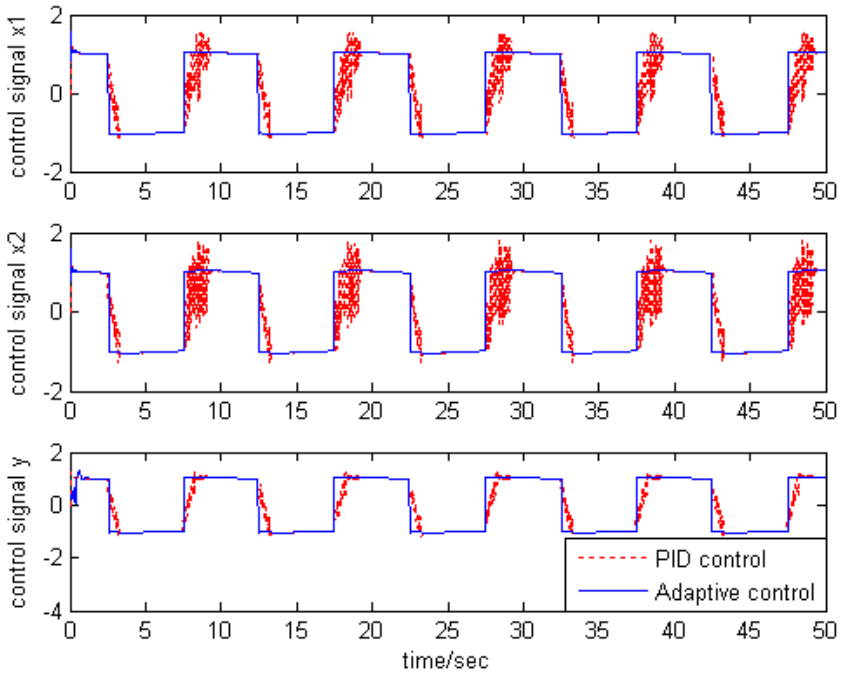

Figure 5.7: Simulated Control Signal for x_1, x_2 and y

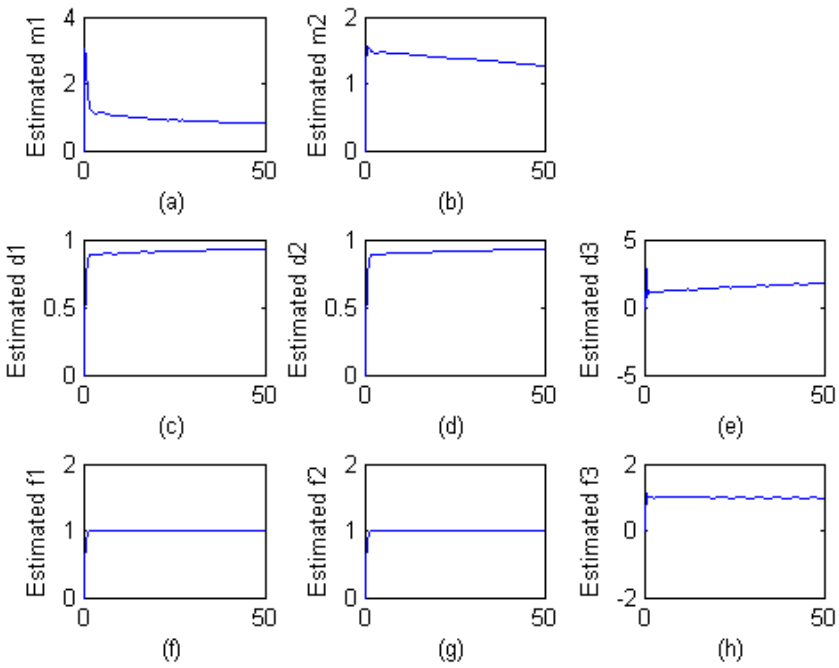

Figure 5.8: Time Histories for Simulated Learning Parameters: m_1, m_2, d_1, d_2, d_3, f_1, f_2 and f_3

the proposed approach quickly yielded significantly improved performance over PID control. On a further note, from Figure 5.8, it can be seen that prior to attaining steady state, the tracking errors (for x_1, x_2 and y) has achieved reasonable performances.

5.6 Implementation Results

The stage used for the experimental setup is the gantry stage as mentioned earlier in Figure 5.2. The control algorithm is implemented in dSPACE via MATLAB real-time workshop. The simulation algorithm can be directly built, using the real-time workshop, into an executable program for dSPACE. The hardware control architecture is centered around a dSPACE DS1103 PPC controller board. The motor specifications are listed in Table 5.1.

Table 5.1: Specifications of Gantry Motors

Content	X-Axis Servo Motor	Y-Axis Servo Motor
	SEM MT22G2-10	Yaskawa SGML-01AF12
Power	350W	100W
Torque	0.70Nm	0.318Nm
Velocity	5000RPM	3000RPM
Resolution	10μm	10μm

For the PID-controlled implementation, PID controllers are tuned as K_p=90, K_i=5 and K_d=1, for the two X-axes (X_1 and X_2) whilst the Y-axis is tuned as K_p=30, K_i=1 and K_d=0. As noted in Table 5.1, the X-axes motors are in the same class and different from the Y-axis motor, hence the X-axes and Y-axis need to be tuned differently. The adaptive controller parameters are configured as: $\gamma_1 = \gamma_2 = \gamma_{31} = \gamma_{32} = \gamma_{33} = \gamma_{41} = \gamma_{42} = \gamma_{43} = 1.8$, K=diag(40 3 5), and Λ=diag(1 1 1).

Trajectories similar to the software simulations are used and the results are shown in Figure 5.9, 5.10, 5.11 and 5.12. These figures present similar characteristics obtained to those from software simulations. The adaptive controller is able to yield individual axis error of under 0.38mm at steady state as compared to the PID performance of 0.96mm for both x_1 and x_2 axis, whilst the y-axis error is kept under 2mm for both controllers, (refer to Figure 5.9). In addition, the adaptive controller is able to minimize the inter-axis offset error (by manipulation of the parameter K), whilst the decoupled PID controller were only able to track individual trajectories independently. This performance is reflected by the resultant inter-axis offset error of 0.32mm using the adaptive controller versus 0.81mm for the decoupled PID controller (refer to Figure 5.10).

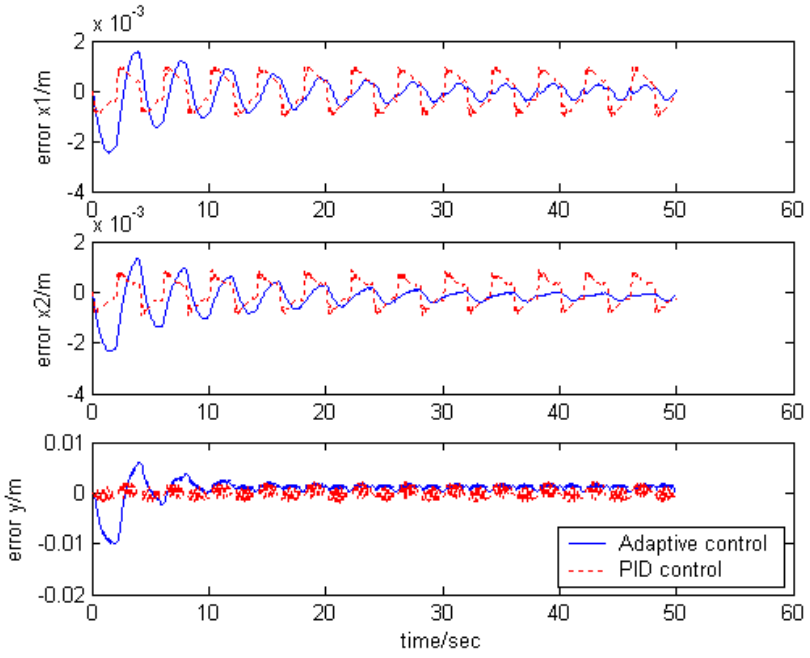

Figure 5.9: Tracking Error for x_1, x_2 and y

Lastly, the time histories of the learning parameters in Figure 5.12 showed gradually adapting parameters. This is expected as the learning gains are small and it is to prevent drastic parameter adjustment in the initial transient stage. Note that even with this small learning gain, the error performances are generally acceptable. The friction parameters for x_1 and x_2 have stabilized and showed similar characteristics, which is expected since both motors are the same model.

5.7 Conclusions

In this chapter, an appropriate dynamic model of a typical *H*-type gantry stage based on the Lagrangian equation is derived. An adaptive controller has been developed to minimize the tracking error as well as inter-axis offset error. The stability of the control scheme has been proven via a Lyapunov-based analysis. Software simulations were

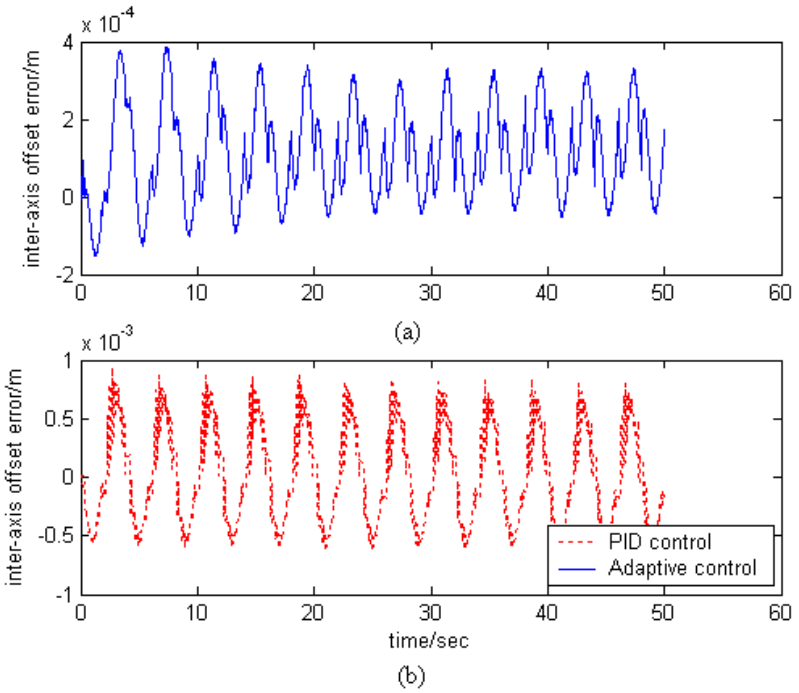

Figure 5.10: Inter-axis Offset Error Between x_1 and x_2 using (a)Adaptive Control and (b) PID Control

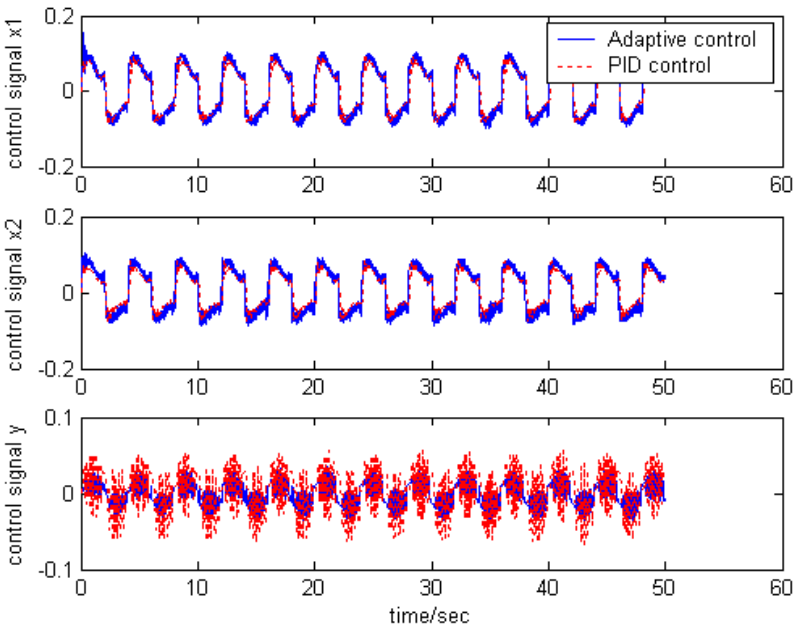

Figure 5.11: Control Signal for x_1, x_2 and y

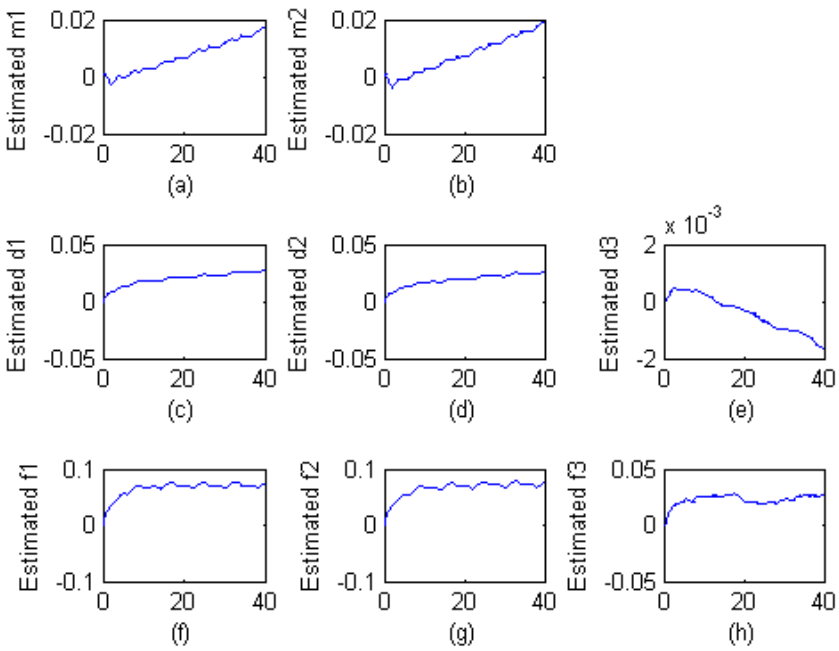

Figure 5.12: Time Histories for Learning Parameters: m_1, m_2, d_1, d_2, d_3, f_1, f_2 and f_3

conducted and the results have shown the superior performances of the adaptive controller over PID control. The subsequent real-time implementation also showed similar appealing performances.

The following are findings which are significant for any user who wish to implement such a scheme:

- It should be noted that the proposed controller is applicable for precision dynamic tracking; where the nonlinear dynamics are significant.

- The first term of the control law: Equation (5.34) is essentially a PD controller with the subsequent terms accommodating for the dynamic loading and frictional effects of the gantry stage.

- The parameters Λ and K are adjusted to improve the performance of x, theta and

y. By selecting diagonal matrices for Λ and K, the motion of x, theta and y are decoupled significantly and hence it is easier to tune.

- Larger learning gain improves the transient response of x and y but it has no effect on inter-axis error. However, too large a learning gain will affect the stability of the system.

- The initialization of the initial condition affect the transient response and has a slight influence on steady state error. A better estimate of the system initial conditions prevents destabilization of the system when stringent trajectories are imposed.

- Although parameters estimation convergence are not definite (the theoretical proof is for the convergence of the filtered error), modal excitation at the appropriate frequencies can provide better estimates.

Chapter 6

Conclusions

Errors in the machine tool motion produce a one-to-one error correspondence in the final workpiece. It is impossible to completely eliminate errors by design and/or manufacturing modifications. Hence, this study provides various soft methodologies for reducing and compensating errors in real-time via the control, thus improving the accuracy of machined workpieces.

6.1 Summary of Contributions

This thesis focuses primarily on improving the positional accuracy of gantry stage. These improvements are along two aspects: corrective approaches are adopted to improve the accuracy of precision motion systems with respect to geometric and dynamic errors, and model-based control strategies are used in the gantry stage to deal with the nonlinear effects that are significantly present and have to be adequately addressed in high accuracy positioning.

Firstly, geometrical compensation is used to improve the accuracy of the precision motion system using a dual-axis high-grade analog optical encoder and Support Vector Ma-

chines (SVM) to calibrate and model the geometrical errors respectively. This proposed approach will reduce significantly the setup time required to perform the experiment as geometrical compensation of the motion system can be performed concurrently for both set of axis. The proposed approach uses the support vector regression method as the basis for modeling; with motivation from the reported problems associated with the look-up table and the other approaches. Simulations and experimental results are provided to highlight the principles and practical applicability of the proposed method resulting from such an approach, as compared to other approaches reported in the literature. Finally, diagonal tests are performed to demonstrate that the proposed compensation approach is able to reduce the geometrical errors effectively.

However, such corrective schemes are restricted to point-to-point positioning applications such as component placement on a PCB-assembly line. Dynamic errors cannot be included in the compensation scheme; which is important for applications that requires continuous trajectory tracking such as e-beam lithography. Hence, utilizing the repetitive nature of a class of applications (such as 2-dimensional wafer inspection), Iterative Learning Control (ILC) is used to provide dynamic geometric compensation. Mathematical analysis showed the boundedness of this approach, while real-time implementation verified the feasibility.

Secondly, based on the H-type configurations of gantry stage, a mathematical model is built using the Lagrangian equation. With the model, an adaptive control method is formulated for the control of the stage, with minimal a priori information assumed of the

model. The modeling of the gantry stage is detailed enough to address the main concerns and yet generic enough to cover various aspects of H-type gantry stage. Mathematical analysis are used to show the boundedness of the error, while real-time implementation verified the proposed methodology.

6.2 Suggestions for Future Work

Although both the control field as well as precision engineering are matured research areas, there are still improvements which can be achieved, as discussed in this study.

From the development in dynamic compensation, there are potential for further improvements. Two identified issues are:

- in the updating law, ILC acts as integrator and hence high frequency terms, such as measurement noise, will be summed up during the learning iterations. The development of control methodologies, such as filters or reset control, can be integrated with the ILC to improve the error performance, and
- in the theoretical analysis, the "boundedness" of the tracking error is proven. However, there is a possibility of adding another degree of freedom into the ILC control law to ensure tracking error converged rather than being bounded.

These issues are relevant only to repetitive applications, in terms of generic dynamic compensation, there are still plenty to develop upon. There is a need to identify the actual sources of errors and develop schemes to properly compensate for them.

Secondly, from the development of the model-based adaptive controller, it was noted

that fast motion of the gantry stage is usually associated with undesirable induced oscillations of the suspended object. These disturbances are a form of dynamical load changes and it can be fairly asymmetrical in nature. Consider for example the suggested gantry in Figure 5.2; In this gantry design, the crux of the issue lies with how the forces are transmitted from the actuators through the guide bar to the planar platform. As the planar platform is a separate entity from the actuators, the forces are directed through the guide bars to the platform. When the planar mass is not traveling directly above the Y-axis actuator, there is an unwanted "Yaw" torque. Furthermore, when the planar mass is not traveling along the center of the two set of X-axis actuators, different forces act on the two separate motors. If the same control signal were applied to both axes, an inter-axis offset error would occur. It is proposed that modifying the control law (5.34) might cater for the different dynamic "disturbances".

Appendix A: Verification of Mapping Error in SVM

The conclusive remark on the adequacy of the resultant mapping model to within 0.6micron is obtain by comparing the calibration lines with the same route along the modelled error map. This comparison is depicted in Figure 1 below, where the modeled errors are compared with the actual errors along the calibration line. The right figure clearly shows the effectiveness of the mapping to be below 0.6micron.

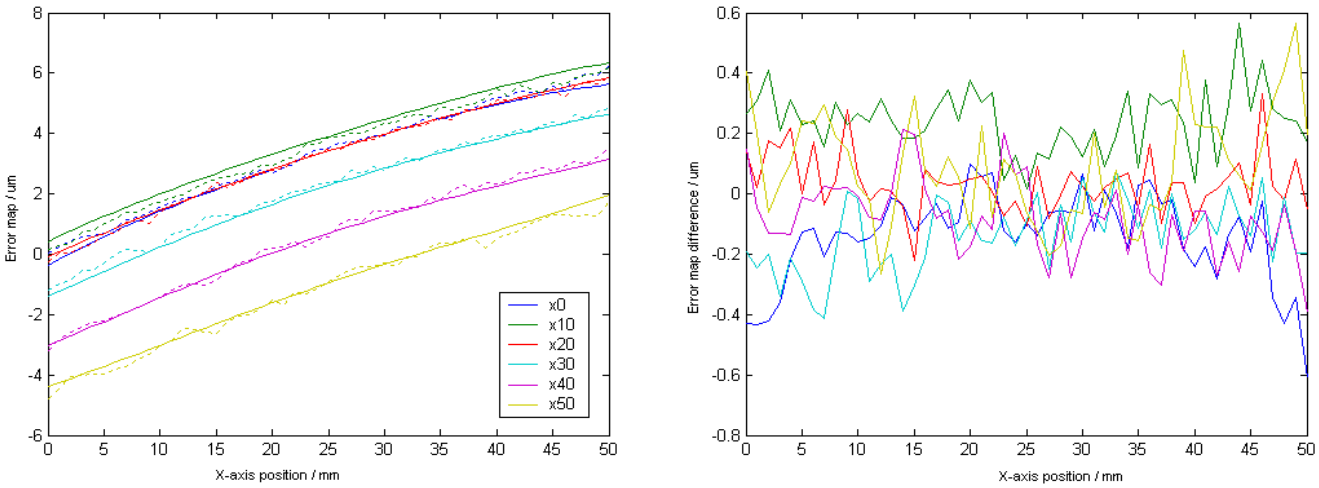

Figure 1: Differences between the calibration results and the error-map along the calibration lines for the X-axis; Actual Value(Left) Computed Differences (Right)

Appendix B: Simulation of Different Trajectories

Theoretically, we can expect any trajectory to be used. This is tested by using varying frequencies as the desired trajectory. The results are shown in Figure 2 below. Note that the sampling time was set at 0.01second and hence the maximum frequency is approximately 2Hz (50samples per iteration). Further increase in the frequency would destabilize the learning, as there are insufficient data points in each cycle.

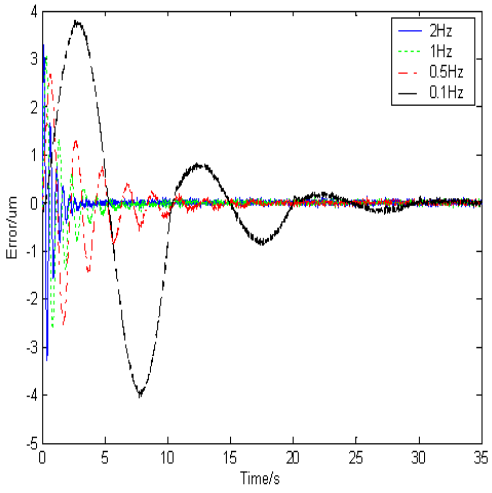

Figure 2: Simulated Response with Varying Frequencies

By further increasing the sampling time to 1 millisecond, the frequency can be increased to 10Hz without affecting the stability, as shown in Figure 3 below. Lastly, note that for all simulation described herewith in this section, the original PD controller for

the "original controlled system" is retuned to create an initial maximum tracking error of about 3micron in the first iteration. This is simply manipulated for ease of comparison.

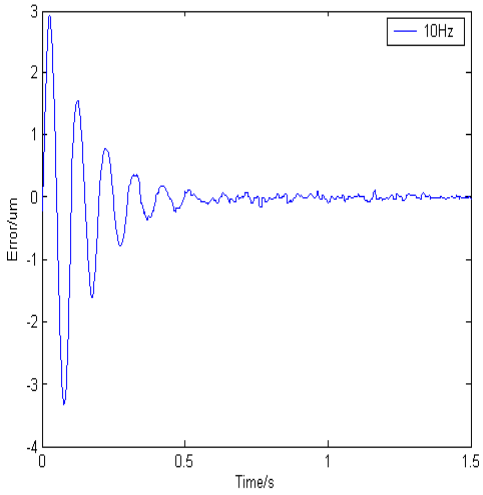

Figure 3: Simulated Response with Higher Frequency by Increasing Sampling Time

Appendix C: Simulation of Sensor noise

The effects of sensor noise was simulated by varying the amplitude of noise. A band-limited white noise was used for the simulation. The results are as depicted in Figure 4.

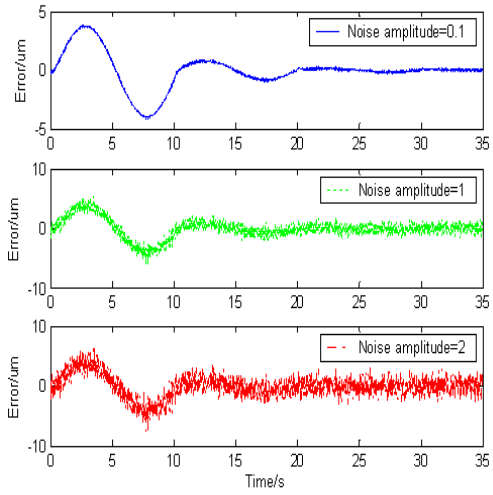

Figure 4: Simulated Response to Varying Noise Amplitude

Bibliography

[1] S.Y. Lim, W. Lin,and Y.P. Leow. Decoupled Planar Positioning System, Singapore Patent,Patent No: PCT/SG01/00190, 2001.

[2] Center for Scalable and Integrated Manufacturing, University of California Berkeley, 3112 Etcheverry Hall, MC 1740, Berkeley, CA 94720-1740, USA, www.sinam.org.

[3] Jain K, Klosner M, Zemel M, and Raghunandan S. Flexible Electronics and Displays: High-Resolution, Roll-to-Roll, Projection Lithography and Photoablation Processing Technologies for High-Throughput Production, Proceedings of the IEEE, Vol. 93(8), pp.1500 - 1510. 2005.

[4] John A. Bosch. Coordinate Measuring Machines and Systems, New York: M. Dekker. 1995.

[5] Seet Hoe Luen, geometrical error compensation of precision machines, doctorate thesis, national university of Singapore, 2000

[6] Alexander H. Slocum. Precision Machine Design, Englewood Cliffs, N.J. : Prentice Hall. 1992.

[7] Heung-Keun Park, Sung-Su Kim, Jin-Moo Park, Tae-Yeon Cho, and Daehie Hong. Dynamics of Dual-Drive Servo Mechanism, IEEE ISIE, Pusan, KOREA, pp.1996-2000. 2001.

[8] Sensors - Robot Eecoder, Society of Robots, http://www.societyofrobots.com/sensors_encoder.shtml

[9] V. G. Badami, S. T. Smith, J. Raja, And R. J. Hocken. A Portable Three-Dimensional Stylus Profile Measuring Instrument, Precision Engineering, Vol. 18(2/3), pp.147-156. 1996.

[10] Todd L. Cloninger, Senthil Balasubramaniam, Brian D. Boudreau, J. Raja, R.J. Hocken. A Simple Technique for Screening Near-Field Probes, Ultramicroscopy, Vol. 57, pp. 223-227. 1995.

[11] Wei Gao, Shuichi Dejima, Hiroaki Yanai, Kei Katakura, Satoshi Kiyono, Yoshiyuki Tomita. A Surface Motor-Driven Planar Motion Stage Integrated with an XYθ_z Surface Encoder for Precision Positioning, Precision Engineering, Vol. 28, pp.329-337. 2004.

[12] K. K. Tan, Huixing X. Zhou, and Tong Heng Lee. New Interpolation Method for Quadrature Encoder Signals, IEEE Transactions on Instrumentation and Measurement, Vol. 51(5), pp.1073-1079. 2002.

[13] Heon Hwang and Si-Chan Kim. Development of Multi-functional Tele-operative Modular Robotic System for Greenhouse Watermelon, Proceedings of the 2003

IEEWASME International Conference on Advanced Intelligent Mechatronics (AIM 2003), pp. 1345-1349. 2003.

[14] Dong-Seok Sun, Tae-Eog Lee, Kyung-Hoon Kim. Component Allocation and Feeder Arrangement for a Dual-Gantry Multi-Head Surface Mounting Placement Tool, International Journal of Production Economics, Vol. 95, pp.245-264. 2005.

[15] John T. Feddema, J. Jill Rivera, and Susan D. Tucker. Knowledge Assistant: A Sensor Fusion Framework for Robotic Environmental Characterization, Proceedings of the 1996 IEEE/SICE/RSJ International Conference on Multisensor Fusion and Integration for Intelligent Systems, pp. 671-678. 1996.

[16] Qi Su and F. Frank Chen. Optimal sequencing of double-gripper gantry robot moves in tightly-coupled serial production systems, IEEE Transactions on Robotics and Automation, Vol. 12(1), pp.22-30. 1996

[17] Craig F. Cutforth and Lucy Y. Pao. Control Using Equal Length Shaped Commands to Reduce Vibration, IEEE Transactions on Control Systems Technology, Vol. 11(1), pp.62-72. 2003.

[18] Ximin Shan and Chia-Hsiang Menq. Robust Disturbance Rejection for Improved Dynamic Stiffness of a Magnetic Suspension Stage. IEEE Trans. on Mechatronics, Vol.7(3), pp.289-295. 2002.

[19] Lin Guo, and Masayoshi Tomizuka. High-Speed and High-Precision Motion Control with an Optimal Hybrid Feedforward Controller, IEEE/ASME Transactions on Mechatronics, Vol. 2(2), pp.110-122. 1997.

[20] Matthijs Boerlage, Rob Tousain, Maarten Steinbuch. Jerk Derivative Feedforward Control for Motion Systems, Proceeding of the American Control Conference, Boston, Massachusetts, pp.4843-4848. 2004.

[21] Steve Dickerson. Command Shaping Control for Material Handling, Proceedings of the American Control Conference, Anchorage, AK, pp. 1734-1735. 2002.

[22] Tsai M.C., I.F. Chiu and M.Y. Cheng. Design and implementation of command and friction feedforward control for CNC motion controllers, IEE Proceedings of Control Theory Application, Vol. 151(1), pp.13-20. January 2004

[23] K.Z. Tang, S.N. Huang, K.K. Tan and T.H. Lee. Combined PID and Adaptive Nonlinear Control for Servo Mechanical Systems, Mechatronics-The Science of Intelligent Machines, Vol. 14(6), pp. 701-714. 2004.

[24] Zuo Z. Liu and Fang L. Luo, Muhammad H. Rashid. QFT-Based Robust and Precision Motion Control System for a High Speed Direct-drive XY Table Positioning Mechanism, IEEE, pp.292-300. 2003.

[25] David J F Hopper. Precision Motion Control of a Manipulator as a Step to Force Control, IEE, Savoy Place, London WCPR OBL. UK. 1994.

[26] Shih-Kang Kuo and Chia-Hsiang Menq. Modeling and Control of a Six-Axis Precision Motion Control Stage, IEEE/ASME Transactions on Mechatronics, Vol. 10(1), pp.50-59. 2005.

[27] Jochen M. Rieber, David G. Taylor. Integrated Control System and Mechanical Design of a Compliant Two-Axes Mechanism, Mechatronics 14, pp.1069-1087. 2004.

[28] Ramy Saad, Saman Halgamuge. Automatically Tuned Hybrid Motion Controller in the Presence of Mechanical Non-Linearities, Proceedings of the 2002 IEEE International Symposium on Intelligent Control, Vancouver, Canada, pp.200-205. 2002.

[29] Yiu Y.K., and Z.X. Li. Control of Parallel Mechanisms-A Geometric Approach, Proceedings of the American Control Conference Anchorage, AK, pp.4720-4725. 2002.

[30] Xuedong Yang and David G. Taylor. H∞ Control Design for Positioning Performance of Gantry Robots, Proceedings of the American Control Conference, Chicago, Illinois, pp.3038-3042. 2000.

[31] Jochen M. Rieber, David G. Taylor. Gain-Scheduled L_2-Gain Based Control of a Flexible Parameter-Varying Robot Link, The 27th Annual Conference of the IEEE Industrial Electronics Society, pp.552-557. 2001.

[32] Chih Lyang Hwang, Song Yu Han and Li Jui Chang. Positioning of Piezo-Driven XY Table Systems using Fuzzy Mixed H^2/H^∞ Optimization-Based Decentralized

Model Reference Control, Proceedings of the IEEE International Conference on Mechantronics, Taipei, Taiwan, pp.39-44. 2005.

[33] Ping-Lang Yen, Wen-I Hsiao and Tien-Sen Lu. Developing a New Low-Cost XY Table using Optical Pickup Head with Adaptive Controller, Proceedings of the IEEE International Conference on Control Applications, Taipei, Taiwan, pp.117-122. 2004.

[34] Catalin F. Baicu, Christopher D. Rahn, and Darren M. Dawson. Backstepping Boundary Control of Flexible-Link Electrically Driven Gantry Robots, IEEE/ASME Transactions on Mechatronics, Vol. 3(1), pp.60-66. 1998.

[35] Rob Rijs and Bram de Jager. Adaptive backstepping control for an XY-table, Proceedings of the American Control Conference, Albuquerque, New Mexico, pp.758-762. 1997.

[36] Samir Mittal and Chia-Hsiang Menq. Precision Motion Control of a Magnetic Suspension Actuator Using a Robust Nonlinear Compensation Scheme, IEEE/ASME Transactions on Mechatronics, Vol. 2(4), pp.268-280. 1997.

[37] B. de Jager. Micro-synthesis control design for an XY-table, Proceedings of the IFAC Symposium on Robust Control Design, Rio de Janeiro, Brasil, pp. 104-108. 1994.

[38] W. J. Rugh and J. S. Shamma. Research on Gain Scheduling (Survey Paper), Automatica, Vol. 36(1O), pp. 1401-1425. 2000.

[39] Bryan C. Murphy, and Won-jong Kim. Intuitive Representation of Gain Schedulers To Facilitate Their Design and Tuning, Proceeding of the 2004 American Control Conference, Boston, Massachusetts, pp.1115-1120. 2004.

[40] Ales Hace, Karel Jezernik, Boris Curk, Martin Terbuc. Robust Motion Control of XY Table for Laser Cutting Machine, IEEE, pp.1097-1102. 1998.

[41] Satoru Goto, Masatoshi Nakamura, ad Nobuhiro Kyura. Accurate Contour Control of Mechatronic Servo Systems using Gaussian Networks, IEEE Transactions on Industrial Electronics, Vol. 43(4), pp.469-476. 1996.

[42] C.H. Lim, Y.K. Tan, S.K.Panda, and J X Xu. Position Control of Linear Permanent Magnet BLDC Servo Using Iterative Learning Control,International Conference on Power System Technology - POWERCON 2004, Singapore, pp.1936-1941. 2004.

[43] James Ratcliffe, Lize van Duinkerken, Paul Lewin, Eric Rogers, Jari Hatonen, Thomas Harte and David Owens. Fast Norm-Optimal Iterative Learning Control for Industrial Applications, American Control Conference, Portland, OR, USA, pp.1951-1956. 2005.

[44] J. J. Hatonen,T. J. Harte, D. H. Owens, J. D. Ratcliffe, P. L. Lewin and E. Rogers. A new robust Iterative Learning Control algorithm for application on a gantry robot, IEEE, pp.305-312. 2003.

[45] Zadeh, L.A. Fuzzy sets. Information and Control, Vol.8(3), pp.338353. 1965.

[46] Pai-Yi Huang, Sinn-Cheng Lin and Yung-Yaw Chen. Real-Coded Genetic Algorithm Based Fuzzy Sliding-Mode Control Design For Precision Positioning, IEEE, pp.1247-1252. 1998.

[47] Murad Samhouri, Asghar Raoufi and Brian Surgenor. Control of a Pneumatic Gantry Robot for Grinding: A Neuro-Fuzzy Approach to PID Tuning, Proceedings of the IEEE Conference on Control Applications, Toronto, Canada, pp.452-458. 2005.

[48] Sungsoo Kim, Baeksuk Chu, Daehie Hong, Heung Keun Park, Jin Moo Park and Tae Yeon Cho. Synchronizing dual drive gantry of chip mounter with LQR approach, Proceedings of the 2003 IEEE/ASME International conference on Advanced Intelligent Mechatronics, pp.838-843. 2003.

[49] K. K. Tan, S. Y. Lim, S. Huang, H. F. Dou, and T. S. Giam. Coordinated Motion Control of Moving Gantry Stages for Precision Applications Based on an Observer-Augmented Composite Controller, IEEE Transactions on Control Systems Technology, VOL. 12(6), pp.984-991. 2004.

[50] Sonia Martinez, Jorge Cortes, and Francesco Bullo. Analysis and Design of Oscillatory Control Systems, IEEE Transactions on Automatic Control, Vol. 48(7), pp.1164-1177. 2003.

[51] Timothy N. Chang, Bhaskar Dani, Zhiming Ji, and Reggie J. Caudill. Contactless Magnetic Transmission System: Vibration Control and Resonance Compensation,

IEEE/ASME Transactions on Mechatronics, Vol. 9(2), pp.458-461. 2004.

[52] G.D. Ianculescu, J. Ly, A.J. Laub, P.M. Papadopoulos. Space Station Freedom Solar Array H∞ Control, Proceedings of the 31st Conference on Decision and Control, Tucson, Arizona, pp.639-640. 1992.

[53] Je-Hie Lee, Uk-You1 Huh, Ho-Joon Park. Improved Contouring Control for Multi-Axis System with Two-Degrees-Of-Freedom Structure, ISIE'97, Guimariies, Portugal, pp.901-905. 1997.

[54] Zuo Zong Liu, Fang Lin Luo, and M. Azizur Rahman. Robust and Precision Motion Control System of Linear-Motor Direct Drive for High-Speed X-Y Table Positioning Mechanism, IEEE Transactions on Industrial Electronics, Vol. 52(5), pp.1357-1363. 2005.

[55] Z.Z. Liu, F.L. Luo and M.H. Rashid. Robust High Speed and High Precision Linear Motor Direct-Drive XY-Table Motion System, IEE Proceedings Control Theory Applications, Vol. 151(2), pp.166-173. 2004.

[56] Ximin Shan, Shih-Kang Kuo, Jihua Zhang, and Chia-Hsiang Menq. Ultra Precision Motion Control of a Multiple Degrees of Freedom Magnetic Suspension Stage, IEEE/ASME Transactions on Mechatronics, Vol. 7(1), pp.67-78. 2002.

[57] Hiroji Yokote, and Kenzo Watanabe. A Hybrid Digital and Analog Controller for DC and Brushless Servomotors, IEEE Transactions on Instrumentation and Measurement, Vol 39(1), pp.259-263. 1990.

[58] Syh-Shiuh Yeh and Pau-Lo Hsu. Analysis and Design of the Integrated Controller for Precise Motion Systems, IEEE Transactions on Control Systems Technology, Vol. 7(6), pp.706-717. 1999.

[59] Marko Bacic, Mark Cannon, Young Il. Lee, and Basil Kouvaritakis. General Interpolation in MPC and its Advantages, IEEE Transactions on Autmoatic Control, Vol. 48(6), pp.1092-1096. 2003.

[60] M. L. Corradini, L. Jetto, and G. Orlando. Robust Stabilization of Multivariable Uncertain Plants via Switching Control, IEEE Transactions on Autmomatic Control, Vol. 49(1), pp.107-114. 2004.

[61] Y. X. Su, C. H. Zheng, and B. Y. Duan. Automatic Disturbances Rejection Controller for Precise Motion Control 0f Permanent-Magnet Synchronous Motors, IEEE Transactions on Industrial Electronics, Vol. 52(3), pp.814-823. 2005.

[62] Y. X. Su, B. Y. Duan, C. H. Zheng, Y. F. Zhang, G. D. Chen, and J. W. Mi. Disturbance-Rejection High-Precision Motion Control of a Stewart Platform, IEEE Transactions on Control Systems Technology, Vol. 12(3), pp.364-374. 2004.

[63] Y. X. Su B. Y. Duan Y. E Zhang. Robust Precision Motion Control for AC Servo System, Proceedings of the 4th World Congress on Intelligent Control and Automation, Shanghai, P.R.China, pp.3319-3323. 2002.

[64] Takashi Emura, and Lei Wang. A High-Resolution Interpolator for Incremental Encoders based on the Quadrature PLL Method, IEEE Transactions on Industrial Electronics, Vol. 47(1), pp.84-90. 2000.

[65] Kenzo Watanabe and Hiroji Yokote. A Microstep Controller of a DC Servomotor, IEEE Transactions on Instrumentation and Measurement, Vol 39(6), pp.867-869. 1990.

[66] Nobumi Hagiwara, Yoshihisa Suzuki and Hideaki Murase. A Method of Improving the Resolution and Accuracy of Rotary Encoders using a Code Compensation Technique, IEEE Transactions on Instrumentation and Measurement, Vol. 41(1), pp.98-101. 1992.

[67] Li Xu and Bin Yao. Adaptive Robust Precision Motion Control of Linear Motors with Ripple Force Compensations: Theory and Experiments, Proceedings of the IEEE International Conference on Control Applications, Anchorage, Alaska, USA, 373-378. 2000.

[68] Junhong Mao, Hiroyuki Tachikawa, Akira Shimokohbe. Double-Integrator Control for Precision Positioning in the Presence of Friction, Precision Engineering 27, pp.419-428. 2003.

[69] Eun-Chan Park, Hyuk Lim, and Chong-Ho Choi. Position Control of X-Y Table at Velocity Reversal using Presliding Friction Characteristics, IEEE Transactions on Control Systems Technology, Vol. 11(1), pp.24-31. 2003.

[70] K.S. Low, M.T. Keck, K.J. Tseng. Parameter Identification and Controller Optimization using GA for a Precision Stage, IEEE PEDS, Indonesia, pp.694-698. 2001.

[71] Young Ho Kim and Frank L. Lewis. Reinforcement Adaptive Learning Neural-Net-Based Friction Compensation Control for High Speed and Precision, IEEE Transactions on Control Systems Technology, Vol. 8(1), pp.118-126. 2000.

[72] Jenq-Shyong Chen. Computer-Aided Accuracy Enhancement for Multi-axis CNC Machine Tool, International Journal of Machine Tools and Manufacture, Vol. 35(4), pp. 593-605. 1995.

[73] Guiquan Chen, Jingxia Yuan, Jun Ni. A Displacement Measurement Approach for Machine Geometric Error Assessment, International Journal of Machine Tools and Manufacture, Vol. 41, pp.149-161. 2001.

[74] Oui-Serg Kim, Sang-Ho Lee, and Dong-Chul Han. Positioning Performance and Straightness Error Compensation of the Magnetic Levitation Stage supported by the Linear Magnetic Bearing, IEEE Transactions on Industrial Electronics, Vol. 50(2), pp.374-378. 2003.

[75] M. A. Donmez, D. S. Blomquist, R. J. Hocken, C. R. Liu and M. M. Barash. A General Methodology for Machine Tool Accuracy Enhancement by Error Compensation, Precision Engineering, Vol.8(4), pp.187-196. 1986.

[76] P.H. Pereira , R.J. Hocken. Characterization and Compensation of Dynamic Errors of a Scanning Coordinate Measuring Machine, Precision Engineering, Vol. 31, pp.22-32. 2007.

[77] Chana Raksiri, Manukid Parnichkun. Geometric and Force Errors Compensation in a 3-Axis CNC Milling Machine, International Journal of Machine Tools and Manufacture, Vol. 44, pp.1283-1291. 2004.

[78] A. K. Srivastava, S. C. Veldhuis and M. A. Elbestawlt. Modelling Geometric and Thermal Errors in a Five-Axis CNC Machine Tool, International Journal of Machine Tools and Manufacture, Vol. 35(9), pp.1321-1337. 1995.

[79] Kevin L. Moore. An Iterative Learning Control Algorithm for Systems with Measurement Noise, Proceedings of the 38th Conference on Decision and Control, Phoenix, Arizona, USA, pp.270-275. 1999.

[80] Bram De Jager. Acceleration Assisted Tracking Control, IEEE Control Systems, pp.20-27. 1994.

[81] K. Lau, R.J. Hocken and W.C. Haight. Automatic Laser Tracking Interferometer System for Robot Metrology, Precision Engineering, Vol. 8(1), pp.3-8. 1986.

[82] K. Lau, R. Hocken and L. Haynes. Robot Performance Measurements using Automatic Laser Tracking Techniques, Robotics and Computer-Integrated Manufacturing, Vol. 2(3/4) pp.227-236. 1985.

[83] A. Dorsey, R.J. Hocken and M. Horowitz. A Low Cost Laser Interferometer System for Machine Tool Applications, Precision Engineering, Vol. 5(1), pp.29-31. 1983.

[84] Christopher D. Mize, John C. Ziegert. Durability Evaluation of Software Error Correction on a Machining Center, International Journal of Machine Tools and Manufacture, Vol. 40, pp. 1527-1534. 2000.

[85] Massimiliano Mattei, Gaetano Paviglianiti, Valerio Scordamaglia. Nonlinear H_∞ Identity Observers for Sensor FDI: An Application Example, IEEE, pp.346-351. 2004.

[86] Kurt Lauridsen. Reliability of Remote Manipulator Systems for use in Radiation Environments,IEE, Savoy Place, London WCPR OBL, UK. 1994.

[87] Paul Gruhn, and Dave Reynolds. Does Your Safety-Instrumented System Really Require SIL3?, Control Engineering Asia, Sun Rise Printing And Supplies Pte Ltd, pp.38. Apr-May 2006.

[88] Ingle KA. Reverse Engineering, Mcgraw Hill; 1994.

[89] R. Ramesh, M.A. Mannan, A.N. Poo. Error Compensation in Machine Tools - A Review Part I: Geometric, Cutting-Force Induced and Fixture Dependent Errors, International Journal of Machine Tools and Manufacture, Vol. 40, pp.1235-1256. 2000.

[90] R. Ramesh, M.A. Mannan, A.N. Poo. Error Compensation in Machine Tools - A Review Part II: Thermal Errors, International Journal of Machine Tools and Manufacture, Vol. 40, pp.1257-1284. 2000.

[91] Evans C.J. Precision Engineering: An Evolutionary View, Cranfield Press, Cranfield, UK. 1989.

[92] Ramesh R., Mannan M. A., and Poo A. N. AI-Based Classification Methodologies for Modeling Machine Tool Thermal Error, Transactions of the North American Manufacturing Research Institution/SME, pp.239-246. 2002.

[93] Mize C. and Ziegert J. Neural Network Thermal Error Compensation of a Machining Center, Precision Engineering, Vol.24(4), pp. 338-346. 2000.

[94] Jenq-Shyong Chen.A Study of Thermally Induced Machine Tool Errors in Real Cutting Conditions, International Journal of Machine Tools and Manufacture, Vol.36(12), pp. 1401-1411. 1996.

[95] Yang Minyang, and Lee Jaejong. Measurement and Prediction of Thermal Errors of a CNC Machining Center using Two Spherical Balls, Journal of Materials Processing Technology, Vol.75(1-3), pp. 180-189. 1998.

[96] Krishnakumar K., and Melkote S. Machining Fixture Layout Optimization Using the Genetic Algorithm, International Journal of Machine Tools and Manufacture, Vol.40(4), pp. 579-598. 2000.

[97] Satyanarayana S. and Melkote S. Determination of Clamping Force Based on Minimization of Workpiece Elastic Deformation, Society of Manufacturing Engineers, NAMRC. 2002.

[98] Kim S.H., Ko T. J., and Ahn J. H. Elimination of Settling Error due to Clamping Forces in On-Machine Measurement, The international Journal of Advanced Manufacturing Technology, Vol.19, pp. 573-578. 2002.

[99] Rong Y., Hu W., Kang Y., Zhang Y., and Yen D. Locating Error Analysis and Tolerance Assignment for Computer-Aided Fixture Design, International Journal of Production Research, Vol.39(15), pp. 3529-3545. 2001.

[100] Okafor A.C., and Ertekin Yalcin M. Derivation of Machine Tool Error Models and Error Compensation Procedure for Three Axes Vertical Machining Center using Rigid Body Kinematics, International Journal of Machine Tools and Manufacture, Vol.40(8), pp. 1199-1213. 2000.

[101] Yao Y. VMMC: a Test-Bed for Machining, Computers in Industry, Vol.47, pp. 255-268. 2002.

[102] Tan K.K., Huang S.N. and Seet H.L. Geometrical Error Compensation of Precision Motion Systems using Radial Basis Function, IEEE Transaction on Instrumentation and Measurement, Vol.49(5), pp. 984 - 991. 2000.

[103] Girosi F. An Equivalence Between Sparse Approximation and Support Vector Machines, Neural Computation, Vol.10, pp.1455-1480. 1998.

[104] Vapnik V. The Nature of Statistical Learning Theory, Berlin: Springer-Verlag, 1995.

[105] Drucker H., Burges C., Kaufman L., Smola A., and Vapnik V. Support Vector Regression Machines, Advances in Neural Information Processing Systems, Vol.9, pp.151-161. 1997.

[106] Muller K.R., Smola A., Ratsch G., Scholkopf B., Kohlmorgen J., and Vapnik V. Predicting Time Series with Support Vector Machines, Proceedings of Artificial Neural Networks, pp.999-1004. 1997.

[107] Mukherjee S.O., Osuna E., and Girosi F. Nonlinear Prediction of Chaotic Time Series using Support Vector Machines, Proceedings of the IEEE Signal Processing Society Workshop, pp.511-520. 1997.

[108] Kuhn, H. W.; Tucker, A. W. (1951). Nonlinear programming. Proceedings of 2nd Berkeley Symposium: 481-492, Berkeley: University of California Press.

[109] J.A.K. Suykens, T. Van Gestel, J. De Brabanter, B. De Moor, J. Vandewalle, Least Squares Support Vector Machines, World Scientific, Singapore, 2002 (ISBN 981-238-151-1)

[110] Burges C.J.C. A Tutorial on Support Vector Machines for Pattern Recognition, Data Mining and Knowledge Discovery, Vol.2, pp.121-167. 1998.

[111] ISO 230-6, test code for machine tools:"Part 6. Determination of positioning accuracy on body and face diagonals (diagonal displacement tests)". 2002.

[112] Mark A.V. Chapman. Limitations of Laser Diagonal Measurements, Precision Engineering, Vol. 27, pp.401-406. 2003.

[113] Arimoto S., S. Kawamura, and F. Miyazaki. Bettering Operations of Robots by Learning, Journal of Robotic Systems 1, pp.123-140. 1984.

[114] Mikael Norrlof. An Adaptive Iterative Learning Control Algorithm with Experiments on an Industrial Robot, IEEE Transactions on Robotics and Automation, Vol.18(2), pp.245-251. 2002.

[115] Kevin L. Moore. An Iterative Learning Control Algorithm for Systems with Measurement Noise, Proceedings of the 38th Conference on Decision and Control, pp.270-275. 1999.

[116] Tan Kok Kiong, Lee Tong Heng, Dou Huifang, and Huang Sunan. Precision Motion Control - Design and Implementation, Springer-Verlag, 2001.

[117] C.S. Teo, K.K. Tan, S.Y. Lim, S. Huang, and K.Z. Tang. Geometric Error Compensation for Multi-Axial Precision Motion Systems Using Support Vectors, Asian Journal of Control: Special Issue on Precision Motion Control and Instrumentation, Vol.7(1), pp.56-62. 2004.

[118] Jochen M. Rieber, and David G. Taylor. Gain-Scheduled L_2-Gain Based Control of a Flexible Parameter-Varying Robot Link, IECON'01, pp.552-557. 2001.

[119] James Ratcliffe, Lize van Duinkerken, Paul Lewin, Eric Rogers, Jari Hatonen, Thomas Harte and David Owens. Fast Norm-Optimal Iterative Learning Control for Industrial Applications, American Control Conference, pp.1951-1956. 2005.

[120] Murad Samhouri, Asghar Raoufi and Brian Surgenor. Control of a Pneumatic Gantry Robot for Grinding: A Neuro-fuzzy Approach to PID Tuning, Proceedings of the IEEE Conference on Control Applications, pp.452-458. 2005.

[121] Rob Rijs, and Bram de Jager. Adaptive Backstepping Control for an XY-table. Proceedings of the American Control Conference, pp.758-762. 1997.

[122] Bram de Jager. Acceleration Assisted Tracking Control, IEEE Control Systems, IEEE Control Systems Magazine, pp.20-27. 1994.

[123] X. Yang and David G. Taylor. H∞ Control Design for Positioning Performance of Gantry Robots, Proceedings of the American Control Conference, pp.3038-3042. 2000.

[124] Jean-Jacques E. Slotine, and Weiping Li. Applied nonlinear control, Imprint Englewood Cliffs, N.J. : Prentice Hall. 1991.

[125] K.K. Tan, T.H. Lee, S. Huang and X. Jiang. Friction Modeling and Adaptive Compensation Using a Relay Feedback Approach. IEEE Trans. on Industrial Electronics, Vol.48(1), pp.169-176. 2001.

[126] Lyapunov A.M. Stability of motion, Academic Press, New-York and London,1966

Author's Publications

Journal Papers:

1. C.S. Teo, K.K. Tan, S.Y. Lim, S. Huang and K.Z. Tang. Geometric Error Compensation for Multi-Axial Precision Motion Systems using Support Vectors, Asian Journal of Control, Special Issue on "Precision Motion Control and Instrumentation", Vol. 7(1), pp.56-62. March 2005.

2. C.S. Teo, K.K. Tan, S.Y. Lim, S. Huang and E.B. Tay. Dynamic Modeling and Adaptive Control of a H-type Gantry stage, Mechatronics-The Science of Intelligent Machines, Vol. 17(7), pp.361-367. Sep 2007.

3. C.S. Teo, K.K. Tan, and S.Y. Lim. Dynamic Geometric Compensation for Gantry Stage using Iterative Learning Control, IEEE Transactions on Instrumentation and Measurement, Accepted for Publication.

Conference Papers:

1. Kok-Kiong Tan, Tong-Heng Lee, Ser-Yong Lim, Twee-Seng Giam and Chek-Sing Teo.

Robust Coordinated Control of Multi-Axis Gantry Stages, The 8th IEEE International Workshop on Advanced Motion Control, Kawasaki, Japan, pp.287-292. 2004.

2. Kok-Zuea Tang, Kok-Kiong Tan, Tong-Heng Lee and Chek-Sing Teo, Neural-Based Correction and Interpolation of Encoder Signals for Precision Motion Control, The 8th IEEE International Workshop on Advanced Motion Control, Kawasaki, Japan, pp.499-504. 2004.

3. T.H.Lee, K.K.Tan, S.N.Huang, C.S.Teo, S.Y.Lim, Adaptive Observer Design Using Neural Networks, The 5th International Conference on Simulated Evolution and Learning, BEXCO: Busan, Korea, paper 333. 2004.

4. Teo Chek Sing, Tan Kok Kiong, Huang Sunan and Lim Ser Yong. Adaptive Control of a 3-Axial H-type Gantry Positioning Stage, The International Symposium on Collaborative Research in Applied Science, University of British Columbia, Vancouver, Canada, pp.182-188. 2005.

5. K.K. Tan, S. Huang, T.H. Lee, C.S. Teo, Andi S. P., C.W. de Silva. Collaborative Research in Fault Detection and Diagnosis, The International Symposium on Collaborative Research in Applied Science, University of British Columbia, Vancouver, Canada, pp.142-148. 2005.

6. C. S. Teo, K.K. Tan, S. Huang and S.Y. Lim. Dynamic Modeling and Adaptive Control of a Multi-Axial Gantry Stage, International Conference on Systems, Man and Cybernetics, Hawaii, USA, pp.3374-3379. 2005.

7. CS Teo, KK Tan, SY Lim. Dynamic Geometric Compensation for Gantry Stage

using Iterative Learning Control, The 32nd Annual Conference of the IEEE Industrial Electronics Society, Paris, FRANCE, paper no. PF-003425. 2006.

8. C.S. Teo, K.K. Tan, S. Huang and S.Y. Lim. Dynamic Modelling and Adaptive Control of a Multidimensional Positioning System, IFAC Workshop on Advanced Process Control for Semiconductor Manufacturing, Furama Riverfront Hotel, Singapore, paper no. 108. 2006.

Chapters in Books:

1. C. S. Teo, K. K. Tan, S. Huang and S. Y. Lim. Adaptive Control of a Gantry System, in "MECHATRONIC SYSTEMS Devices, Design, Control, Operation, and Monitoring", RC Press, Taylor and Francis, Boca Raton, FL. Chapter 11.

2. K.K. Tan, S. Huang, T.H. Lee, C.S. Teo, Andi S. P., C.W. de Silva. Fault Detection and Diagnosis in Mechatronic Systems: A Study of Tools in Milling Machine via State Observer, in "MECHATRONIC SYSTEMS Devices, Design, Control, Operation, and Monitoring", RC Press, Taylor and Francis, Boca Raton, FL. Chapter 25.